



**UNIVERSITY OF NAIROBI**

**BATCH ADSORPTION OF MALACHITE GREEN FROM AQUEOUS  
SOLUTIONS USING LOW-COST RICE HUSKS AND SYNTHETIC  
POLYMER ADSORBENTS: KINETIC AND EQUILIBRIUM MODELLING**

**BY**

**VERONICA M. MUINDE**

**I80/92722/2013**

**A Thesis Submitted in Fulfillment of the Requirements for Award of the Degree of Doctor  
of Philosophy in Chemistry of the University of Nairobi**

**2021**

## DECLARATION

I declare that this thesis is my original work and has not been submitted elsewhere for examination, award of a degree or publication. Where other people's work or my work has been used, this has properly been acknowledged and referenced in accordance with the University of Nairobi's requirements.

Signature ...  .....

Date...05/07/2021.....

**Veronica M. Muinde**  
**180/92722/2013**  
Department of Chemistry  
School of Physical Sciences  
University of Nairobi

This thesis is submitted for examination with our approval as research supervisors:

Prof. John M. Onyari  
Department of Chemistry  
University of Nairobi  
P.O Box 30197-00100  
Nairobi, Kenya  
[jonyari@uonbi.ac.ke](mailto:jonyari@uonbi.ac.ke)

Signature



Date

9/7/2021 ...

Dr. Benson M. Wamalwa  
Department of Chemistry  
University of Nairobi  
P.O Box 30197-00100  
Nairobi, Kenya  
[Benson.wamalwa@uonbi.ac.ke](mailto:Benson.wamalwa@uonbi.ac.ke)



07/07/2021

Dr. John N. Wabomba  
Department of Chemistry  
University of Nairobi  
P.O Box 30197-00100  
Nairobi, Kenya  
[jwabomba@uonbi.ac.ke](mailto:jwabomba@uonbi.ac.ke)



05/07/2021

## **DEDICATION**

To my family members and friends.

## ACKNOWLEDGEMENTS

I acknowledge my supervisors, Professor John M. Onyari, Dr. Benson M. Wamalwa and Dr. John N. Wabomba for their mentorship and assistance which they accorded me during my study. Many thanks to DAAD for offering me a scholarship which facilitated me to pursue this program.

My sincere appreciation to Professor Steve Howdle, University of Nottingham (United Kingdom), School of Chemistry for awarding me a GlaxoSmithKline (GSK) Ph.D. Associate scholarship for three months. The scholarship enabled me to train on polymer synthesis and characterization in his research lab using state of the art equipment. I acknowledge his research group (both Ph.D. and Postdoc students) for the support they accorded me during my three months research visit at the university. I am indebted to Professor Robert Mokaya (Pro Vice Chancellor for Global engagement) for all the assistance he gave me throughout my stay in Nottingham.

I acknowledge my employer, the University of Nairobi for allowing me to pursue this program. All members of staff, department of chemistry for supporting me throughout my study period. My heartfelt gratitude to Dr. Richard Mutinda Nthumbi for his invaluable assistance. Many thanks to Dr. Wycliffe C. Wanyonyi of Kabianga University for his advice and assistance regarding my research work.

Finally, I acknowledge my family members for their support, prayers and patience.

## ABSTRACT

Safe and abundant water is crucial for the good health of human beings and animals. Across Africa, a third of the population has no access to clean water and sanitation and this affects the continent's economic productivity adversely due to water-related diseases.

The contamination of water by organic dyes such as malachite green has become a global challenge owing to their toxicity. Stringent discharge guidelines have been imposed on Kenyan industries releasing dye-loaded effluents to the environment and this has accelerated the search for efficient and economically viable low-cost sorbent materials.

Rice husks, chitosan- zinc oxide and poly ( $\epsilon$ -caprolactone) – rice husks blend films were categorized as potential low-cost and highly effective sorbents for the uptake of malachite green from aqueous media.

Adsorbent characterization was achieved using selected analytical tools such as scanning electron microscope, thermogravimetric analyzer, Fourier transform infrared and powder X-ray diffractometer instruments. The equilibrium experiments were achieved through the application of batch experiments and the analysis of the solutions was done using a UV-Vis spectrophotometer. The equilibrium data was evaluated using three commonly utilized models namely Langmuir, Freundlich and Temkin models whereas the kinetic data was evaluated via first and second-order rate graphs. The intraparticle diffusion model was applied in testing the sorption mechanisms.

The sorbent materials were found to be mesoporous, thermally stable and contained carbonyl, hydroxyl, phenyl and amino groups on their surface.

The quantity of the colorant removed was impacted by the solution pH, colorant concentration, sorbent particle size, solution temperature, adsorbent quantity and contact time. The adsorbent

quantities utilized for the adsorption of MG onto RH, CS-ZnO and polycaprolactone – rice husks (PCL-RH) were 0.1, 0.6 and 0.3 g respectively with an optimal pH of 7 (RH & PCL-RH) and 8 for CS-ZnO. The percentage adsorption for the dye using the three adsorbents rose with increasing material dose, uptake time and reducing particle sizes. Conversely, the sorption efficacy reduced with increasing dye strength. The thermodynamic data signified an exothermic reaction process.

The sorption equilibrium data was perfectly depicted by the Langmuir uptake model in comparison with the other two isotherms with  $R^2$  values  $> 0.90$ . The maximum adsorption capacities of RH, PCL-RH and CS-ZnO were 6.5, 9.09 and 11 mg/g respectively.

The rate of MG removal onto the three adsorbents corresponded to the second-order chemical kinetics denoting that chemisorption depicted the rate-determining step and therefore intraparticle diffusion was not exclusively controlling the reaction.

These results demonstrate that unmodified RH, chitosan–ZnO composites and PCL- RH blend films could be utilized as complementary low-cost and eco-friendly materials for textile water purification.

**TABLE OF CONTENTS**

**DECLARATION ..... II**

**DEDICATION .....III**

**ACKNOWLEDGEMENTS .....IV**

**ABSTRACT..... V**

**LIST OF TABLES .....XV**

**LIST OF FIGURES ..... XVI**

**LIST OF SCHEMES .....XX**

**LIST OF ABBREVIATIONS .....XXII**

**CHAPTER ONE ..... 1**

**INTRODUCTION ..... 1**

1.1: BACKGROUND OF THE STUDY ..... 1

1.2: CHALLENGES ASSOCIATED WITH THE RELEASE OF UNTREATED EFFLUENTS INTO WATER RESOURCES..... 1

1.3: CURRENT TECHNOLOGIES USED TO TREAT EFFLUENTS ..... 2

1.4: LOW-COST ADSORBENTS ..... 2

1.5: STATEMENT OF THE PROBLEM ..... 3

1.6: OBJECTIVES ..... 4

1.6.1: *Overall Objective* ..... 4

1.6.2:	<i>Specific Objectives</i> .....	4
1.7:	JUSTIFICATION AND SIGNIFICANCE OF THE STUDY .....	5
<b>CHAPTER TWO</b> .....		<b>6</b>
<b>LITERATURE REVIEW</b> .....		<b>6</b>
2.1:	DYES .....	6
2.1.1:	<i>Synthetic Dyes</i> .....	6
2.1.2:	<i>Basic Malachite Green (MG)</i> .....	7
2.2:	ADSORPTION.....	8
2.2.1:	<i>Adsorption Isotherm</i> .....	9
2.2.2:	<i>Langmuir Isotherm</i> .....	9
2.2.3:	<i>Freundlich Isotherm</i> .....	10
2.2.4:	<i>Temkin Isotherm</i> .....	11
2.3:	KINETICS OF ADSORPTION .....	12
2.3.1:	<i>Lagergren First-Order Kinetics</i> .....	12
2.3.2:	<i>Pseudo Second Order Kinetics</i> .....	13
2.3.3:	<i>Weber – Morris Intraparticle Diffusion</i> .....	13
2.4:	THERMODYNAMIC STUDIES .....	14
2.5:	ADSORBENTS INVESTIGATED IN THIS WORK .....	15
2.5.1:	<i>Rice Husks</i> .....	15
2.5.2:	<i>Chitosan – Zinc Oxide (CS- ZnO)</i> .....	16
2.5.3:	<i>Poly (<math>\epsilon</math>-Caprolactone) Polymer</i> .....	18
2.5.3a:	<i>Condensation of 6-hydroxy caproic acid</i> .....	19

2.5.3b:	<i>Ring-Opening Polymerization of Lactones</i> .....	19
2.5.4:	<i>ε-PCL-Rice Husks Film Blends</i> .....	22
<b>CHAPTER THREE</b> .....		<b>24</b>
<b>MATERIALS AND METHODS</b> .....		<b>24</b>
3.1:	MATERIALS .....	24
3.2:	PREPARATION OF MALACHITE GREEN SOLUTION .....	24
3.3:	PREPARATION OF ADSORBENTS .....	24
3.3.1:	<i>Preparation of Rice Husks (RH)</i> .....	24
3.3.2:	<i>Synthesis of Chitosan-ZnO Material</i> .....	25
3.3.3:	<i>Synthesis of Poly (ε-Caprolactone)</i> .....	26
3.3.4:	<i>Preparation of Plain ε-Polycaprolactone (ε-PCL) Films</i> .....	27
3.3.5:	<i>Preparation of ε-Polycaprolactone – Rice Husks (ε-PCL-RH) Blended Films</i> .....	27
3.4:	CHARACTERIZATION OF ADSORBENTS.....	28
3.4.1:	<i>Analysis of Organic Functional Groups in the Rice Husks</i> .....	28
3.4.2:	<i>Surface Morphology Analysis of RH and MG Loaded RH</i> .....	28
3.4.3:	<i>Physisorption Analysis for RH</i> .....	28
3.4.4:	<i>Thermogravimetric Analysis of RH</i> .....	29
3.4.5:	<i>Powder X-Ray Diffractometry Analysis of RH</i> .....	29
3.4.6:	<i>FTIR Analysis of Chitosan-Zinc Oxide Material</i> .....	29
3.4.7:	<i>Thermogravimetric Assessment for CS- ZnO</i> .....	30
3.4.8:	<i>XRD Analysis of CS- ZnO Composite</i> .....	30
3.4.9:	<i>Physisorption Analysis of CS - ZnO</i> .....	30

3.4.10:	<i>Zeta Potential Measurement of CS-ZnO material .....</i>	30
3.4.11:	<i>Energy Dispersive X-Ray Fluorescence of CS-ZnO Composite .....</i>	31
3.4.12:	<i><sup>1</sup>H NMR Analysis of Poly (<math>\epsilon</math>-Caprolactone).....</i>	31
3.4.13:	<i>Differential Scanning Calorimetry Measurement for <math>\epsilon</math>- PCL.....</i>	32
3.4.14:	<i>Size Exclusion Chromatography (SEC) Analysis of Poly (<math>\epsilon</math>- Caprolactone).....</i>	32
3.4.15:	<i>Dynamic Mechanical Analysis for Poly (<math>\epsilon</math>- Caprolactone) .....</i>	32
3.5:	<b>BATCH EXPERIMENTS FOR UPTAKE OF MG USING RH .....</b>	33
3.5.1:	<i>Impact of Interaction Time and Initial Colorant Concentration .....</i>	33
3.5.2:	<i>Influence of pH for the Uptake of Malachite Green on Rice Husks .....</i>	33
3.5.3:	<i>Influence of Stirring Rate.....</i>	33
3.5.4:	<i>Influence of Rice Husks Particle Mesh Size.....</i>	34
3.5.5:	<i>Impact of Solution Temperature .....</i>	34
3.5.6:	<i>Influence of Ionic Strength.....</i>	35
3.6:	<b>ADSORPTION OF MALACHITE GREEN USING CHITOSAN-ZINC OXIDE.....</b>	35
3.6.1:	<i>Impact of Interaction Time and Colorant Concentration .....</i>	35
3.6.2:	<i>Impact of Amount of Chitosan-ZnO.....</i>	36
3.6.3:	<i>Impact of MG Solution pH.....</i>	36
3.7:	<b>BATCH EXPERIMENTS USING PCL-RH BIOFILMS.....</b>	36
3.7.1	<i>Influence of Dosage on MG Uptake.....</i>	36
3.7.2	<i>Impact of Contact Time on MG Abstraction by PCL-RH Blended Films.....</i>	37
3.7.3:	<i>Impact of Initial Colorant Concentration on Uptake of MG by PCL-RH Blend Films .....</i>	37

3.8:	KINETICS AND MECHANISM EXPERIMENTS FOR THE REMOVAL PROCESS.....	37
3.9:	STATISTICAL ANALYSIS .....	37
<b>CHAPTER FOUR.....</b>		<b>38</b>
<b>RESULTS AND DISCUSSION .....</b>		<b>38</b>
4.1:	<i>Characterization of RH .....</i>	38
4.1.1:	<i>FTIR Spectra for Raw and Dye Reacted RH .....</i>	38
4.1.2:	<i>Scanning Electron Microscope Assessment for Rice Husks .....</i>	39
4.1.3:	<i>Energy-Dispersive X-Ray Assessment for Rice Husks.....</i>	40
4.1.4:	<i>XRD Assessment for Rice Husks.....</i>	41
4.1.5:	<i>Thermogravimetric Analysis of Rice Husks.....</i>	42
4.1.6:	<i>BET Surface Area Assessment for RH .....</i>	44
4.2:	CHARACTERIZATION OF CS – ZNO SORBENT MATERIAL .....	45
4.2.1:	<i>FTIR Evaluation.....</i>	45
4.2.2:	<i>TGA Investigation of CS- ZnO Adsorbent .....</i>	47
4.2.3:	<i>XRD Phase Assessment of Chitosan- ZnO Material.....</i>	48
4.2.4:	<i>Physisorption Investigation of Chitosan-ZnO Sorbent Material.....</i>	49
4.2.5:	<i>Zeta Potential Analysis .....</i>	50
4.2.6:	<i>EDXRF Chemical Analysis for CS-ZnO .....</i>	51
4.3:	CHARACTERIZATION OF E-POLYCAPROLACTONE ( $\epsilon$ - PCL) POLYMER.....	52
4.3.1:	<i><math>^1\text{H}</math> NMR Analysis for <math>\epsilon</math>- PCL.....</i>	52
4.3.2:	<i>Assessment of Poly (<math>\epsilon</math>-Caprolactone) using Size Exclusion Chromatography (SEC)</i> .....	54

4.3.3:	<i>Assessment of Poly (<math>\epsilon</math>-Caprolactone) by Differential Scanning Calorimetry</i> .....	55
4.3.4:	<i>Dynamic Mechanical Analysis for Poly (<math>\epsilon</math>-caprolactone)</i> .....	56
4.3.5:	<i>FTIR Spectrum for Pure <math>\epsilon</math>-PCL</i> .....	57
4.4:	CHARACTERIZATION OF POLY(E-CAPROLACTONE) - RICE HUSKS FILMS .....	58
4.4.1:	<i>Thermogravimetric Analysis of PCL - RH</i> .....	58
4.4.2:	<i>X-Ray Diffraction Analysis</i> .....	59
4.4.3:	<i>FTIR Spectra Analysis of Raw and MG Loaded PCL-RH Films</i> .....	60
4.5:	BATCH EXPERIMENTS FOR UPTAKE OF MALACHITE GREEN ON RICE HUSKS .....	62
4.5.1:	<i>Determined Maximum Absorption Wavelength of MG</i> .....	63
4.5.2:	<i>Calibration Curve</i> .....	63
4.5.3:	<i>Influence of Interaction Time on Malachite Green Uptake onto Rice Husks</i> .....	64
4.5.4:	<i>Influence of Initial Colorant Strength</i> .....	65
4.5.5:	<i>Influence of Dosage on Malachite Green Adsorption</i> .....	66
4.5.6:	<i>Effect of Monovalent Ions on Malachite Green Adsorption</i> .....	67
4.5.7:	<i>Impact of Rice Husks Particle Size on Malachite Green Adsorption</i> .....	68
4.5.8:	<i>Impact of Solution pH on Malachite Green Uptake by Rice Husks</i> .....	69
4.5.9:	<i>Impact of Agitation Speed on Malachite Green Uptake</i> .....	70
4.5.10:	<i>Impact of Temperature on Malachite Green Adsorption</i> .....	71
4.6:	EQUILIBRIUM ISOTHERMS FOR UPTAKE OF MG BY RH .....	72
4.6.1:	<i>Langmuir Isotherm for Uptake of Malachite Green</i> .....	72
4.6.2:	<i>Freundlich Isotherm for Malachite Green Adsorption</i> .....	73
4.6.3:	<i>Temkin Isotherm for Malachite Green Adsorption on RH</i> .....	74

4.7:	KINETIC STUDIES OF MALACHITE GREEN ADSORPTION ONTO RH .....	75
4.7.1:	<i>Pseudo- First-Order Rate Kinetics on MG uptake .....</i>	75
4.7.2:	<i>Pseudo- Second - Order Reaction Rate for Uptake of MG on Rice Husks.....</i>	76
4.7.3:	<i>Intraparticle Diffusion Model.....</i>	77
4.7.4:	<i>Thermodynamic Studies.....</i>	78
4.8:	BATCH ADSORPTION EXPERIMENTS FOR CHITOSAN- ZNO MATERIAL .....	80
4.8.1:	<i>Impact of Dye Concentration.....</i>	80
4.8.2:	<i>Impact of Interaction Time.....</i>	80
4.8.3:	<i>Impact of CS-ZnO Dose.....</i>	81
4.8.4:	<i>Influence of pH.....</i>	82
4.9:	EQUILIBRIUM ISOTHERMS FOR REMOVAL OF MG BY THE CHITOSAN-ZNO SORBENT..	84
4.9.1:	<i>Langmuir Model for the Uptake of MG by CS-ZnO Material .....</i>	84
4.9.2:	<i>Freundlich Model for Uptake of MG on CS-ZnO Nanocomposite.....</i>	85
4.9.3:	<i>Temkin Uptake Model.....</i>	86
4.10:	KINETIC MODELLING FOR UPTAKE OF MG BY CS-ZNO COMPOSITE.....	87
4.10.1:	<i>Mechanism for Adsorption of MG onto CS-ZnO Material .....</i>	87
4.10.2:	<i>Intra- Particle Diffusion Rate Model for Uptake of MG on CS-ZnO Material ..</i>	89
4.11:	BATCH UPTAKE FOR MG ON POLY( $\epsilon$ -CAPROLACTONE)-RICE HUSKS (PCL-RH) BLEND FILMS .....	90
4.11.1:	<i>Impact of Dose on the Uptake of MG on PCL-RH.....</i>	90
4.11.2:	<i>Impact of Interaction Time on the Adsorption of MG by Plain PCL and PCL-RH Materials.....</i>	91
4.11.3:	<i>Impact of Initial Colourant Strength on MG Removal by PCL-RH Films.....</i>	92

4.12:	SORPTION KINETICS FOR THE ABSTRACTION OF MG BY PCL-RH.....	93
4.13:	THE INTRA-PARTICLE DIFFUSION MODEL FOR UPTAKE OF MG BY PCL-RH.....	95
4.14	COMPARISON OF RH, CS-ZNO AND PCL-RH WITH OTHER SORBENTS FOR UPTAKE OF MG FROM AQUEOUS MEDIA .....	96
4.2:	EQUILIBRIUM ISOTHERMS FOR UPTAKE OF MG BY E-POLYCAPROLACTONE-RICE HUSKS FILMS .....	97
4.2.1:	<i>Langmuir model for the abstraction of MG on PCL-RH biofilms.....</i>	97
4.2.2:	<i>Freundlich isotherm for the abstraction of MG by PCL-RH blend films.....</i>	98
4.2.3:	<i>Temkin Isotherm for Abstraction of MG on PCL-RH Blend Films .....</i>	100
4.3:	ADSORBENT COST EVALUATION .....	101
<b>CHAPTER FIVE .....</b>		<b>102</b>
<b>CONCLUSIONS AND RECOMMENDATIONS.....</b>		<b>102</b>
5.1:	CONCLUSIONS .....	102
5.2:	RECOMMENDATIONS.....	104
<b>REFERENCES.....</b>		<b>105</b>
<b>APPENDICES.....</b>		<b>127</b>

## LIST OF TABLES

<b>Table 3.1:</b>	Volume of IM NaCl and distilled water for MG uptake by rice husks.....	35
<b>Table 4. 1:</b>	EDX analysis results for RH material.....	41
<b>Table 4. 2:</b>	Isotherm Values for the Removal of MG by Unmodified Rice Husks.....	73
<b>Table 4. 3:</b>	Kinetic Rate Values for Sorption of MG by Rice Husks.....	78
<b>Table 4.4:</b>	Activation Energy and Thermodynamic Values for MG Uptake by RH.....	79
<b>Table 4. 5:</b>	Isotherm values for the abstraction of MG by CS-ZnO composite .....	87
<b>Table 4. 6:</b>	Chemical Kinetics Values for the Abstraction of MG by CS-ZnO nanomaterial ..	90
<b>Table 4.7:</b>	Chemical Kinetic Components for Biosorption of MG onto PCL-RH.....	95
<b>Table 4. 8:</b>	Comparison of Various Literature Sorbents with the three Adsorbents Used in this Study for MG Uptake.....	96
<b>Table 4. 9:</b>	Isotherm Constants for the Abstraction of MG by PCL-RH Biofilms .....	100

## LIST OF FIGURES

Figure 2.1:	Structure of Malachite Green Oxalate .....	8
Figure 2.2:	Structure of leucomalachite green .....	8
Figure 2.3:	Rice husks obtained from the Mwea milling factory.....	16
Figure 2.4:	Chemical structure of Chitin.....	18
Figure 2.5:	Chemical structure of Chitosan.....	18
Figure 2.6:	Chemical structure of Poly( $\epsilon$ -caprolactone) .....	19
Figure 4.1:	FTIR spectra for raw and MG loaded rice husks .....	39
Figure 4.2:	SEM micrographs of (a) raw rice husks (b) reacted rice husks with MG.....	40
Figure 4.3:	PXRD patterns of rice husks.....	42
Figure 4.4:	TGA Thermogram of rice husks adsorbent. ....	44
Figure 4.5:	BET N <sub>2</sub> isotherm for rice husks.....	45
Figure 4.6:	FTIR spectrum of Chitosan.....	46
Figure 4.7:	FTIR spectrum for Chitosan-ZnO composite. ....	47
Figure 4.8:	TGA thermogram for Chitosan-ZnO sorbent .....	48
Figure 4.9:	XRD diffractogram for CS-ZnO sorbent .....	49
Figure 4.10:	BET adsorption-desorption isotherm for CS-ZnO.....	50
Figure 4.11:	Zeta potential for CS- ZnO material .....	51
Figure 4.12:	EDXRF analysis of CS- ZnO material.....	52
Figure 4.13:	<sup>1</sup> H NMR spectrum for the synthesized $\epsilon$ - Polycaprolactone.....	54
Figure 4.14:	SEC-MALS curves of PCL in the bulk (120 °C) using benzyl alcohol as the initiator.....	55

Figure 4.15:	Overlay DSC thermogram curves for 10 KDa and 15 KDa poly( $\epsilon$ -caprolactone) .	56
Figure 4.16:	DMA curve for melting temperature ( $T_m$ ) of poly( $\epsilon$ -caprolactone).....	57
Figure 4.17:	FTIR spectrum of pure $\epsilon$ -PCL.....	58
Figure 4.18:	TGA thermogram of PCL- RH blend films .....	59
Figure 4.19:	XRD diffractogram of PCL-RH blend film. ....	60
Figure 4.20:	FTIR spectrum for unreacted/raw PCL-RH blend films.....	61
Figure 4.21:	FTIR spectrum for malachite green loaded PCL-RH blend.....	62
Figure 4.22:	Maximum absorption curve for malachite green dye.....	63
Figure 4.23:	Malachite green calibration curve .....	64
Figure 4.24:	Influence of interaction time on MG sorption.....	65
Figure 4.25:	Variation of % MG adsorbed onto RH as a function of time.....	66
Figure 4.26:	Plot of % sorption vs time for removal of MG by RH.....	67
Figure 4.27:	Variation of % adsorption vs NaCl concentration for removal of MG onto RH	68
Figure 4.28:	Impact of RH mesh size on MG uptake .....	69
Figure 4.29:	Impact of solution pH on uptake of MG by RH.....	70
Figure 4.30:	Impact of shaking rate on sorption of MG on RH.....	71
Figure 4.31:	Influence of temperature for the uptake of MG onto RH adsorbent .....	72
Figure 4.32:	Langmuir model for the uptake of MG onto rice husks .....	73
Figure 4.33:	Freundlich model for the uptake of MG on rice husks .....	74
Figure 4.34:	Temkin isotherm for the uptake of MG onto rice husks .....	75
Figure 4.35:	PFO kinetics graph for the uptake of MG by rice husks.....	76
Figure 4.36:	PSO kinetic reaction for the uptake of MG by RH .....	77

Figure 4.37:	Intra particle diffusion graph for uptake MG by RH .....	78
Figure 4.38:	Thermodynamic graph of removal of MG by RH material .....	79
Figure 4.39:	Impact of initial dye concentration on the % sorption of MG. ....	80
Figure 4.40:	Influence of interaction time on MG abstraction onto plain chitosan and CS-ZnO materials.....	81
Figure 4.41:	Influence of dosage on uptake of MG on CS-ZnO composite.....	82
Figure 4.42:	Influence of pH on the abstraction of malachite green on CS-ZnO composite. .	84
Figure 4.43:	Langmuir model for the abstraction of MG by chitosan-ZnO composite.....	85
Figure 4.44:	Freundlich sorption model for the uptake of MG on CS-ZnO composite. ....	86
Figure 4.45:	Temkin model for the abstraction of MG dye onto CS-ZnO composite.....	87
Figure 4.46:	PFO kinetics graph for the abstraction of MG by CS-ZnO nanocomposite .....	88
Figure 4.47:	Second-order rate graph for removal of MG on CS- ZnO .....	89
Figure 4.48:	Intraparticle diffusion plot for biosorption of MG on CS – ZnO material.....	90
Figure 4.49:	Impact of dose on % abstraction of MG on PCL-RH film blend.....	91
Figure 4.50:	Influence of interaction time on % removal of MG on plain PCL & PCL-RH films.....	92
Figure 4.51:	Influence of initial dye strength with time on abstraction of MG by PCL-RH films.....	93
Figure 4.52:	Pseudo first-order graph for the abstraction of MG on PCL-RH films.....	94
Figure 4.53:	PSO reaction for the abstraction of MG by PCL-RH nanomaterial .....	95
Figure 4.54:	Intraparticle particle diffusion graph for the uptake of MG by PCL-RH films ..	96
Figure 4.55:	Langmuir model for the abstraction of MG on PCL-RH films.....	98
Figure 4.56:	Freundlich model for uptake of MG by PCL-RH material .....	99

Figure 4.57: Temkin model for removal of MG by PCL-RH biofilms ..... 100

## LIST OF SCHEMES

Scheme 2.1:	Anionic polymerization reaction of $\epsilon$ - caprolactone. ....	20
Scheme 2.2:	Mechanism for cationic ROP reaction. ....	21
Scheme 2.3:	Monomer – activation ROP.....	21
Scheme 3.1:	Synthesis of CS-ZnO Sorbent .....	26
Scheme 3.2:	Synthesis of $\epsilon$ -Polycaprolactone using tin (II) octoate catalyst. ....	27

## Appendices

<b>Appendix 1:</b>	EDS elemental spectrum for rice husks .....	127
<b>Appendix 2:</b>	<sup>1</sup> H NMR spectrum for ε-Caprolactone .....	128
<b>Appendix 3:</b>	<sup>13</sup> C NMR spectrum for ε-Caprolactone .....	129
<b>Appendix 4:</b>	<sup>1</sup> H NMR spectrum for ε-PCL (5000g/mol) .....	130
<b>Appendix 5:</b>	<sup>1</sup> H NMR spectrum for ε-PCL (10,000g/mol) .....	131
<b>Appendix 6:</b>	Ring opening polymerization of ε-Caprolactone (CL) with stannous octoate (sn(Oct) <sub>2</sub> as the catalyst and benzyl alcohol as the initiator .....	131
<b>Appendix 7:</b>	EDXRF analysis settings for CS-ZnO material .....	131
<b>Appendix 8:</b>	Mean elemental concentration levels of CS-ZnO material .....	132
<b>Appendix 9:</b>	Chemical structure of carbinol form of malachite green .....	132
<b>Appendix 10:</b>	Chemical structure of malachite green chloride .....	132

## LIST OF ABBREVIATIONS

$^1\text{H}$ NMR	Proton Nuclear Magnetic Resonance
AC	Activated carbon
BET	Brunauer- Emmett – Teller
BzOH	Benzyl alcohol
$\text{CDCl}_3$	Deuterated Chloroform
COD	Chemical oxygen demand
DMA	Dynamic mechanical analyzer
DSC	Differential Scanning Calorimeter
EDX	Energy-dispersive X-ray spectroscopy
EDXRF	Energy dispersive X-ray fluorescence
FTIR	Fourier Transform Infrared Spectroscopy
GPC	Gel permeation chromatography
JCPDS	Joint committee on powder Diffraction standards
kDa	Kilodaltons
MALS	Multi-angle light scattering
MG	Malachite Green
$M_n$	Number average molecular weight
PDI	Polydispersity index
PFO	Pseudo- first order
PLA	Poly lactide
PSO	Pseudo- second order
R	Universal gas constant

RH	Rice Husk
ROP	Ring-opening polymerization
SEC	Size exclusion chromatography
SEM	Scanning electron microscopy
Sn (Oct) <sub>2</sub>	Tin (II) 2 - ethyl hexanoate
STP	Standard Temperature and Pressure
T <sub>g</sub>	Glass transition temperature
TGA	Thermogravimetric analysis
THF	Tetrahydrofuran
T <sub>m</sub>	Melting temperature
UV-VIS	Ultraviolet-visible
ΔG°	Change in standard Gibbs free energy
ΔH°	Change in standard enthalpy
ΔS°	Change in standard entropy
ε-CL	Epsilon caprolactone
ε-PCL	Epsilon polycaprolactone

# CHAPTER ONE

## INTRODUCTION

### **1.1: Background of the Study**

Wastewater from most industries in Kenya (e.g., food, textile, leather, paper, pulp, plastics, etc.) contain huge amounts of pollutants such as dyes (Chanzu *et al.*, 2012). For instance, malachite green (MG) is usually utilized for coloring leather, cotton, silk, paper products and in the manufacture of inks and paints (Hameed & El- Khaiary, 2008b). Majority of these colorants such as MG are hazardous and should be removed prior to discharging the effluents into the receiving water.

### **1.2: Challenges Associated with the Release of Untreated Effluents into Water Resources**

Untreated or inefficiently treated effluents are the chief source of both surface and groundwater pollution. The organic substances that are discharged with the effluents to the watercourses consume large oxygen levels for biodegradation purposes thus disrupting the ecological stability of rivers and lakes (Chuah *et al.*, 2005; Priya & Selvan, 2017). Sewage also carries microbial pathogens that cause diseases (Suemitsu *et al.*, 1986).

Domestic effluent, agricultural run-off, and industrial waste comprise of phosphorus and nitrogen, that upsurge the quantity of nutrients in aquatic systems and consequently may cause eutrophication problems (Strokal *et al.*, 2014). Furthermore, when effluents containing synthetic dyes are discharged into water bodies, they reduce photosynthetic activity (Bhatnagar & Jain, 2005) thus affecting the stability of aquatic ecosystems. Industrial effluent treatment methods are often not effective in the removal of pollutants such as synthetic dyes.

### **1.3: Current Technologies Used to Treat Effluents**

There are various technologies used for wastewater treatment and they have varying degrees of success. Some of them include coagulation-flocculation (Wang *et al.*, 2007) and degradation using visible light (Saravanan *et al.*, 2014). Moreover, disinfection using ultraviolet, chlorine and ozone (Zheng *et al.*, 2017), ion exchange (Rengaraj *et al.*, 2001), adsorption (Mittal *et al.*, 2010), electro-oxidation (Särkkä *et al.*, 2015), biodegradation (Goswami *et al.*, 2018) and membrane process (Chu *et al.*, 2008) approaches have also been utilized in wastewater treatment.

Conversely, these approaches have some shortcomings and limitations. For instance, techniques centered on oxidation and ion exchange have exhibited reduced efficacy for the abstraction of small quantities of contaminants (Regel-Rosocka, 2010). Furthermore, coagulation needs pH regulation and initiates additional problems of sludge removal while ozonation, although it removes color efficiently, does not reduce chemical oxygen demand (COD) intensities (Bhatnagar & Minocha, 2006; Han *et al.*, 2014).

Among the various technologies available for wastewater treatment, the sorption method is better relative to other techniques owing to their suitability, simple operation and simple fabrication (Mohammed *et al.*, 2014). Moreover, this method eliminates or reduces various types of toxins and hence it has broader applicability in wastewater treatment (Bhatnagar & Minocha, 2006).

### **1.4: Low-Cost Adsorbents**

Over the years, activated carbon (AC) has been utilized as an efficient material for the adsorption of colorants from aqueous media. However, commercial AC is considered costly (Kurniawan *et al.*, 2006) and therefore current research is directed towards the development of inexpensive adsorbents for water purification. Low-cost materials for dye removal include natural, industrial

by-product wastes and agricultural waste (Ferrero, 2007). Some of their attractive features include abundance, accessibility at reduced or no expense, eco-friendly and excellent performance in eradicating pollutants from aqueous media (Dubey & Gopal, 2007).

Previous research has demonstrated that various low-cost materials such as lotus leaf (Han *et al.*, 2014), brewers' spent grain (Chanzu *et al.*, 2019), cabbage waste powder (Wekoye *et al.*, 2020), sunflower seed hull (Zou *et al.*, 2015) and cucumber peels (Stavrinou *et al.*, 2018) have high efficacy in the adsorption of various pollutants. Further, other low-cost materials such as water hyacinth (Mishra & Tripathi, 2009), rice straw-derived char (Hameed & El- Khaiary, 2008a), rice husk ash (Mbui *et al.*, 2002), potato peel (Kyzas & Deliyanni, 2015) and watermelon peels (Memon *et al.*, 2008) have also been investigated for wastewater purification purposes.

Some of the proposed low-cost materials include: rice husks (RH), chitosan-ZnO composite (CS-ZnO) and poly( $\epsilon$ -caprolactone)-rice husks (PCL-RH).

### **1.5: Statement of the Problem**

Over the years, textile effluents from dye manufacturing industries have continued to contaminate both surface and underground waters owing to fast industrialization across the world; thus, increasing loss of drinking water. Synthetic dyestuffs have deleterious effects especially in aquatic systems since they interfere with photosynthetic activity and also pose danger to aquatic life owing to the loading of aromatic compounds, chlorides and heavy metals into water systems (Chanzu *et al.*, 2012).

Dyes such as MG are hazardous (Khatti & Singh, 2009), stable and non-degradable owing to their intricate aromatic conformation in their arrangement (Mahmoodi, 2013). The abstraction of

these synthetic colorants from textile wastewater before disposal is imperative to safeguard human health.

Although many studies have been conducted on synthetic dyes in water, little information is available on remediation studies using natural polymers such as rice husks (RH), chitosan-ZnO composite (CS-ZnO) and poly( $\epsilon$ -caprolactone)-rice husks (PCL-RH) as biodegradable low- cost and efficient sorption materials. Whereas biodegradable polymers such as poly( $\epsilon$ -caprolactone) have been investigated for biomedical application (Kweon *et al.*, 2003), their use in the abstraction of dyes from wastewaters has not been explored.

## **1.6: Objectives**

### **1.6.1: Overall Objective**

To assess the efficacy of selected low-cost adsorbents in removing malachite green from aqueous solutions.

### **1.6.2: Specific Objectives**

- i) To determine the physicochemical properties of rice husks adsorbent materials using spectroscopic techniques.
- ii) To synthesize and characterize polycaprolactone and prepare polycaprolactone- rice husks film blends for the sorption of malachite green dye.
- (iii) To synthesize chitosan-zinc oxide composite adsorbent material and characterize by selected analytical techniques including Fourier transform infrared (FTIR), Thermogravimetric analyzer (TGA), X-ray diffractometer (XRD), Zeta ( $\zeta$ ) potential and energy dispersive X-ray (EDX) fluorescence.

- iv) To determine through batch experiments the optimum process parameters for the abstraction of malachite green dye from aqueous media by polycaprolactone-rice husks films and other adsorbent materials.
- v) To investigate batch adsorption kinetics and equilibrium models for the uptake process of malachite green from aqueous media by the adsorbent materials.

### **1.7: Justification and Significance of the Study**

Activated carbon (AC) has been researched broadly for the abstraction of various colorants and it has shown high sorption capacities. However, owing to its high cost and regeneration shortcomings, cheaper and economical alternative adsorbents have been sought.

The drawbacks of AC have led to the exploration of low-cost sorbent materials for the removal of synthetic colorants from textile wastewater (Hameed, 2009; Khattri & Singh, 2009). Materials such as rice husks, poly( $\epsilon$ -caprolactone), poly( $\epsilon$ -caprolactone) – rice husks film blends and chitosan-ZnO (CS-ZnO) are viable biodegradable and efficient resources.

These materials may be sustainably employed as low-priced sorbents for the abstraction of colorants such as MG from wastewater. Purification of wastewater will ultimately avail clean water for various uses and additionally, it will ensure a sustainable environment that is within the framework of Sustainable Development Goal (SDG) number 6. Findings from this work will inform strategic decisions aimed at decreasing water contamination in Kenya.

## CHAPTER TWO

### LITERATURE REVIEW

#### 2.1: Dyes

More than 10,000 dyes are used in various industries globally (Nethaji *et al.*, 2010). Generally, these colorants are synthetic and they contain an intricate aromatic configuration that renders them nondegradable (Khan *et al.*, 2013). Excessive use of dyes leads to the production of huge quantities of colored effluents every year which are ultimately discharged into water bodies.

The colored effluents discharged into water bodies are very noxious to flora and fauna and they also decrease the photosynthetic process and fundamental production in flora (Dahri *et al.*, 2014). Some colorants, for instance, Malachite Green (MG), Methylene Blue (MB) and other cationic colorants are oncogenic and thus it is critical to abstract them from wastewater for environmental and aesthetical purposes (Kushwaha *et al.*, 2014).

##### 2.1.1: Synthetic Dyes

Synthetic dyes are aromatic compounds (Mahmoodi, 2014) produced through chemical synthesis. The aromatic rings in dyes are comprised of delocalized electrons and different functional groups. They have chromophores and auxochromes which are responsible for the dye color and intensity respectively (Özbay *et al.*, 2013). Examples of these chromophores are: -N=N-, -C=O-, -NO<sub>2</sub>-, -C=C-, -C=N-, and quinoid rings whereas common auxochromes include -NH<sub>3</sub>-, -COOH-, -SO<sub>3</sub>H and -OH (Rai *et al.*, 2005).

Dyes can be categorized based on electrical charge such as anionic (direct, acid and reactive colorants), cationic (basic colorants) and non-ionic dispersed colorants. Anionic and non-ionic

dyes typically comprise of azo or anthraquinone chromophores (Özbay *et al.*, 2013). Some examples of the basic dyes include MG, MB and crystal violet. Methyl orange and Eriochrome Black T are classified as anionic dyes (Attallah *et al.*, 2016) whereas Disperse blue SBL (DB SBL), Vat Scarlet R (VS R) and Acid Dark blue 2G (ADB 2G) are classified as non-ionic disperse dyes (Li *et al.*, 2010). Sorption of MB and Congo red dyes using *Eichhornia crassipes* has been explored (Wanyonyi *et al.*, 2013; Wanyonyi *et al.*, 2014).

### **2.1.2: Basic Malachite Green (MG)**

MG is a green (Green crystalline powder) colorant that is normally used in the textile industry. It may exist either as the chloride (Appendix 10) or oxalate salt (chromatic form) (Fig. 2.1), the carbinol base (Appendix 9) or the reduced leucomalachite green (Fig. 2.2) form (Culp & Beland, 1996). The dye is utilized for coloring cotton, silk, leather, and paper (Ahmad & Kumar, 2010). It is also used as a parasiticide, fungicide, antiprotozoal and antibacterial agent (Kumar & Kumar, 2015). MG is endorsed for exterior use; its oral ingestion is poisonous, harmful and oncogenic owing to the presence of nitrogen (Bulut *et al.*, 2008).

MG is extremely poisonous to mammal cells and behaves as a tumor-boosting vehicle (Akar *et al.*, 2013). MG reduces food consumption; development and fertility rates; initiates liver impairment, spleen, kidney and heart; imposes lacerations on skin, eyes, lungs and bones (Chanzu, *et al.*, 2012). Malachite green degrades to give leucomalachite green (Fig. 2.2) which is one of its major metabolites (Nethaji *et al.*, 2010).

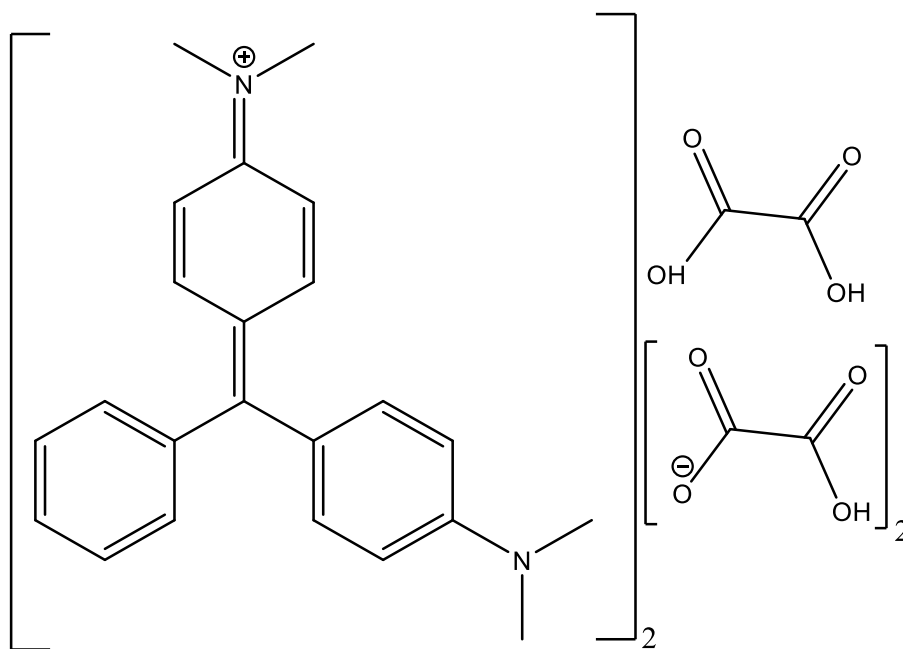


**Figure 2.1:** Structure of Malachite Green Oxalate

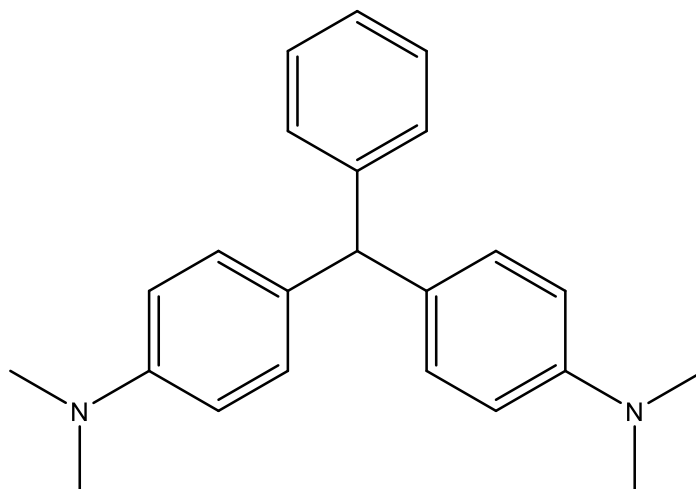


**Figure 2.2:** Structure of leucomalachite green

## 2.2: Adsorption

It is a chemical process that occurs once a gas or liquid solute accumulates on the surface of a solid or a liquid (sorbent) producing a molecular or atomic film. It differs from absorption, where

a material disperses into a liquid or solid to make a solution (Jiang *et al.*, 2018). The phrase *sorption* incorporates both methods, whereas *desorption* is the opposite process. It is a quantifiable correlation illustrating the balance between the intensities of sorbate in solution (mass/volume) and their strength (mass sorbate/mass sorbent). Sorption is generally expressed through isotherms, that is, parameters that link the quantity of sorbate on the sorbent material, with its pressure (for gases) or intensity (for liquids) (Talip *et al.*, 2009).

### **2.2.1: Adsorption Isotherm**

It correlates the concentration of a solute on the sorbent surface to the strength of the solute in the liquid where the sorbent is in contact (Allen *et al.*, 2004). These quantities are ordinarily verified empirically. To illustrate the equilibrium isotherm for the biosorption process, Langmuir, Freundlich and Temkin isotherms are normally adopted (Yadamari *et al.*, 2011)

### **2.2.2: Langmuir Isotherm**

The model is centered on the postulates (Chen *et al.*, 2010) that: (i) each active site interrelates with a sole sorbate molecule, (ii) sorbate particles are sorbed on well-localized sites, (iii) no interaction between neighboring sorbed particles, and (iv) the sorption sites are all dynamically equal.

The model illustrates the portion of the surface that is covered by sorbate molecules for a specific temperature and pressure of the sorbate.

Equation 2.1 represents the non-linearized Langmuir model (Langmuir, 1916).

$$q_e = \frac{K_L q_{Max} C_e}{1 + K_L C_e} \quad (2.1)$$

Where  $q_e$  represents the equilibrium solute concentration on the sorbent (mg/g - adsorbent);  $C_e$  stands for the equilibrium solute strength in the solution (mg/L);  $q_{max}$  is the maximum uptake capability of sorbent (mg/g) and  $K_L$  signifies the Langmuir factor (L/mg).

The linearized form of the Langmuir equation is given in equation 2.2 (Kumar & Sivanesan, 2005).

$$\frac{C_e}{q_e} = \frac{1}{K_L q_{Max}} + \frac{C_e}{q_{Max}} \quad (2.2)$$

Langmuir factor values,  $q_{max}$  and  $K_L$  are obtained from the gradient and intercept of the linearized graph of  $C_e/q_e$  versus  $C_e$ . The fundamental characteristic of this isotherm may be articulated using a separation component ( $R_L$ ), which is determined according to equation 2.3 (Weng *et al.*, 2009);

$$R_L = \frac{1}{1 + K_L C_i} \quad (2.3)$$

The  $R_L$  value denotes the nature of sorption model. For example, for linear ( $R_L = 1$ ), Favorable ( $0 < R_L < 1$ ), Unfavorable ( $R_L > 1$ ) whereas Irreversible ( $R_L = 0$ ).

### 2.2.3: Freundlich Isotherm

Freundlich model (Freundlich, 1906) is an empirical equation utilized to describe the sorption process on a heterogeneous surface (Hameed *et al.*, 2007). Equation 2.4 is the nonlinear form of the isotherm:

$$q_e = K_f C_e^{1/n} \quad (2.4)$$

Where  $q_e$  is the adsorbed quantity of the dye at equilibrium (mg/g),  $K_f$  denotes the Freundlich factor (mg/g),  $C_e$  signifies the equilibrium concentration (mg/L) and  $1/n$  represents the heterogeneity component.

This model can be developed from Langmuir's expression by presuming that the distribution of sites on the sorbent exists, which has distinctive affinities for various sorbates with each site acting according to Langmuir representation (Srivastava *et al.*, 2009).  $K_f$  measures the capability of the sorbent whereas “ $n$ ” measures the fluctuation affinity of the sorbate with the variation in adsorption. When  $n = 1$ , the model is linear and suggests that all the uptake sites on the sorbent have an equivalent attraction for the sorbates (Farajzadeh & Fallahi, 2005). When  $n > 1$ , this signifies that the affinities reduce with escalating sorption capability. The linearized form of this isotherm is given by equation 2.5:

$$\log q_e = \log K_f + \frac{1}{n} \log C_e \quad (2.5)$$

The factors  $1/n$  and  $K_f$  are evaluated from the gradient and intercept of the linearized graph of  $\log q_e$  against  $\log C_e$ .

#### **2.2.4: Temkin Isotherm**

This model comprises of a feature that describes the sorbate–sorbent relationship (Hameed & Ahmad, 2009; Shirmardi *et al.*, 2013). It proposes an equivalent sharing of binding energies over the quantity of exchanging uptake sites on the surface (Dezhampanah *et al.*, 2014). Equation 2.6 represents the non-linearized form of the model.

$$q_e = \frac{RT}{b} \ln(K_t C_e) \quad (2.6)$$

Where  $q_e$  is the sorbed quantity of the colorant at equilibrium (mg/g),  $R$  is the universal gas coefficient ( $8.314 \text{ Jmol}^{-1}\text{K}^{-1}$ ),  $T$  is the absolute temperature,  $K_t$  denotes the equilibrium binding constant (L/mg),  $b$  is the Temkin factor (J/mol) and  $C_e$  represents the concentration of the dye at equilibrium (mg/L).

The linear arrangement (Equation 2.7) of the Temkin model is expressed as:

$$q_e = B \ln K_t + B \ln C_e \quad (2.7)$$

$B = RT/b$  and  $K_t$  are constants.

The isotherm constants  $K_t$  and  $B$  are determined from the gradient and intercept of plots of  $q_e$  vs  $\ln C_e$  respectively.

### **2.3: Kinetics of Adsorption**

To explore the mechanisms of the sorption method and probable rate-limiting stages that comprise of mass transfer and chemical processes, kinetic rate models are applied to assess the experimental data (Dahri *et al.*, 2014). Some of the commonly employed models include Lagergren first-order (Bharathi & Ramesh, 2013; Makeswari & Santhi, 2013), Lagergren second-order kinetics (Ho & Mckay, 1999) and Weber- Morris (Weber & Chakravorti, 1974) intraparticle diffusion.

#### **2.3.1: Lagergren First-Order Kinetics**

This is an empirical rate equation that describes the kinetic behavior of solute sorption at the solid/ solution interface (Moussout *et al.*, 2018).

The Lagergren first-order equation (Hameed *et al.*, 2009) is stated in equation 2.8:

$$\log(q_e - q_t) = \log q_e - \frac{t}{2.303} K_1 \quad (2.8)$$

Where  $q_t$  is the quantity of adsorbate removed /gram of sorbent (mg/g) at time  $t$  (Minutes),  $q_e$  signifies the sorption capability (mg/g), and  $K_1$  is the Lagergren first-order constant ( $\text{min}^{-1}$ ). The model is applied to establish the influence of time on the sorption process.

### 2.3.2: Pseudo Second Order Kinetics

The model is centered on the postulation that the rate-controlling step is chemisorption (Sharma & Nandi, 2013). It is applied to equilibrium data to predict the sorption kinetics. It is articulated in equation 2.9:

$$t/q_t = 1/K_2 q_e^2 + 1/q_e t \quad (2.9)$$

where  $K_2$  signifies second-order rate coefficient ( $\text{g.mg}^{-1}\text{min}^{-1}$ ) whereas  $q_e$  denotes equilibrium sorption capacity (mg/g). The linearized graph of  $t/q_t$  vs  $t$  is normally employed for computation of  $q_e$  of pseudo-second-order and the  $k_2$ .

### 2.3.3: Weber – Morris Intraparticle Diffusion

This model is employed to classify the diffusion process in sorption processes. It is represented by equation 2.10 (Weber & Chakravorti, 1974):

$$q_t = K_{id} t^{1/2} + c \quad (2.10)$$

where  $K_{id}$  denotes the intraparticle diffusion constant ( $\text{mgg}^{-1}\text{min}^{1/2}$ ) whereas  $C$  is the intercept that symbolizes the width of the boundary layer.

The greater the C value, the bigger the boundary layer effect. Quantities of  $K_{id}$  and C are established from the gradient and y-intercept from the linearized graph of  $q_t$  vs  $t^{1/2}$  respectively (Han *et al.*, 2014).

When the particles are stirred throughout the experiment period, it is presumed that mass transport from the bulk liquid to the exterior plane is not the rate-limiting component but maybe film or intraparticle diffusion (Dahri *et al.*, 2014). When the graph of  $q_t$  vs  $t^{1/2}$  crosses through zero (Origin), then intraparticle diffusion is the rate-defining step (Poojari *et al.*, 2015).

#### 2.4: Thermodynamic Studies

These experiments are carried out to explore the variation of temperature with sorption process. The thermodynamic factors of adsorption for example change in Gibb's free energy ( $\Delta G^\circ$ ) in  $\text{kJmol}^{-1}$ , enthalpy ( $\Delta H^\circ$ ) in  $\text{kJmol}^{-1}$ , and entropy, ( $\Delta S^\circ$ ) in  $\text{kJmol}^{-1}\text{K}^{-1}$  (Hameed *et al.*, 2007) are computed using the following equations 2.11 and 2.12 (Nodeh *et al.*, 2016):

$$\ln K_c = \Delta S^\circ / R - \Delta H^\circ / RT \quad (2.11)$$

$$\Delta G^\circ = \Delta H^\circ - T\Delta S^\circ \quad (2.12)$$

Where R symbolizes gas constant ( $8.314 \text{ Jmol}^{-1}\text{K}^{-1}$ ), T is the absolute temperature (K) whereas  $K_c$  signifies the thermodynamic equilibrium constant.

Values of  $\Delta H^\circ$  and  $\Delta S^\circ$  are evaluated from the gradient and intercept of a graph of  $\ln K_c$  vs  $1/T$ . When  $\Delta H^\circ$  is negative, it infers that the sorption rate is exothermic whereas a positive value suggests an endothermic process (Fu *et al.*, 2015). The positive figure of  $\Delta S^\circ$  indicates increased

randomness of the sorption rate process whereas a positive quantity of  $\Delta G^{\circ}$  infers a spontaneous sorption process (Dahri *et al.*, 2014).

## **2.5: Adsorbents Investigated in This Work**

### **2.5.1: Rice Husks**

Rice husks (Fig. 2.3) is a by-product from rice processing factories and it accounts for approximately 20 % of the 500 million tons of rice produced worldwide (Johar *et al.*, 2012). In Kenya, rice is grown in Mwea Tembere (Kirinyaga County), Ahero, West Kano (Kisumu County) and Bunyala (Busia County). It is among the first three staple foods consumed in Kenya. Rice husks (RH) comprise a granular structure with high chemical stability, mechanically strong and it is insoluble in water. It contains about 32 % cellulose, 21 % lignin, 21 % hemicellulose, 3 % unrefined protein and 20 % silica (Chowdhury *et al.*, 2011). The usage of unmodified or modified RH as a sorbent for the uptake of contaminants from wastewater has drawn significant attention recently since it is found in plenty as agricultural waste.

RH has previously been modified to increase sorption capacity (Jaman *et al.*, 2009). The features of this adsorbent vary with the technique of modification which impacts the removal efficacy (Chuah *et al.*, 2005). Feng *et al.*, (2004) stated that keeping RH at elevated temperatures ( $> 700$  °C) improved the surface area (SA) and raised the uptake capability. They established that finer RH ash removed more heavy metals for instance lead and mercury and that the uptake process rose with pH upsurge.



**Figure 2.3:** Rice husks obtained from the Mwea milling factory.

### **2.5.2: Chitosan – Zinc Oxide (CS- ZnO)**

Chitosan (CS) is a nitrogenous polysaccharide that is obtained from chitin (Fig. 2.4) via the deacetylation process. CS is the second-highest plentiful natural polymer next to cellulose (Aydın & Aksoy, 2009). Chitin is extensively distributed naturally because it is acquired from the exoskeletons of crustaceans (Teng *et al.*, 2001) with fungi and some bacteria as a key constituent (Kumari & Kumar, 2014).

CS has been explored for several applications like dye adsorption (Bekçi *et al.*, 2008), drug delivery (Hu *et al.*, 2013), heavy metal removal (Nghah *et al.*, 2006), tissue engineering (Sarasam & Madihally, 2005), colorant degradation and antibacterial action properties (Haldorai & Shim, 2013), pesticide removal from water (Dehaghi *et al.*, 2014) and food packing (Shukla *et al.*, 2013). Presently, there are gaps in the exploitation of CS derivatives synthesized from ZnO for the removal of colorants.

Comparing CS (Fig. 2.5) to other natural polymers, it has drawn significant attention in water remediation due to its extensive amount of organic surface groups (-NH<sub>2</sub> and -OH). The existence of these surface groups in its structure makes it possible to be modified easily. Chitosan and chitosan-based compounds for example, CS-ZnO can remove noxious contaminants from water for instance colorants and heavy metals (Shukla *et al.*, 2013). This natural polymer possesses desirable qualities e.g., biocompatibility, biodegradation, non-toxicity, antibacterial action and hydrophilicity attributes. Furthermore, it is affordable, renewable and has remarkable uptake efficacy (Hu *et al.*, 2013).

Metal oxide-based composites for instance ZnO have drawn much attention as sorbent materials owing to their interesting features such as strong adsorption ability and large surface to volume ratio (Srivastava *et al.*, 2013). This makes them attractive candidates for wide-ranging applications.

CS -ZnO blends have been studied for antibacterial action (Ana & Angel, 2015), photocatalytic properties (Mujeeb *et al.*, 2018) and also as sorbent materials for colorants and pesticides (Govindan *et al.*, 2012). Furthermore, ZnO nanoparticles were used in this work to immobilize the CS particles and also suppress their clustering during the sorption rate process and additionally to increase the quantity of active sorption sites of CS.

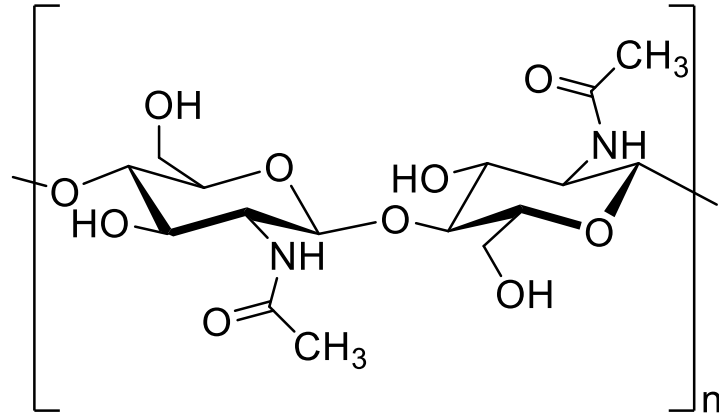


**Figure 2.4:** Chemical structure of Chitin

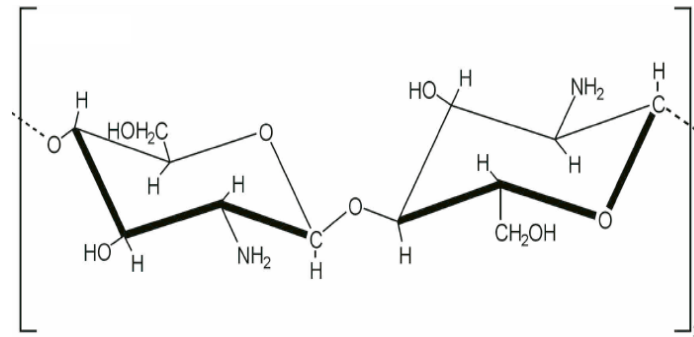


**Figure 2.5:** Chemical structure of Chitosan

### 2.5.3: Poly ( $\epsilon$ -Caprolactone) Polymer

Lactones are cyclic esters derived from a hydroxycarboxylic acid by loss of water intramolecularly. Poly( $\epsilon$ -caprolactone) which is abbreviated as  $\epsilon$ -PCL is a semi-crystalline aliphatic polyester (Fig. 2.6) comprised of hexanoate repeat units (Labet & Thielemans, 2009). Over the years, it has gained a lot of attraction in research due to its desirable features such as biocompatibility and biodegradability. Some of the applications of  $\epsilon$ -PCL are in the disciplines of controlled release drug delivery procedures (Sattayanon *et al.*, 2013), tissue engineering (Kweon *et al.*, 2003) and food packaging (Swapna *et al.*, 2011).

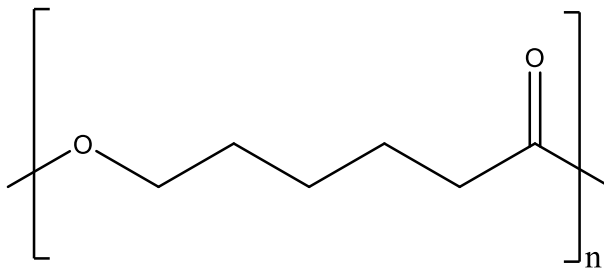


**Figure 2.6:** Chemical structure of Poly( $\epsilon$ -caprolactone)

Two methods are commonly used in the synthesis of  $\epsilon$ -PCL:

- i) The condensation of 6-hydroxy caproic (6-hydrohexanoic) acid (Varma *et al.*, 2005).
- ii) The ring-opening polymerization (ROP) of  $\epsilon$ -caprolactone (Darensbourg & Karroonnirun, 2010).

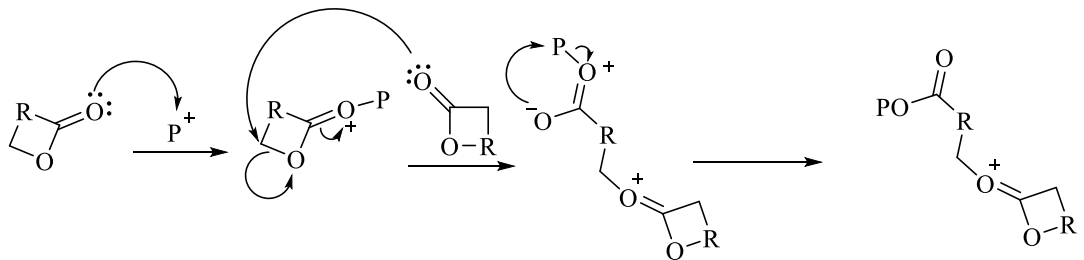
### 2.5.3a: Condensation of 6-hydroxy caproic acid

Condensation polymers are produced by the removal of water (or alcohol) during polymerization through a vacuum. One drawback of this method is the formation of polymers with low molecular weight and broad polydispersity index (Labet & Thielemans, 2009), hence the method is not preferred for the synthesis of  $\epsilon$ -PCL.

### 2.5.3b: Ring-Opening Polymerization of Lactones

The polymerization is normally conducted in bulk (solvent-free) or in suspension (tetrahydrofuran, dioxane, toluene etc.), dispersion or emulsion (Sosnowski *et al.*, 1996). The temperature of bulk polymerization ranges from 100 to 150 °C while in solution polymerization, low temperatures (0 to 25 °C) are employed to decrease side reactions (Gadzinowski *et al.*, 1996). Some of the catalysts used in ROP reactions include: zinc, tin, aluminium and iron compounds which are Lewis acids.

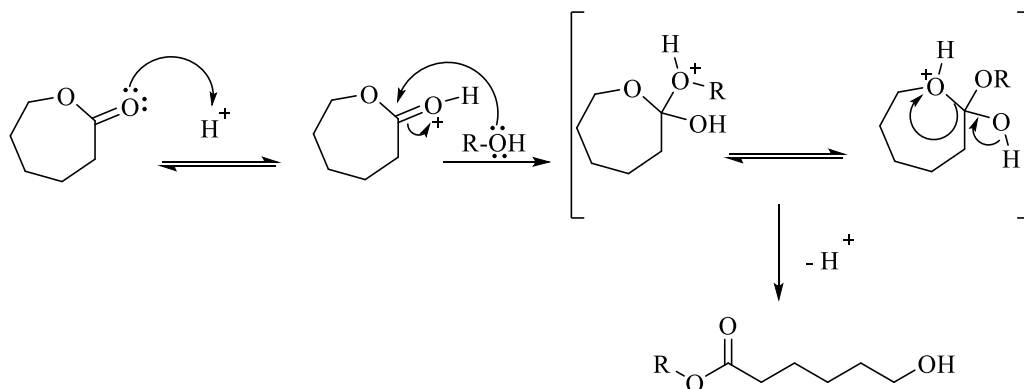




**Scheme 2.2:** Mechanism for cationic ROP reaction.

### iii) Monomer-activated Ring-Opening Polymerization

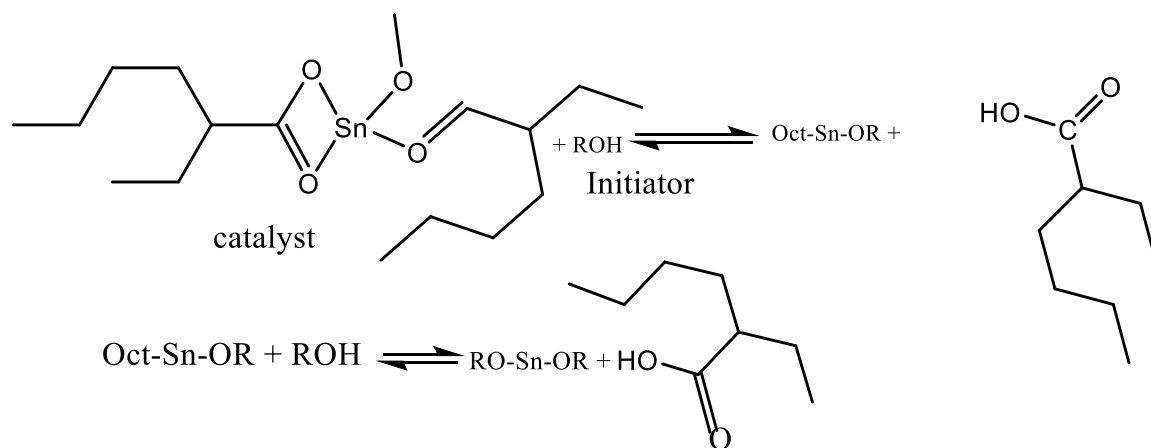
This encompasses the activation of monomer molecules by a catalytic agent, then by activated monomer attack on the polymer chain end (Scheme 2.3).



**Scheme 2.3:** Monomer – activation ROP.

### iv) Coordination – Insertion ROP

This is a very popular type of ROP. It is essentially a quasi-anionic type of ROP. The reaction propagation process is projected to progress via the coordination of the monomer to the catalytic agent (Storey & Sherman, 2002) and the incorporation of the monomer into the metal-oxygen link of the catalytic agent (Scheme 2.4). Throughout the propagation time, the developing chain is fixed to the metal through an alkoxide link (Stanford & Dove, 2010).



**Scheme 2.4:** Co-ordination insertion ring-opening polymerization.

#### 2.5.4: $\epsilon$ -PCL-Rice Husks Film Blends

The development of biodegradable polymers has drawn a lot of interest due to the environmental problems associated with plastic waste (Zhao *et al.*, 2008). Poly( $\epsilon$ -caprolactone) has found various applications in various fields owing to its biocompatibility and biodegradability qualities (Ahmadzadeh *et al.*, 2018). The large-scale application of PCL especially in the abstraction of colorants from wastewater has not been fully investigated owing to its high cost and poor intrinsic properties (Zhao *et al.*, 2008). PLA/Spent (PLA stands for polylactide acid) brewery grains blend has been investigated for adsorption of malachite green (MG) adsorption (Chanzu *et al.*, 2012).

Blending PCL with other natural polymers such as rice husks can improve in overcoming these drawbacks. Rice husks (RH), is a lignocellulosic material with numerous benefits such as abundance, low- cost, high specific strength and biodegradability. Integrating RH into PCL polymer can successfully decrease the manufacturing cost of the latter by substituting the costly polymer with affordable RH fillers without compromising its biodegradation performance. In the

current study, PCL-RH film blends have been explored for MG uptake from aqueous solutions. Both the RH and PCL are biodegradable thus environmentally benign.

## CHAPTER THREE

### MATERIALS AND METHODS

#### 3.1: Materials

Rice husks were acquired from Mwea Tembere, a rice refining company in Kenya. Malachite green oxalate with a 95% purity ( $C_{52}H_{54}N_4O_{12}$ ; Mwt 927.01 g/mol;  $pK_a = 6.9$  &  $\lambda_{620}$  nm), sodium chloride, hydrochloric acid, ethanoic acid, sodium hydroxide and zinc acetate (Analytical grade) were obtained from Kobian Scientific, Kenya.

Chitosan (100 - 300 kDa) with a 95 % deacetylation was procured from Sigma – Aldrich (UK).  $\epsilon$ -caprolactone (99%), tin (II) 2 – ethyl hexanoate (98 %), anhydrous benzyl alcohol (99%), tetrahydrofuran (99.5 %), diethyl ether (99 %), dichloromethane (99.8 %), deuterated chloroform (99.9 %) and acetone (99.5 %) were procured from Sigma – Aldrich (UK). High purity argon gas was procured from BOC gases (UK).

#### 3.2: Preparation of Malachite Green Solution

A 1000 ppm stock solution was made with double-distilled deionized water. Sequential dilution of the standard solution was performed and a standard curve graph plotted.

#### 3.3: Preparation of Adsorbents

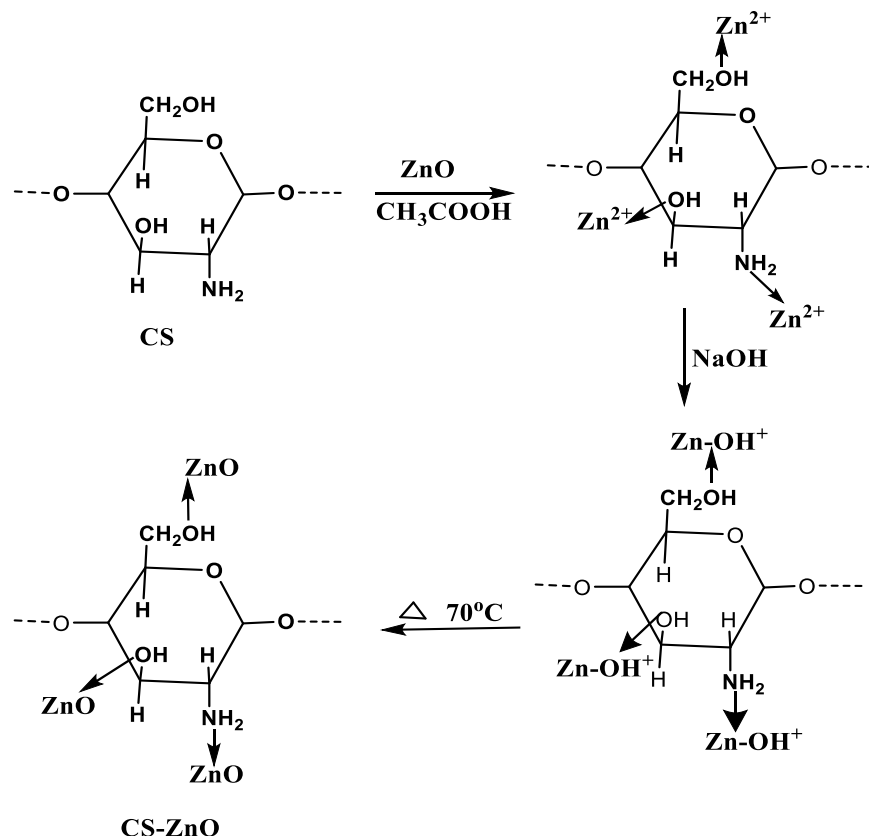
##### 3.3.1: Preparation of Rice Husks (RH)

The rice husks were cleaned using double-distilled water to eliminate all the adhering contaminants. They were then air-dried and ultimately oven-dried (Memmert UM 400, Germany) at 105 °C for 48 hours to eliminate any residual moisture. The adsorbent was subsequently sifted into three distinct particle sizes ( $< 300$ ,  $> 300 < 425$ , and  $> 425$   $\mu\text{m}$ ) and stored in sealed containers to be utilized in the later analytical tests.

### 3.3.2: Synthesis of Chitosan-ZnO Material

Zinc oxide nanoparticles were prepared by chemical precipitation technique which uses zinc acetate as a precursor (Dehaghi *et al.*, 2014). 0.05 M NaOH was added to 0.01 M zinc acetate dihydrate solution. The mixture was stirred to ensure homogeneity. The precipitate obtained was cleaned with double distilled water, filtered and later dried out at 25 °C for two days. The resulting powder product was calcined at 430 °C with a muffle furnace, (Daihan digital FHX – 05, Wonju, South Korea) for 35 minutes. One gram of the synthesized zinc oxide nanoparticles (NP) were dissolved in 2 % (v/v) ethanoic acid where ZnO transformed into Zn cations (Dhanavel *et al.*, 2014).

To this solution, one gram of chitosan (CS) was added and then sonicated for about 30 minutes. 1M of NaOH solution was later added dropwise until a pH of 10 was attained. The obtained solution was placed in a thermostatic water bath set at 70 °C for approximately 3 hours to get raw CS- ZnO product (Scheme 3.1). The CS-ZnO precipitate was sieved and rinsed with distilled water 5 times for neutralization. The resulting product was oven-dried at 65 °C for about 1 hour and then stored for subsequent experiments.



**Scheme 3.1:** Synthesis of CS-ZnO Sorbent

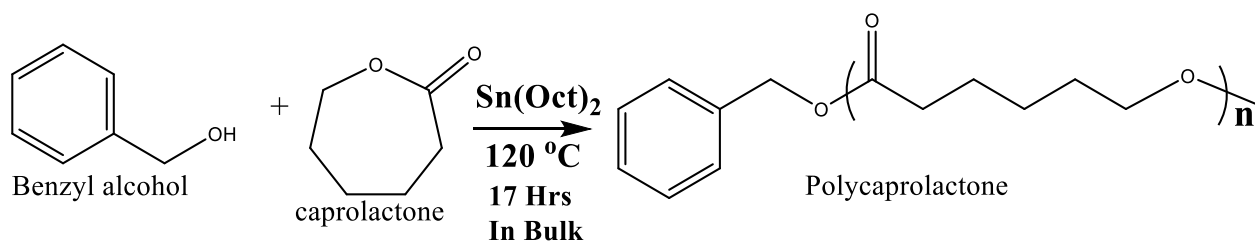
### 3.3.3: Synthesis of Poly ( $\epsilon$ -Caprolactone)

Tin (II) 2 – ethyl hexanoate was vacuum dried at 25 °C for 24 hours before use.  $\epsilon$ -Caprolactone was dried using calcium hydride for 48 hours, vacuum distilled and then kept under an inert atmosphere. Poly( $\epsilon$ -caprolactone) was synthesized in bulk through the ROP method (Scheme 3.2). Tin (II) 2 – ethyl hexanoate was used as the reaction catalyst, the initiator was benzyl alcohol whereas  $\epsilon$ -CL was used as the monomer. Three different molecular weights for  $\epsilon$ -PCL were targeted i.e., 5000, 10,000 and 15,000 kD.

Benzyl alcohol,  $\epsilon$ -CL and Sn (Oct)<sub>2</sub> were appropriately weighed based on the particular targeted molecular weight. The weighed reactants were put in a 20-milliliter round-bottomed glass flask,

then sealed using a suba sealer. The reactants were degassed using argon (Ar) gas for 30 minutes through a Schlenk line. The glass flask was later inserted into a preheated oil bath which was set at 120 °C.

The reactions were conducted for 16 hours and then terminated by adding tetrahydrofuran (THF). The synthesized polymers were purified by precipitation method using cold diethyl ether and then vacuum dried (Baheti *et al.*, 2018). The dry  $\epsilon$ -PCL samples were transferred into respective well-labeled vials awaiting characterization.



**Scheme 3.2:** Synthesis of  $\epsilon$ -Polycaprolactone using tin (II) octoate catalyst.

### 3.3.4: Preparation of Plain $\epsilon$ -Polycaprolactone ( $\epsilon$ -PCL) Films

The films were prepared using solvent casting method. Briefly, the method used by Chanzu *et al.*, (2012) was adopted with some modifications. About 5 g of  $\epsilon$ -PCL (Mwt of 15,000 g/mol) was weighed and put in 50 milliliters of DCM in a 250 mL Erlenmeyer glass flask and then spread on a glass plate making a thin film using a glass rod. The film was oven-dried at 25 °C for 24 hours. The dry  $\epsilon$ -PCL films were stored for subsequent experiments.

### 3.3.5: Preparation of $\epsilon$ -Polycaprolactone – Rice Husks ( $\epsilon$ -PCL-RH) Blended Films

About 5 g of  $\epsilon$ -PCL (15,000 g/mol) was weighed and placed in 100 milliliters of DCM in a 250 mL Erlenmeyer glass flask. Rice husks (5 g) of  $< 300\text{ }\mu\text{m}$  particle size were added to the

mixture followed by thorough shaking. The obtained mixture was emptied onto a glass plate and applied into a thin film using a glass rod and then oven-dried at 25 °C for three days. The dry  $\epsilon$ -PCL-RH blended films were stored in airtight containers for subsequent experiments.

### **3.4: Characterization of Adsorbents**

#### **3.4.1: Analysis of Organic Functional Groups in the Rice Husks**

FTIR analysis was performed on a PerkinElmer photometer, (PerkinElmer Spectrum 100 FTIR, USA) with a preset scanning range between 4000 - 400  $\text{cm}^{-1}$ . The Pellet method, which employs KBr for chemical investigation was applied. Surface groups in both unreacted and dye-loaded RH were determined from the spectra acquired.

#### **3.4.2: Surface Morphology Analysis of RH and MG Loaded RH**

The imaging of the rice husks was accomplished with Tescan Vega 3 XMU, (Czech Republic) SEM that was integrated with an energy dispersive X-Ray spectrophotometer for elemental assessment. Both raw RH (< 300  $\mu\text{m}$ ) and malachite green loaded rice husks samples were fixed to 10 mm metal mounts using carbon tapes and then sputter-coated with gold at an acceleration voltage of 20 kV.

#### **3.4.3: Physisorption Analysis for RH**

The RH surface area (SA) and porosity were evaluated by the  $\text{N}_2$  gas adsorption-desorption technique on a micromeritics ASAP 2020 BET (USA) analyzer with liquefied  $\text{N}_2$  at 77 K. Approximately 1g samples of rice husk (<300  $\mu\text{m}$ ) was degassed using  $\text{N}_2$  at 120°C to remove moisture before analysis. The SA for RH was computed using the Brunner- Emmet- Teller equation whereas for porosity parameters, Barret- Joyner – Halenda (BJH) isotherm method was adopted (Nethaji *et al.*, 2010).

#### **3.4.4: Thermogravimetric Analysis of RH**

Thermal analysis of RH samples was performed using TAQ 500 TGA (Elstree, United Kingdom). Approximately 10 mg samples of RH (<300 μm) were weighed and subjected to thermogravimetric analysis (TGA) in both nitrogen and air atmosphere. The temperature was raised from 30 to 500 °C at a temperature ramp of 10 °C/min.

#### **3.4.5: Powder X-Ray Diffractometry Analysis of RH**

X-ray diffractometry patterns of finely pulverized RH were acquired using a Bruker D8 Advance AXS GmbH (Berlin, Germany). Cu  $k_{\alpha}$  energy source ( $\lambda = 0.15406$  nm) at 40 kv and 130 mA in the preset scan angles ( $2\theta$ ) of 5 – 70° at a speed of 0.5 min<sup>-1</sup> and room temperature were applied. The crystallite size of RH was established using Scherrer expression 3.1 (Yusuff, 2018):

$$D = K \frac{\lambda}{\beta} \cos \theta \quad (3.1)$$

Where D is the crystallite size, K symbolizes shape component ( $\approx 0.9$ ),  $\lambda$  denotes X-ray wavelength,  $\beta$  is the line widening at half the highest intensity whereas  $\theta$  signifies the diffraction angle.

#### **3.4.6: FTIR Analysis of Chitosan-Zinc Oxide Material**

Typical CS-ZnO spectra were obtained on an IRAffinity -1S, FTIR (Shimadzu, Kyoto, Japan) spectrophotometer using attenuated total reflectance (ATR, diamond) sampling method. The pulverized CS-ZnO material was scanned from 500 to 4000 cm<sup>-1</sup>.

#### **3.4.7: Thermogravimetric Assessment for CS- ZnO**

Thermogravimetric data was acquired using a TGA Q500 V20.13 (USA) build 39 analyzer. The analysis was done under nitrogen atmosphere. Approximately 35 milligrams of the powdered material were heated starting from 25 to 650 °C at a rate of 10 °C/min.

#### **3.4.8: XRD Analysis of CS- ZnO Composite**

Well pulverized CS-ZnO material was studied on a D8 Advance, Bruker AXS GmbH. About 1 g powder sample was placed on the sample holder, levelled well, placed on the equipment and then analyzed. Cu K $\alpha$  energy source ( $\lambda = 0.15406$  nm) was utilized over  $2\theta$  angles ranging from  $10^0$  to  $70^0$  at room temperature.

#### **3.4.9: Physisorption Analysis of CS - ZnO**

A finely ground CS- ZnO sample was examined for surface area and porosity characteristics via sorption technique on a micro metrics BET analyzer. The samples were degassed and then the measurements were accomplished at 77 K with N<sub>2</sub> as the adsorbate.

#### **3.4.10: Zeta Potential Measurement of CS-ZnO material**

Sample analysis was carried out via a Zetasizer Nano ZS (Malvern Panalytical, Ltd, UK) using a light scattering technique. 2- (N- Morpholino) ethane sulfonic acid having a conductivity of 3.18 mS/cm, pH of 6 and a concentration of 10 mM was utilized as the dispersing agent. The measurements were performed utilizing single-use zeta cells at 25 °C.

### 3.4.11: Energy Dispersive X-Ray Fluorescence of CS-ZnO Composite

The elemental analysis of CS-ZnO composite was achieved on a Rigaku NEX CG (USA) EDXRF spectrophotometer. The equipment settings were as follows: a current of 2 mA, applied power of 50 W and a voltage of 50 kV (Appendix 7). 1 g sample of finely ground CS- ZnO composite was analyzed under an air atmosphere. Four secondary targets (RX9, Cu, Mo and Al) were applied for the assessment.

### 3.4.12: <sup>1</sup>H NMR Analysis of Poly (ε-Caprolactone)

The technique was employed to calculate % monomer conversion, the degree of polymerization (DP<sub>n</sub>) and the number- average molecular weight (M<sub>n</sub>) as described by Nguyen *et al.*, (2014). The number-average molecular weight (M<sub>n</sub>) was computed through end group assessment from the NMR spectrum obtained. The monomer (ε-Caprolactone) was also characterized using both <sup>1</sup>H and <sup>13</sup>C NMR.

The following expressions were utilized for the calculations involving the PCL polymer.

$$\% \text{ conversion} = \frac{\int \text{Polymer}}{\int \text{polymer} + \int \text{monomer}} * 100$$

$$DP_n = \frac{\int \text{signal of repeating unit of polymer}}{\int \text{signal of end groups}}$$

$$M_n \text{ NMR} = DP_n * \text{molar mass of } \epsilon\text{- CL (repeating unit)}$$

The spectra measurements were performed on a 300 MHz Bruker DPX – 300 (Bruker, Ettlingen, Germany) spectrophotometer to determine percentage monomer conversion, degree of polymerization (DP<sub>n</sub>), and molecular weight (M<sub>n</sub>) for the crude ε- polycaprolactone sample. For purified ε- PCL polymer, a Bruker DPX – 400 spectrophotometer (400 MHz) was used. The vacuum dried sample was dissolved in 600 μL of deuterated chloroform (CDCl<sub>3</sub>), vortexed and then the solution was placed into a well labelled NMR tube for analysis.

#### **3.4.13: Differential Scanning Calorimetry Measurement for $\epsilon$ - PCL**

Thermal analysis for  $\epsilon$  - polycaprolactone was done on a DSC Q 2000 (TA instruments, UK) under nitrogen flow (50 mL/min). Indium metal standards which were supplied by TA instruments were used to calibrate the equipment. A temperature program ranging between -90 – 100 °C was used to monitor changes in heat flow over four cycles. The third and fourth cycles were used to erase the thermal history of the polymer being investigated.

To accomplish this, a scan rate of 10 °C/min was employed with a 5-minute isotherm at both ends of the temperature range to mark the end of the cycle. In a typical experiment, a polymer sample of 0.98 mg was loaded into a T-zero aluminium pan and an empty reference pan was used. Data analysis was done using universal analysis by TA software.

#### **3.4.14: Size Exclusion Chromatography (SEC) Analysis of Poly ( $\epsilon$ - Caprolactone)**

The analysis was performed on a 1260 Infinity Multidetector GPC (California, united states). PL – gel mixed – D columns interfaced with a refractometer and a multi-angle light scattering detector (MALS) were used. The equipment was first calibrated utilizing polystyrene standards possessing a narrow polydispersity index. Approximately, 2 mg of  $\epsilon$ -PCL were dissolved in 2 mL of HPLC grade THF, filtered into a GPC vial using a 0.2  $\mu$ m microfilter and then analyzed. The mobile phase flow rate was set at 1 mL/min whereas the total run time was 30 minutes. The data was processed using Astra software.

#### **3.4.15: Dynamic Mechanical Analysis for Poly ( $\epsilon$ - Caprolactone)**

The melting temperature ( $T_m$ ) of  $\epsilon$ -PCL was achieved on a TA Instruments Q800 DMA (USA). Approximately 100 mg of powder sample was evenly pressed on an aluminium sheet sample holder. The sample holder was then fastened onto a three-point clamp on a single cantilever

bending. The heating was accomplished from 25 to 100 °C with a ramp of 5 °C/ minute and an applied frequency of 1 Hz. Liquid N<sub>2</sub> was used to cool the equipment. The normalized modulus was plotted vs the temperature and then the obtained results were compared to those of DSC.

### **3.5: Batch Experiments for Uptake of MG Using RH**

#### **3.5.1: Impact of Interaction Time and Initial Colorant Concentration**

The laboratory tests were studied utilizing 40 milliliters of the dye solution in 250 milliliter conical glass flasks. A dose of 0.1 g of the RH with a mesh size of  $> 300 < 425\mu\text{m}$  was utilized. The conical flasks were agitated on a M49235 Thermolyne, (UK) orbital shaker at 200 rpm. Variable solution concentrations of MG colorant (2.3 to 9.3 mg/L) were made for the analysis of the impact of colorant initial strength on the uptake of the dye. Lab measurements of the prepared MG solution was accomplished on a UV- Vis 1700 (Shimadzu, Japan) spectrophotometer, at a  $\lambda_{\text{max}}$  of 620 nm.

#### **3.5.2: Influence of pH for the Uptake of Malachite Green on Rice Husks**

Malachite green solutions with varying pH (3 to 9) were made using double distilled water. The pH was regulated to the preferred value using 0.1M NaOH or 0.1M HCl. 0.1g of the dried RH sorbent was put in each of the triplicate conical flasks containing 40 milliliters of 9.3 mg/L colorant solution. The flasks were shaken at 200 rpm at variable time intervals and later the solution absorbance of the residual dye concentration was determined.

#### **3.5.3: Influence of Stirring Rate**

The impact of the stirring rate was explored by applying an array of stirring speeds (50 – 250 rpm). Approximately 0.1 g of the RH sorbent material was placed in three well-labelled glass conical flasks each containing 40 milliliters of MG solution at neutral pH. The initial MG

strength was fixed at 9.3 mg/L while a particle mesh of  $> 300 < 425 \mu\text{m}$  was adopted. The flasks were agitated at the preset shaker speeds.

#### **3.5.4: Influence of Rice Husks Particle Mesh Size**

To assess the impact of mesh size on the uptake of MG colorant by RH sorbent, RH of selected sizes ( $< 300$ ,  $> 300 < 425$ , and  $> 425 \mu\text{m}$ ) was used. 0.1 g of RH were placed in triplicate Erlenmeyer flasks having 40 mL of the 9.3 mg/L colorant solution at neutral pH. The glass flasks were stirred at a speed of 200 rpm.

#### **3.5.5: Impact of Solution Temperature**

Removal of malachite green by RH ( $< 300 \mu\text{m}$ ) was studied at 296.15, 303.15, 313.15 and 323.15  $^{\circ}\text{K}$  at neutral pH. The initial dye strength was fixed at 9.3 mg/L while the sorbent amount remained at 0.1g. 40 milliliters of MG solution was added to each of the three well labelled Erlenmeyer flasks containing the accurately weighed rice husks material. The solution mixture was stirred at 200 rpm at preset time intervals and then the absorbance readings were done at 620 nm.

The percentage (%) uptake of the colorant and the amount of dye abstracted by RH,  $q_e$  (mg/g) were computed via equations (3.2) and (3.3) respectively:

$$\% \text{ Adsorption} = 100(C_o - C_e)/C_o \quad (3.2)$$

$$q_e = (C_o - C_e)V/M \quad (3.3)$$

Where  $C_o$  and  $C_e$  are initial and equilibrium intensities (mg/L) of the colorant,  $q_e$  denotes the quantity of colorant removed by the RH material at equilibrium (mg/g),  $V$  is the volume of the colorant utilized (L) whereas  $M$  stands for the quantity of the RH sorbent utilized in grams.

### 3.5.6: Influence of Ionic Strength

One molar (1 M) NaCl solution was prepared and utilized for the ionic strength experiments. The malachite green (MG) dye concentration and volume were both fixed at  $1 \times 10^{-5}$  M and 36 mL, respectively. About 0.1 g of RH having a mesh size of 300 – 425  $\mu\text{m}$  was added to the salt-modified dye solutions at neutral pH and room temperature. To each of the 250 mL Erlenmeyer flask, a varying volume of 1M NaCl solution and distilled water were added as indicated in Table 3.1 below. The flasks were stirred at 200 rpm whereas the UV- Vis measurements were performed at a wavelength of 620 nm.

**Table 3.1:** Volume of 1M NaCl and distilled water for MG uptake by rice husks.

Flask	1	2	3	4	5	6	7	8	9
Vol. of 1M NaCl (mL)	0	0.5	1	1.5	2	2.5	3	3.5	4
Vol. of distilled water (mL)	4	3.5	3	2.5	2	1.5	1	0.5	0

### 3.6: Adsorption of Malachite Green Using Chitosan-Zinc Oxide

#### 3.6.1: Impact of Interaction Time and Colorant Concentration

About 0.6 g of chitosan – ZnO and plain chitosan sorbent materials were separately placed into three different well labelled 250 mL glass flasks each having 40 mL of the colorant solution at neutral pH. The MG concentration was varied from 2.3 up to 9.3 mg/L and the tests were studied for 180 minutes. The glass flasks were shaken at a rate of 200 rpm and later the solution was measured at 620 nm using a UV–Visible spectrophotometer.

### **3.6.2: Impact of Amount of Chitosan-ZnO**

The influence of CS –ZnO material on MG uptake was investigated by varying quantities of the sorbent dosage from 0.4 to 1.2 g for MG colorant concentration of 9.3 mg/L. The percentage (%) uptake was determined at specific time intervals whilst maintaining all the other batch parameters constant.

### **3.6.3: Impact of MG Solution pH**

The impact of pH was examined by utilizing colorant solutions at diverse pH values (pH 3 - 9). The initial pH was amended to the preferred value by addition of 0.1M HCl or 0.1 M NaOH. About 0.6 g of CS-ZnO sorbent was placed into three different well labelled glass conical flasks each having 40 milliliters of dye solution. The flasks were stirred at 200 rpm on an orbital shaker at preset time intervals and then the analysis was achieved at an absorption of 620 nm. The % adsorption and the quantity of dye removed onto the chitosan- ZnO were computed via equations (3.2) and (3.3) under section 3.5.5.

## **3.7: Batch Experiments Using PCL-RH Biofilms**

### **3.7.1 Influence of Dosage on MG Uptake**

The quantity of the adsorbate (PCL-RH) utilized ranged from 0.1 to 0.5 g. 40 milliliters of 9.3 mg/L neutral malachite green solution were placed in three different Erlenmeyer flasks. The glass flasks were then placed on an orbital shaker where they were shaken at 200 rpm at room temperature. Aliquots of the MG solution were withdrawn at specified times during the 150 minutes of experiment time.

### **3.7.2 Impact of Contact Time on MG Adsorption by PCL-RH Blended Films**

0.3 g of PCL-RH and plain PCL sorbate materials were separately utilized in conjunction with 40 milliliters of 9.3 mg/L MG solution at neutral pH. Both the adsorbent and the adsorbate were placed on glass flasks and then agitated at 200 rpm in an orbital shaker at 25 °C. The absorbance was measured at 620 nm.

### **3.7.3: Impact of Initial Colorant Concentration on Uptake of MG by PCL-RH Blend Films**

0.3 g of  $\epsilon$ -polycaprolactone – rice husks (PCL-RH) material was utilized for the batch experiments. The MG concentration was varied from 2.3 to 9.3 mg/L. 40 milliliters of neutral MG solution at room temperature were placed on triplicate Erlenmeyer flasks and stirred at 200 rpm on an orbital shaker. The analysis of the MG solution was done at  $\lambda_{\max}$  of 620 nm.

### **3.8: Kinetics and Mechanism Experiments for the Removal Process**

Global kinetic expression based on lumped analysis of adsorption kinetic data for instance pseudo-first-order (PFO) and pseudo-second-order (PSO) rate equations were employed for the interpretation of the sorption rate data in the study (Wang *et al.*, 2018). The mechanism of the dye removal onto selected low-cost adsorbents was determined using intraparticle diffusion.

### **3.9: Statistical analysis**

Data processing was achieved through linear regression coupled with standard curves and presented as graphs and statistical tables. MS- Excel spreadsheets, Sigma plot and origin software were used for data processing. Student's t-test was applied to assess results whereas the Dixon Q test was applied to check for the outliers in the data thus enhancing data reliability. Other statistical parameters namely mean and standard deviation (Std Dev.) were also computed.

## CHAPTER FOUR

### RESULTS AND DISCUSSION

#### 4.1: Characterization of RH

##### 4.1.1: FTIR Spectra for Raw and Dye Reacted RH

The FTIR examination of the adsorbent was done to establish the organic surface groups present. The spectra of the raw and malachite green (MG) loaded rice husks displayed various absorption peaks (Fig. 4.1). The wide band stretching from 3317.41 to 3900.02  $\text{cm}^{-1}$  reveals the existence of  $-\text{OH}$  and  $-\text{NH}$  surface groups. The absorption bands detected at 2913.68 and 1364.37  $\text{cm}^{-1}$  are ascribed to the stretching and bending of the C-H bond in methyl surface bands correspondingly (Kushwaha *et al.*, 2014). Further, the absorption band emerging at 2520.51  $\text{cm}^{-1}$  is typical of  $-\text{OH}$  linked with carboxylic acids while the stretch starting from 2014.69 to 2162.07  $\text{cm}^{-1}$  is imputable to  $-\text{C}\equiv\text{C}$  for alkynes. The absorption band stretching from 1629.45 to 1732.02  $\text{cm}^{-1}$  is distinctive of a carbonyl superficial band.

The occurrence of the  $-\text{OH}$  band together with the carbonyl group suggests the existence of carboxylic surface groups in the RH. The band stretching from 1459.11 to 1508.07  $\text{cm}^{-1}$  is representative of aromatic exterior groups while the intense absorption band commencing from 1031.69 to 1046.79  $\text{cm}^{-1}$  is imputable to the C-O group. The RH surface groups such as  $-\text{OH}$ ,  $-\text{NH}$ , carbonyl plus carboxyl surface groups are fundamental adsorption sites for sequestering organic pollutants (Poojari *et al.*, 2015). Some peaks shifted after the adsorption process (3317.41 - 3341.91, 3730.52 - 3788.79, 3900.02 up to 3911.20, 2520.51 - 2580.85 and 1629.45 - 1635.73  $\text{cm}^{-1}$ ) while other absorption bands vanished (3548.75 and 3511.30  $\text{cm}^{-1}$ ) after the

adsorption process. This was evident that uptake of MG by RH was successful and new chemical bonds were formed between the adsorbent and the adsorbate.

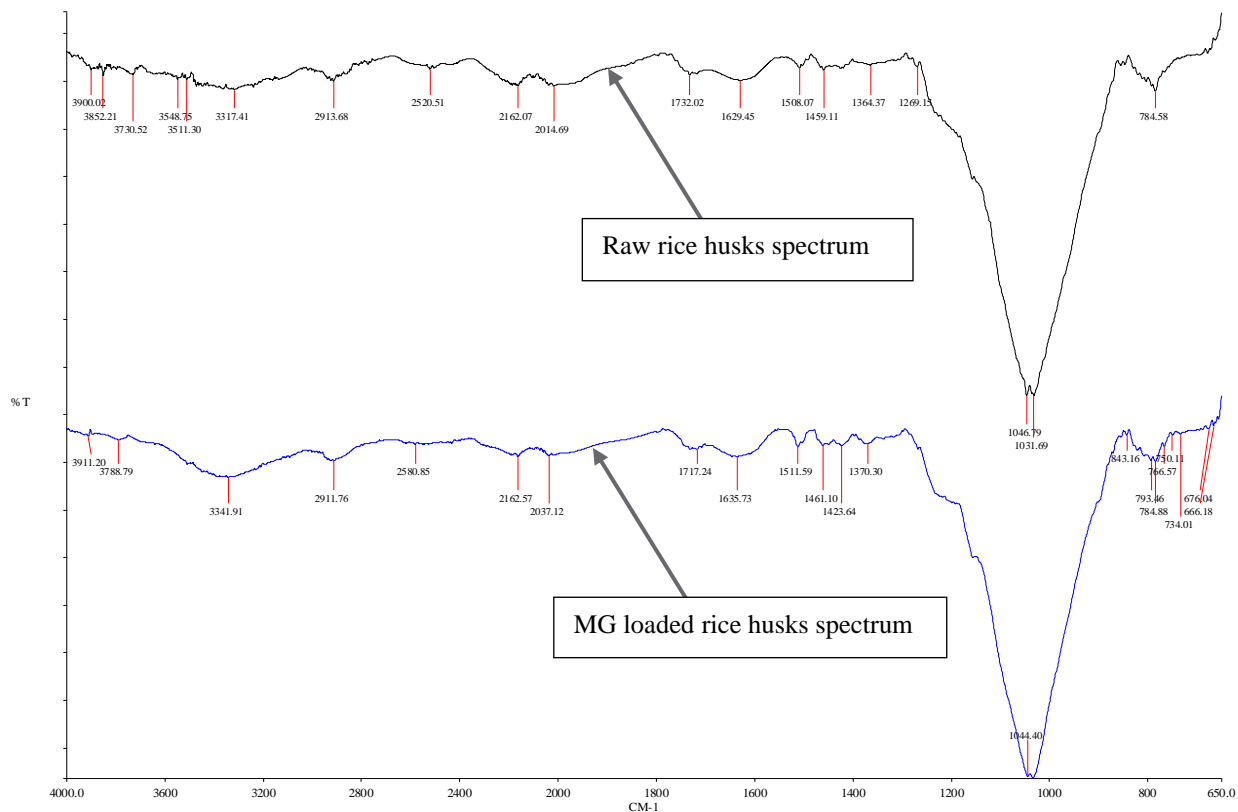


**Figure 4.1:** FTIR spectra for raw and MG loaded rice husks

#### 4.1.2: Scanning Electron Microscope Assessment for Rice Husks

To assess the efficacy of the sorption process, imaging of the adsorbent was performed after sputter-coating the material with gold. Figures 4.2a and 4.2b represent the SEM micrographs obtained. Figure 4.2a signifies the micrograph of the raw RH before the sorption process. The SEM results revealed that the raw unmodified RH has an irregular permeable surface and cavities that could be liable for the uptake of the MG dye. Figure 4.2b symbolizes the MG-reacted malachite green rice husks. It is apparent that, after the uptake of the colorant by the RH, the surface of the sorbent material became smooth inferring that the unoccupied sorption sites of

the RH were ultimately covered with the MG contaminant and thus the abstraction of MG by rice husks was effective. Hameed (2009) reported comparable findings for the uptake of methylene blue from aqueous media by grass waste.

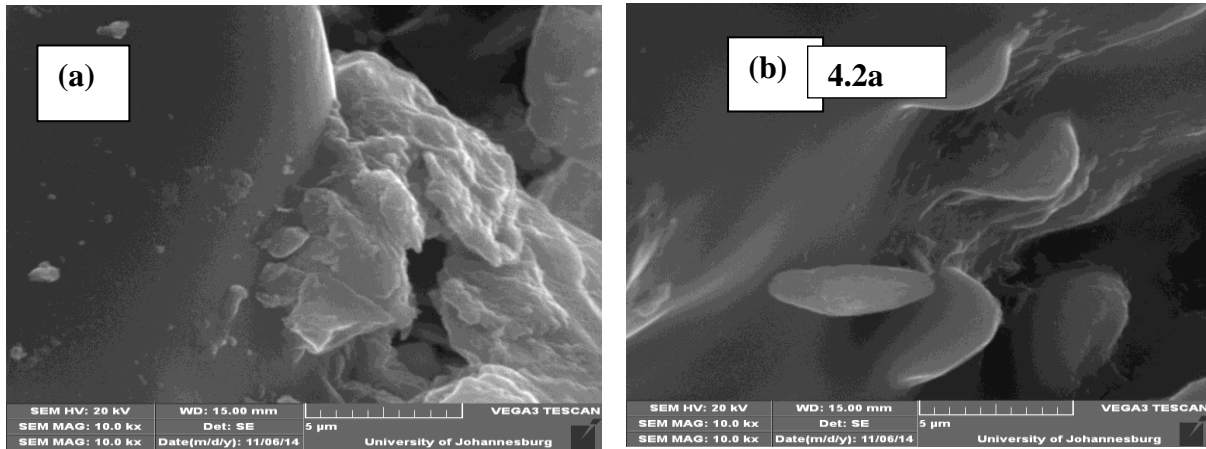


**Figure 4.2:** SEM micrographs of (a) raw rice husks (b) reacted rice husks with MG.

#### 4.1.3: Energy-Dispersive X-Ray Assessment for Rice Husks

The technique was applied to evaluate the elemental composition of the adsorbent. The material comprised of large quantities of oxygen and silicon (42.8 and 51.82% correspondingly) and lower amounts of magnesium, aluminium, sulfur, phosphorus, calcium manganese and iron (Table 4.1 and Appendix 1). These elements are fundamental in the formation of chemical bonds throughout the sorption process.

**Table 4. 1:** EDX analysis results for RH material

<b>Element</b>	<b>Weight%</b>	<b>Atomic%</b>
O	42.80	57.42
Mg	0.22	0.19
Al	0.59	0.47
Si	51.82	39.61
P	0.44	0.31
S	0.31	0.20
Ca	2.08	1.12
Mn	0.45	0.18
Fe	1.28	0.49
Totals	100.00	

#### **4.1.4: XRD Assessment for Rice Husks**

The XRD patterns for rice RH are represented in figure 4.3. The RH was found to be non-crystalline with broad diffused peaks appearing at  $2\theta = 22.5^\circ$ ,  $35^\circ$  and  $45^\circ$ . The amorphous nature of the rice husks is attributed to high amounts of lignin, cellulose and hemicellulose (Johar *et al.*, 2012). Comparable findings were depicted by Yuvakkumar *et al.*, (2014) where the broad peak at  $2\theta = 22.5^\circ$  was ascribed to presence of amorphous silica.

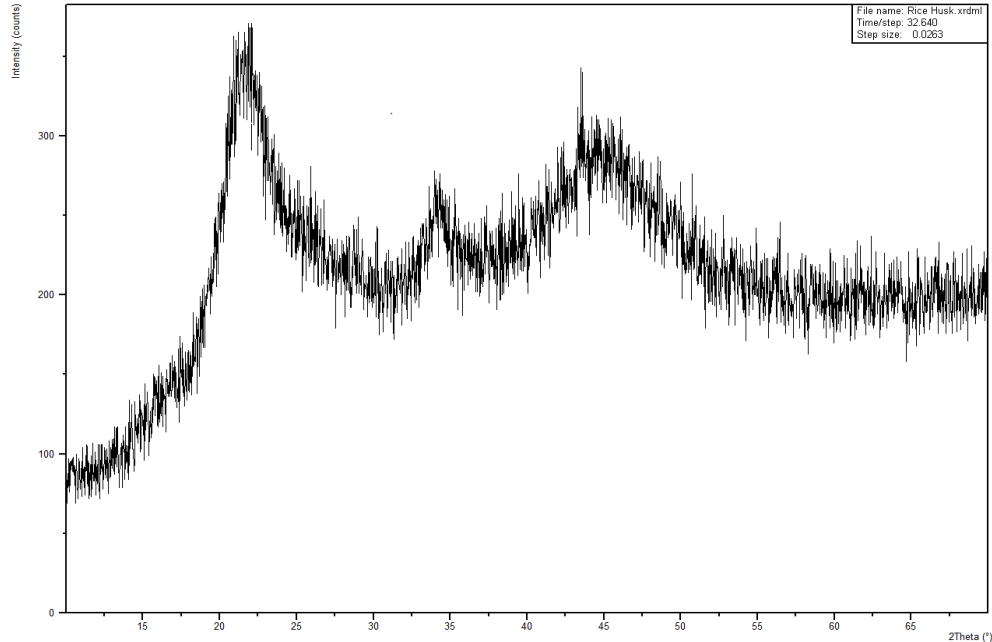


**Figure 4.3:** PXRD patterns of rice husks.

#### 4.1.5: Thermogravimetric Analysis of Rice Husks

The thermal stability of RH adsorbent was investigated under both air and nitrogen (Inert) atmospheres (Fig. 4.4). There was noticeable weight loss from 33 to 110 °C for both curves which is ascribed to the vaporization of adsorbed water (Mansaray & Ghaly, 1998). In the inert atmosphere, there was weight loss which started at 240 °C and ended at 490 °C whereas in airflow the weight loss started at 225 °C and ended at 500 °C. This kind of degradation drift is imputable to thermal degradation of hemicellulose, cellulose and lignin which are the major constituents of rice husks (Genieva *et al.*, 2008; Yin & Goh, 2011). In the case of degradation under oxygen flow, there was CO<sub>2</sub> presence and consequently, the production of char occurred at 500 °C.



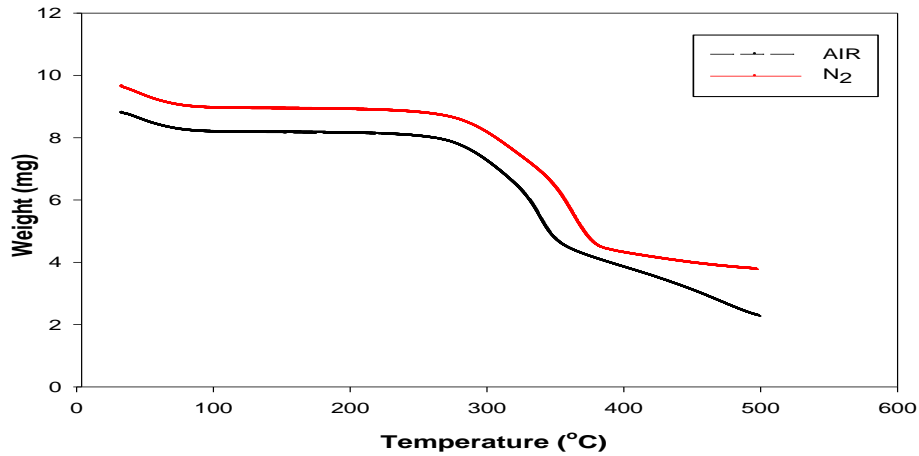


**Figure 4.4:** TGA Thermogram of rice husks adsorbent.

#### 4.1.6: BET Surface Area Assessment for RH

The single point ( $P/P_0$ ) surface area evaluation for the RH was  $9.8 \text{ m}^2/\text{g}$  while its pore volume was  $0.068671 \text{ cm}^3/\text{g}$ . The pore size of the sorbent material was  $280.4 \text{ \AA}$  ( $28.4 \text{ nm}$ ), indicating that the RH was mesoporous in nature (Kaneko, 1994). These factors influence the magnitude of the sorption process. Fig. 4.5 represents the BET adsorption-desorption isotherm.

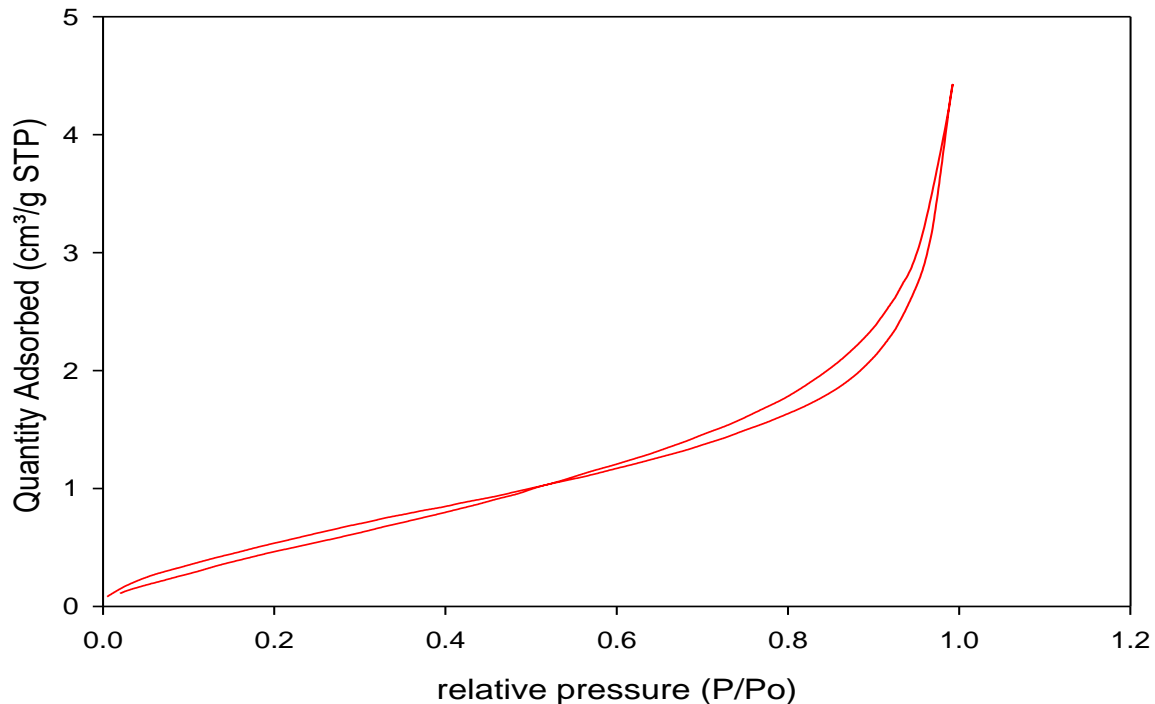


**Figure 4.5:** BET N<sub>2</sub> isotherm for rice husks.

## 4.2: Characterization of CS – ZnO Sorbent Material

### 4.2.1: FTIR Evaluation

FTIR spectrum for pure chitosan (Fig. 4.6) showed a prominent band at 3290.56 cm<sup>-1</sup> which was imputable to -OH and -NH<sub>2</sub> vibration. The band at 2870.08 cm<sup>-1</sup> was attributed to the -CH<sub>3</sub> and CH<sub>2</sub> groups of CS while 1647.21 cm<sup>-1</sup> is owed to the C=O amide 1 vibration. The COO<sup>-</sup> bending imputable to carboxylic acid salt was detected at 1369.46 cm<sup>-1</sup> as described by other investigators (Moradi *et al.*, 2014). The small shoulder at 1141.6 cm<sup>-1</sup> signifies β (1- 4) glucosidic stretch while the absorption band at 1014.56 cm<sup>-1</sup> is assigned to C- O – C in the glucose ring (Moradi *et al.*, 2014; Shukla *et al.*, 2013).

Compared to the neat CS, the absorption peaks corresponding to  $\text{-NH}_2$  and  $\text{-OH}$  surface absorption groups in the CS- ZnO material (Fig.4.7) moved to upper wavenumbers i.e.,  $3718.76\text{ cm}^{-1}$  implying an effective interface between the CS and ZnO groups. This reveals that ZnO nanoparticles were successfully immobilized on the CS material (Mujeeb *et al.*, 2018). The synthesized composite exhibited absorption bands at  $659.66$  and  $543.93\text{ cm}^{-1}$ , imputable to O-Zn-O stretching, as demonstrated in the previous studies (John *et al.*, 2015). The absorption bands detected at  $2924$  and  $2870\text{ cm}^{-1}$  are attributable to asymmetric  $\text{SP}^3$  stretching of  $\text{CH}_3$  and  $\text{CH}_2$  of CS polymer.

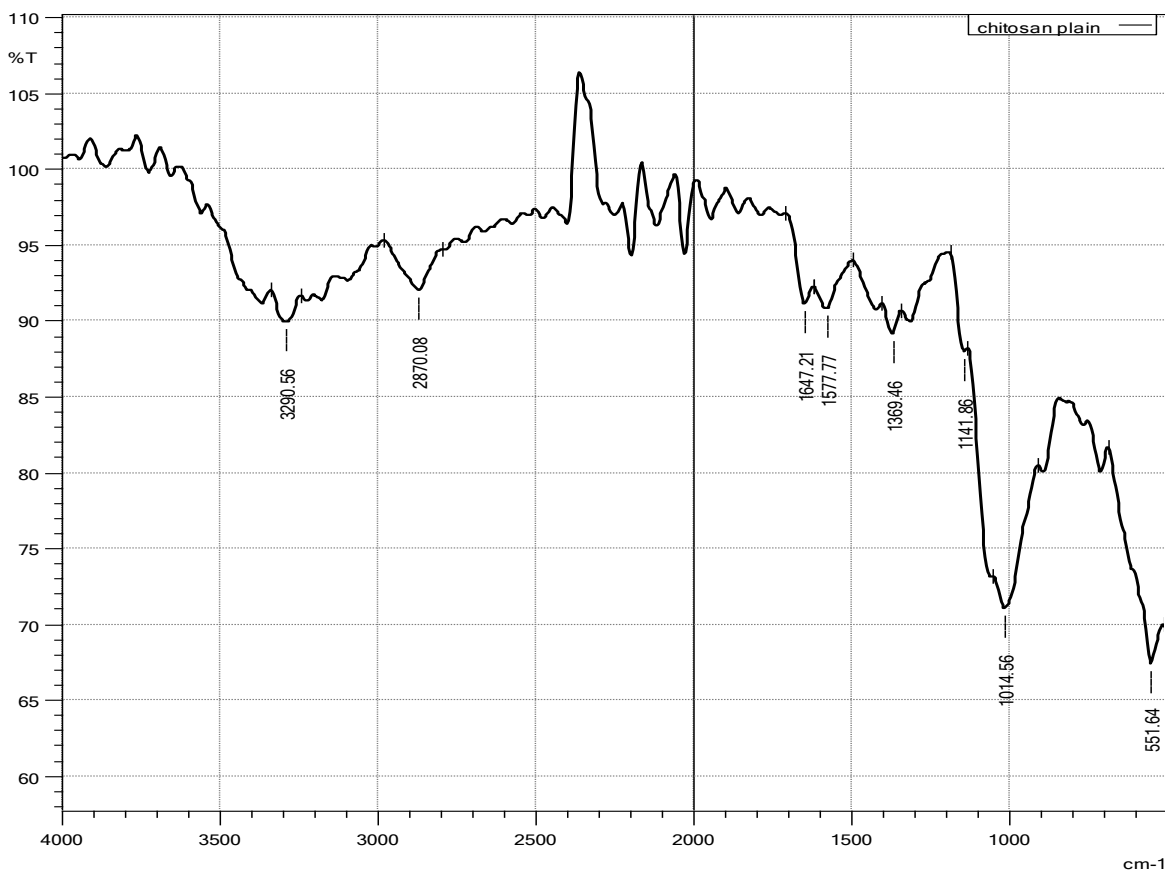


**Figure 4.6:** FTIR spectrum of Chitosan.

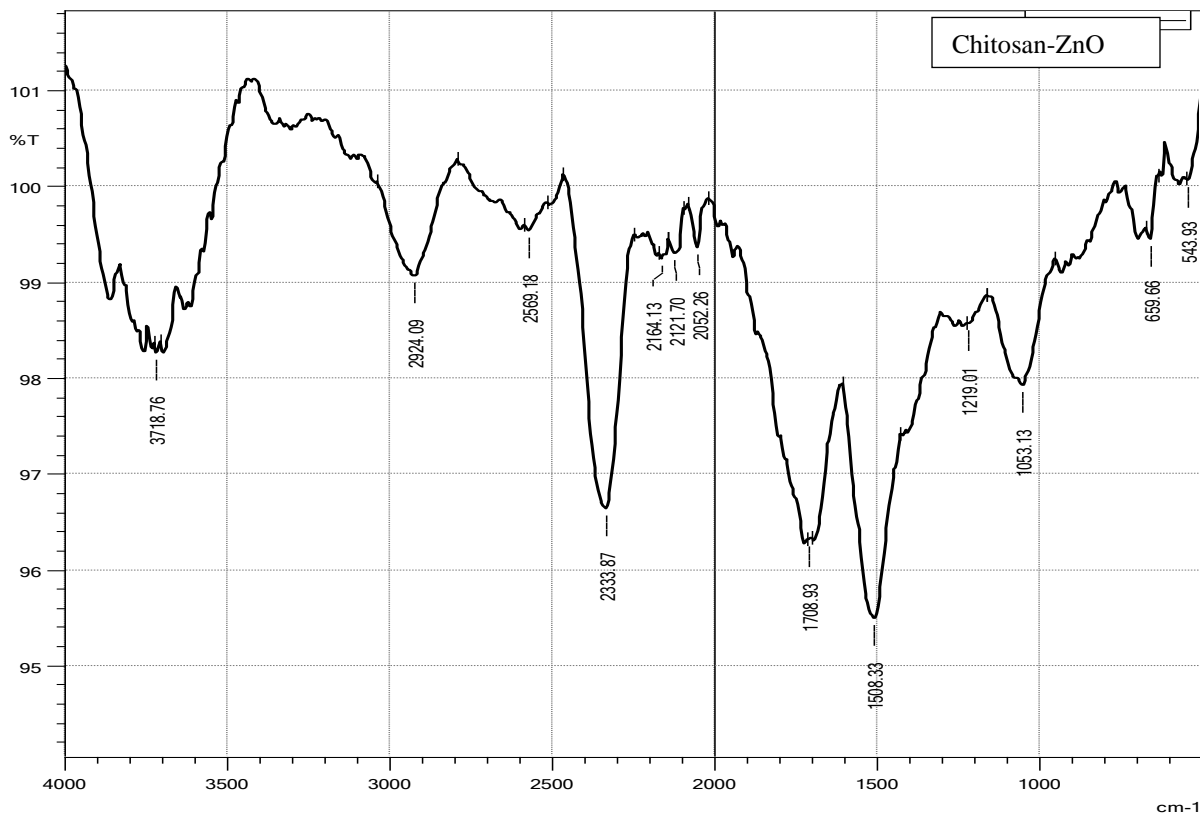


**Figure 4.7:** FTIR spectrum for Chitosan-ZnO composite.

#### 4.2.2: TGA Investigation of CS- ZnO Adsorbent

The sorbent material exhibited a three-phase thermal degradation (Fig. 4.8). The material weight loss of 3.22 mg from 100 to 109.8 °C is attributed to residue moisture evaporation. Further, the 7.89 mg weight loss reflected from 109.8 to 325.7°C represents the degradation of chitosan. Comparable results were presented by Sanuja *et al.*, (2015). The slope between 325.68 – 526.41 °C is imputable to the carbonization process (Youssef *et al.*, 2015) that eventually yielded a 16.87 mg residue.

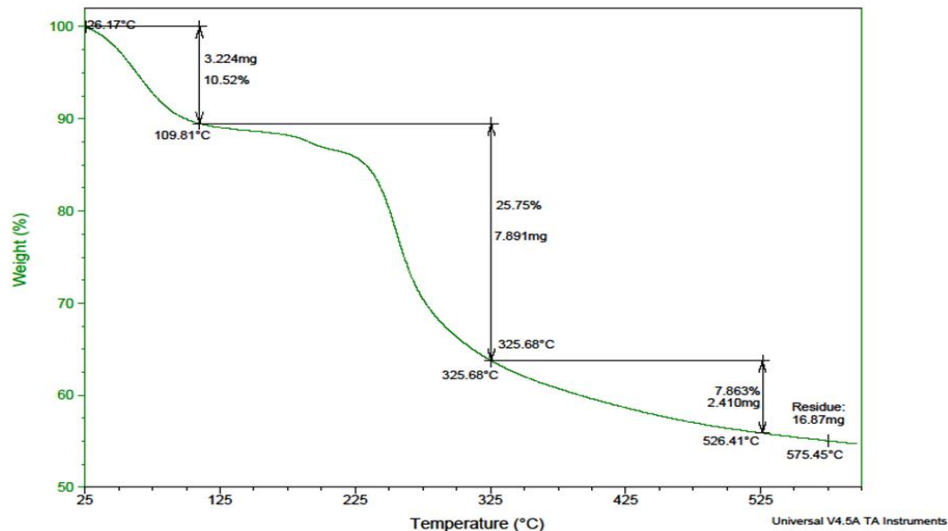


**Figure 4.8:** TGA thermogram for Chitosan-ZnO sorbent

#### 4.2.3: XRD Phase Assessment of Chitosan- ZnO Material

Fig. 4.9 denotes the XRD pattern of the CS-ZnO sorbent. The diffraction peak detected at  $2\theta = 20^\circ$  is from the neat CS material (Saeed *et al.*, 2014). The findings unveiled that CS is a semi-crystalline material. The diffractogram patterns observed at  $2\theta$  points of  $31.8^\circ$ ,  $34.5^\circ$ ,  $36.6^\circ$ ,  $47.4^\circ$ ,  $56.6^\circ$ ,  $62.7^\circ$ ,  $66.4^\circ$ ,  $68.1^\circ$ , and  $69.1^\circ$  were assigned to (100), (002), (101), (102), (110), (103), (200), (112) and (201) crystal configuration of ZnO with hexagonal wurtzite arrangement. The XRD lines match the standard values illustrated in the Joint Committee on Powder Diffraction Standards data card no: 36-1451 (Srivastava *et al.*, 2013; John *et al.*, 2015). The Powder XRD findings unveiled successful chemical integration of the hexagonal form of ZnO on the chitosan material by precipitation approach.

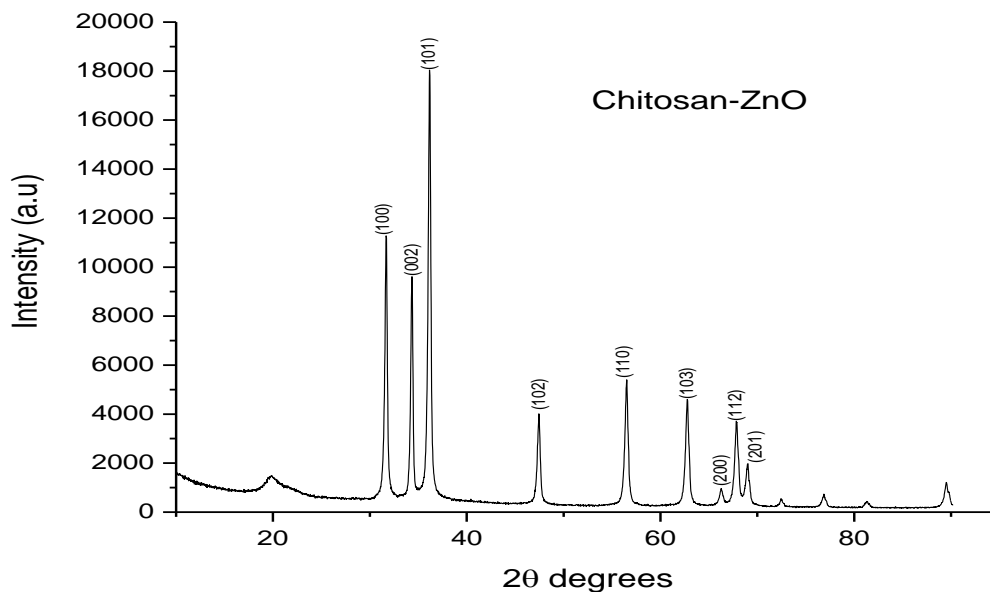


**Figure 4.9:** XRD diffractogram for CS-ZnO sorbent

#### 4.2.4: Physisorption Investigation of Chitosan-ZnO Sorbent Material

The analysis was executed to give an insight into the porosity of the sorbent. The BET findings (surface area) for the CS-ZnO material were  $8 \text{ m}^2/\text{g}$ , pore volume of  $6.91 \times 10^{-2} \text{ cm}^3/\text{g}$  and a pore diameter of 33 nm. The  $\text{N}_2$  sorption isotherm (Fig. 4.10) is classified as type IV corresponding to IUPAC classification revealing that the synthesized adsorbent was mesoporous (Wang *et al.*, 2008) since it exhibits a pore diameter that ranges from 2 to 50 nm.

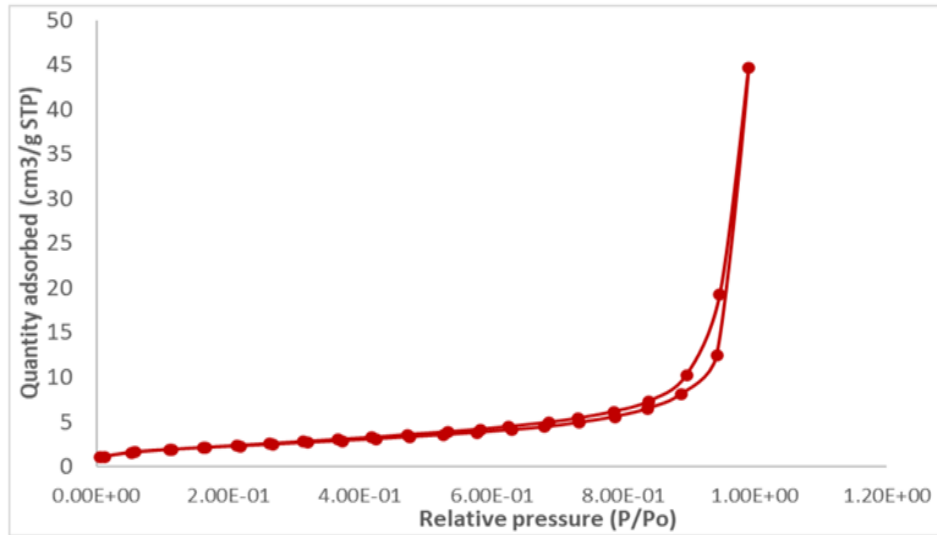


**Figure 4.10:** BET adsorption-desorption isotherm for CS-ZnO.

#### 4.2.5: Zeta Potential Analysis

This analysis was performed to establish the surface charge and steadiness of the nanoparticles in a colloidal solution. It can alter the uptake ability of the sorbent material (Wang *et al.*, 2009). The zeta potential for the CS-ZnO material was  $-3.86 \pm 0.01$  mV (Fig. 4.11), thus demonstrating enhanced stability of the particles at approximately neutral pH.

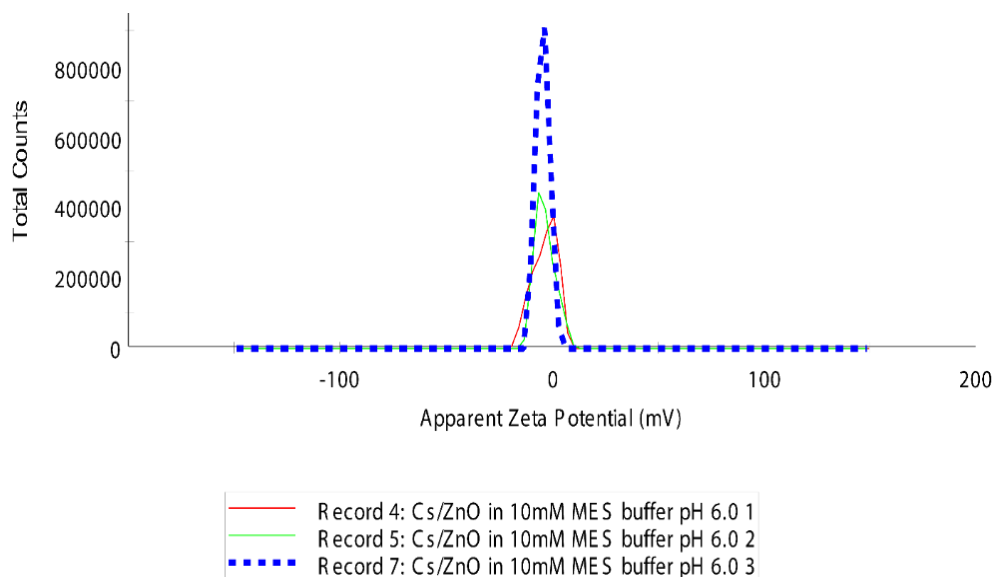


**Figure 4.11:** Zeta potential for CS- ZnO material

#### 4.2.6: EDXRF Chemical Analysis for CS-ZnO

The study findings disclosed existence of phosphorus (P), iron (Fe), and zinc (Zn) in the sorbent material (Fig. 4.12 and Appendix 8). The molybdenum secondary target demonstrated great excitation efficiency for Fe and Zn while the RX9 secondary target showed elevated efficiency for phosphorus. Escape peaks (Kang *et al.*, 2002) for Zn were detected and that might be attributed to an artifact from the equipment detector which is produced by the photoelectrical effect associated with elevated count rates of the targeted element. The sorbent (CS-ZnO) exhibited considerable quantity of Zn ( $96500 \pm 53.2$  mg/kg) relative to Fe ( $753 \pm 45.3$  mg/kg) and P ( $166 \pm 26.6$  mg/kg). The existence of Zn in the adsorbent proved successful integration of ZnO into the CS framework. The observed trend of elemental abundance in the investigated material was  $Zn > Fe > P$ .

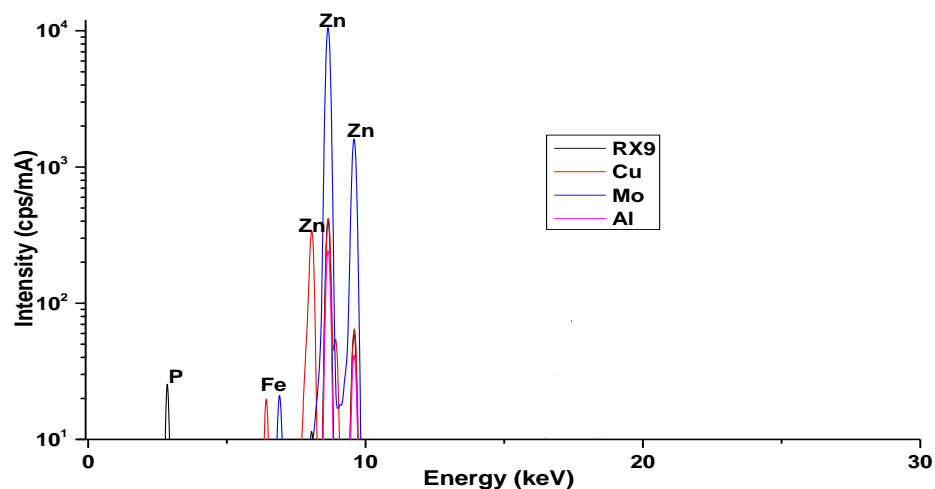


**Figure 4.12:** EDXRF analysis of CS- ZnO material.

### 4.3: Characterization of $\epsilon$ -Polycaprolactone ( $\epsilon$ - PCL) Polymer

#### 4.3.1: <sup>1</sup>H NMR Analysis for $\epsilon$ - PCL

The <sup>1</sup>H NMR is employed to determine the chemical composition for a polymer synthesized and also to compute the number – average molecular weight ( $M_n$ ) of the polymer. This analytical instrument is also used to calculate the degree of polymerization ( $DP_n$ ) and the % conversion of a monomer into a polymer.

The peaks at 1.40 ppm (2H,  $-\text{CO}(\text{CH}_2)_2\text{CH}_2(\text{CH}_2)_2\text{O}-$ ), 1.64 ppm (4H,  $-\text{COCH}_2\text{CH}_2\text{CH}_2\text{CH}_2\text{CH}_2\text{O}-$ ), 2.29 ppm (2H,  $-\text{COCH}_2-(\text{CH}_2)_4\text{O}-$ ), and 4.07 ppm (2H,  $-\text{CO}(\text{CH}_2)_4-\text{CH}_2\text{O}-$ ), were ascribed to  $\epsilon$ -PCL whereas the peak resulting from methylene protons adjacent to hydroxyl end group appearing as a triplet is at 3.65 ppm (2H,  $-\text{CO}(\text{CH}_2)_4\text{CH}_2\text{OH}$ ) (Fig. 4.13). The peak at 5.13 ppm appearing as a singlet (2H,  $\text{PhCH}_2\text{O}-$ ), is imputable to the oxymethylene protons next to the ester linkage for benzyl alcohol in the resulting repeating unit. The resultant peak from the aromatic protons of the benzyl moiety is at 7.36 ppm (5H, aromatic).

The obtained findings are comparable to previously reported outcomes from other studies (Xu *et al.*, 2014).

The two peaks appearing at 1.85 and 3.76 ppm could be due to the tetrahydrofuran (THF) solvent residue (Fulmer *et al.*, 2010) in the sample caused by incomplete vacuum drying. THF was utilized to terminate the polymerization reaction.

The targeted molecular weights were 5000, 10000 and 15,000 g/mol. The respective spectra for 5,000 and 10,000 g/mol are given in appendices 4 and 5. The  $M_n$   $^1\text{H}$  NMR for the synthesized  $\epsilon$ -PCL polymers were 3653, 5979 and 5709 g/mol respectively (Appendix 6).

From the obtained results, it is clear that the molecular weight calculated from  $^1\text{H}$  NMR data was lower than the targeted ones. This discrepancy of results could be ascribed to possible inactivation of the catalyst as the reaction progressed even though the percentage conversion of the monomer was higher than 90% in all the reactions. Further, “backbiting” reactions due to long reaction hours (17 Hrs) might have contributed to the low molecular weights of the polymers.

The  $^1\text{H}$  NMR of the monomer ( $\epsilon$ - Caprolactone) exhibited five signals at 4.2 to 1.6 ppm (Appendix 2) whereas the  $^{13}\text{C}$  NMR for the same compound displayed six signals (Appendix 3). The signal for the carbonyl group of the cyclic ester occurred at 177 ppm. The oxymethylene group was observed at 64.1 ppm whereas the signals ascribed to the four methylene groups occurred at 34.1 to 24.6 ppm (Appendix 3).

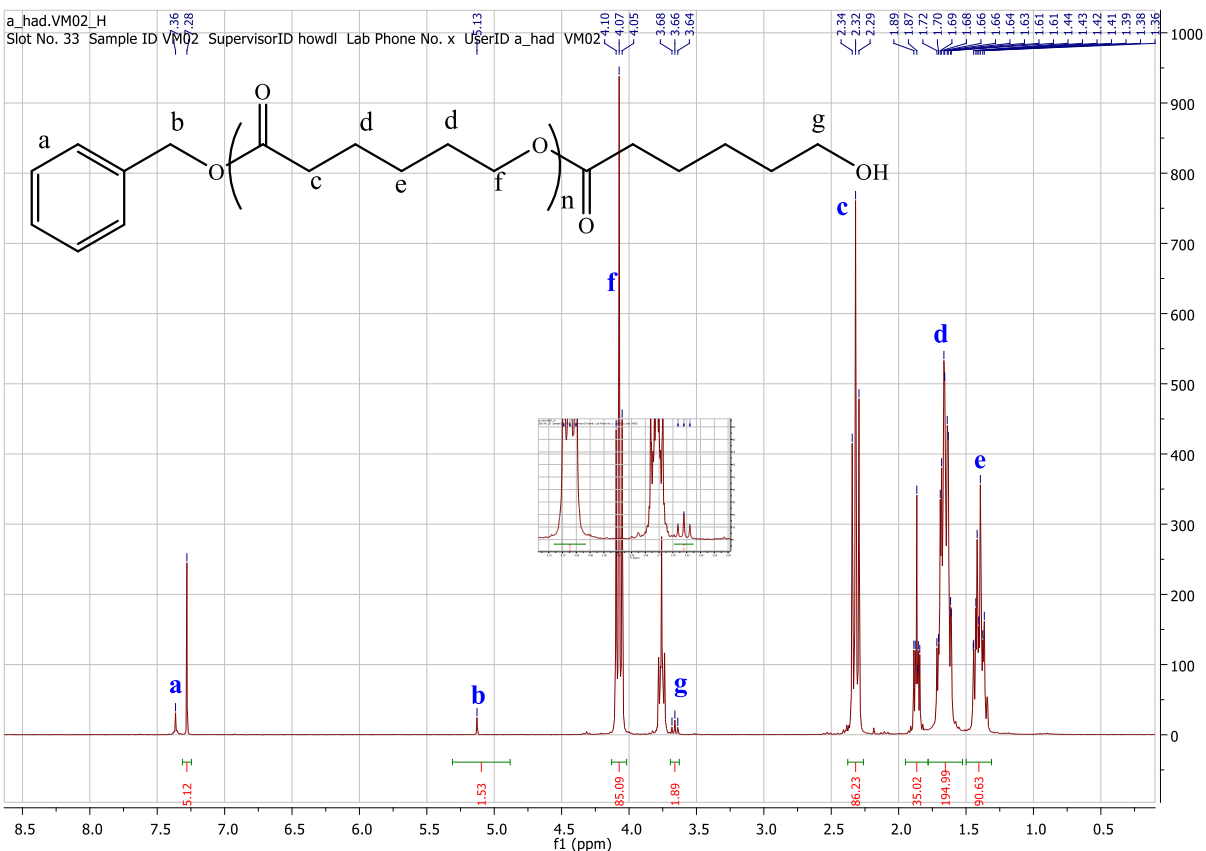


**Figure 4.13:**  $^1\text{H}$  NMR spectrum for the synthesized  $\epsilon$ - Polycaprolactone

#### 4.3.2: Assessment of Poly ( $\epsilon$ -Caprolactone) using Size Exclusion Chromatography (SEC)

The SEC instrument interfaced with a multi-angle light scattering detection (SEC-MALS), which is a technique that aids in the computation of the  $M_n$  and polydispersity index (PDI) of a synthesized polymer was used. The experimental SEC-MALS molecular weights were lower than the targeted ones (Fig. 4.14) despite the high percentage of monomer conversion and lower polydispersity indices (Appendix 6). The reason for this disagreement in  $M_n$  is that transesterification reaction could have occurred during the polymerization of the monomer ( $\epsilon$ -caprolactone). This is due to both inter and intramolecular side reactions which are prevalent during the advanced phases of polymerization in bulk principally at high temperatures. It causes

the widening of the polydispersity index and loss of regulation of the polymerization process (Labet & Thielemans, 2009).

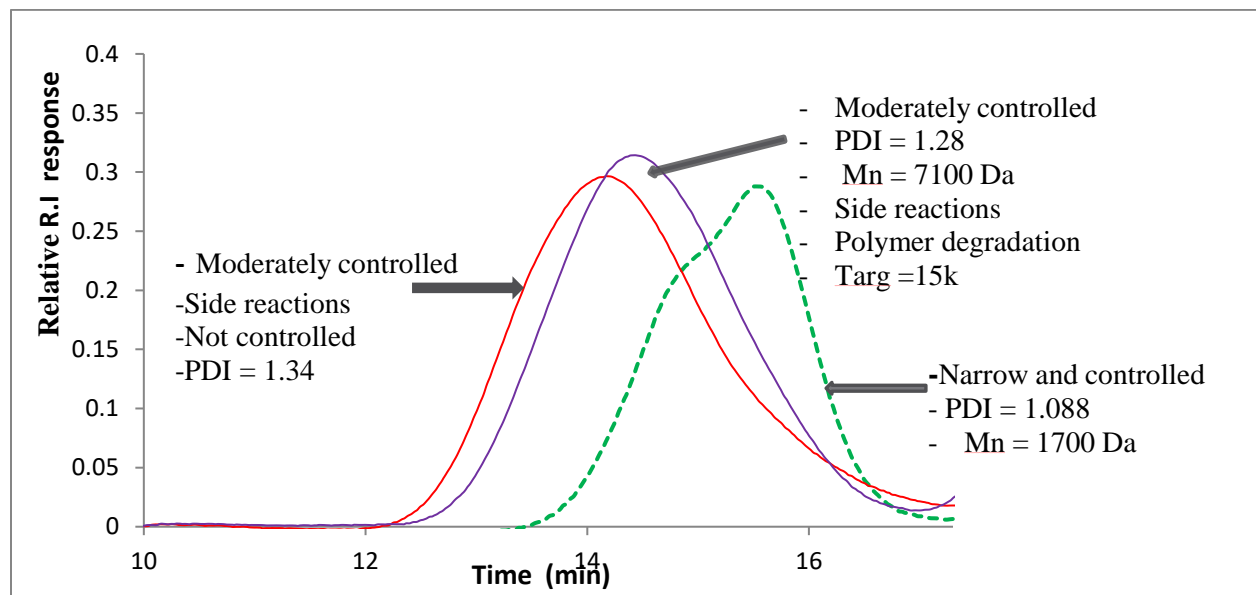


**Figure 4.14:** SEC-MALS curves of PCL in the bulk (120 °C) using benzyl alcohol as the initiator

#### 4.3.3: Assessment of Poly ( $\epsilon$ -Caprolactone) by Differential Scanning Calorimetry

The thermal performance of  $\epsilon$ -PCL was investigated by applying the DSC technique. The polymer was found to be semi-crystalline with a melting temperature ( $T_m$ ) of approximately 54 °C (Fig. 4.15). Conversely, the peak for glass transition temperature ( $T_g$ ) was not detected. This is attributable to probably insufficient cooling of the DSC equipment since  $T_g$  is measured at very low temperatures. Further, this might have been caused by an abrupt change in heat transfer between the sample and the pan. Typical DSC values stated in the literature  $\epsilon$ -PCL range between 56 to 65 °C for  $T_m$  and -65 to -60 °C for  $T_g$ .

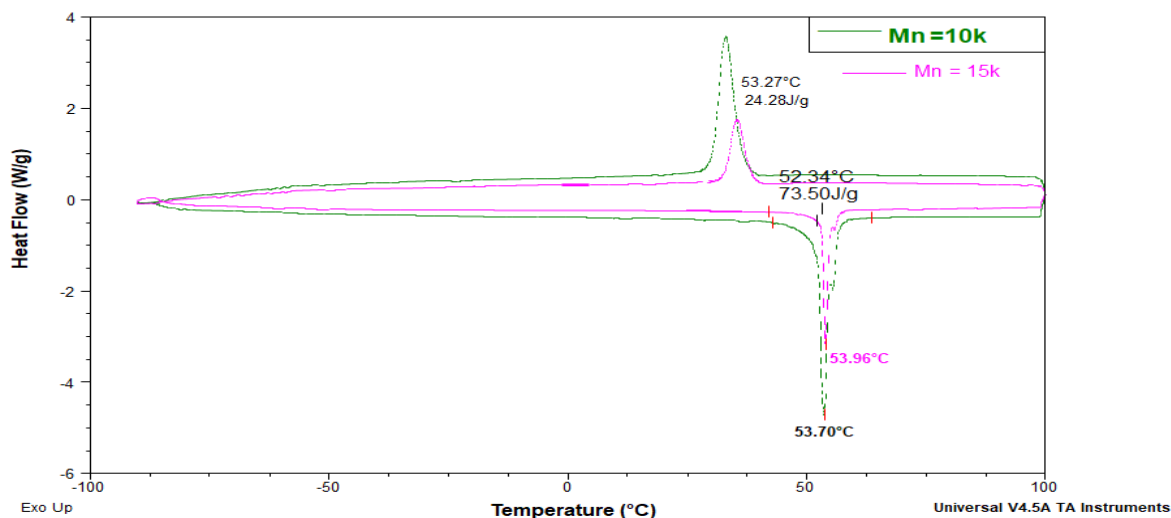


**Figure 4.15:** Overlay DSC thermogram curves for 10 KDa and 15 KDa poly( $\epsilon$ -caprolactone)

#### 4.3.4: Dynamic Mechanical Analysis for Poly ( $\epsilon$ -caprolactone)

DMA is a more sensitive technique in the investigation of the thermal behavior of polymeric materials compared to DSC. It was utilized in this work as a confirmatory test for the thermal properties of poly ( $\epsilon$ -caprolactone). The melting temperature of PCL was 64 °C (Fig. 4.16), a value that was higher than the one (54 °C) obtained using the DSC technique. Moreover, the DMA value is comparable to what is reported in the literature (56 to 65 °C). The peak for  $T_g$  could not be detected since the cooling of the equipment was achievable up to 25 °C and the  $T_g$  for PCL is normally -60°C.

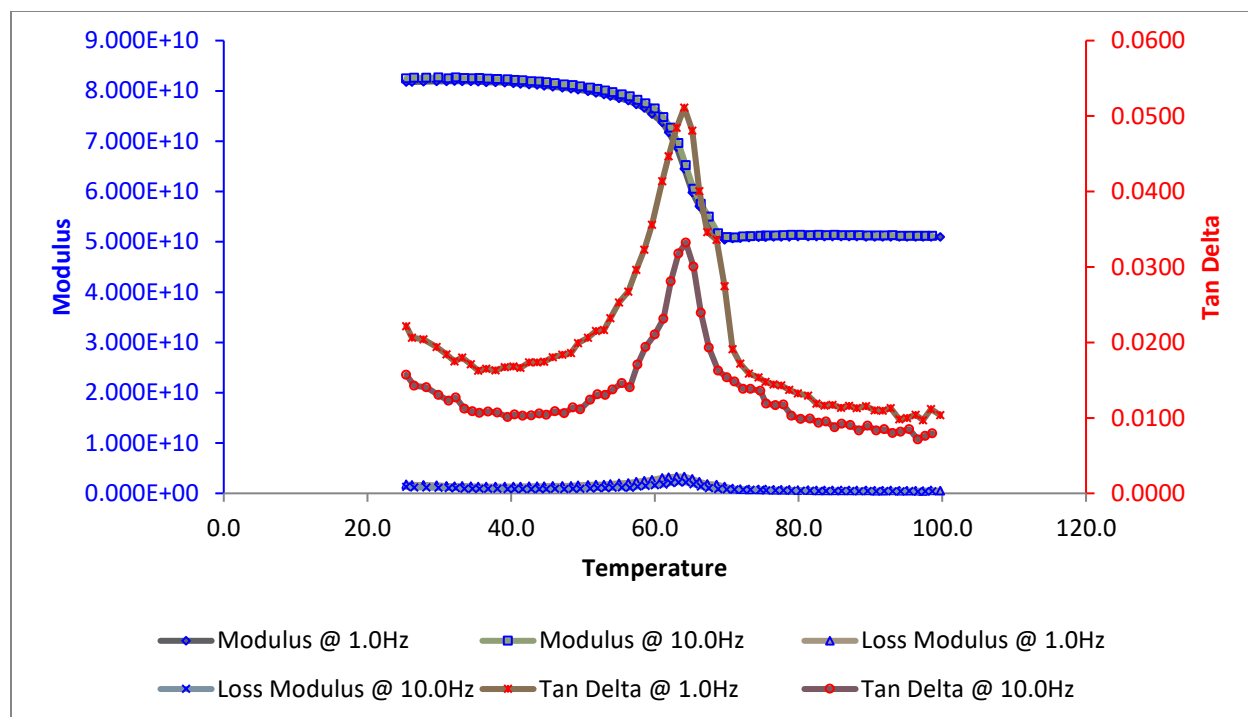


**Figure 4.16:** DMA curve for melting temperature ( $T_m$ ) of poly( $\epsilon$ -caprolactone).

#### 4.3.5: FTIR Spectrum for Pure $\epsilon$ -PCL

The FTIR spectrum of the semi-crystalline PCL reveals typical absorption bands of an aliphatic polyester (Fig. 4.17). The absorption peaks at  $2943.37$  and  $2864.29$   $\text{cm}^{-1}$  signify the C-H stretching of the methylene functional groups (Phillipson *et al.*, 2014). The absorption peak at  $1720.50$   $\text{cm}^{-1}$  is ascribed to the carbonyl surface group whereas the peaks between  $1043.49$  –  $1471.69$   $\text{cm}^{-1}$  are due to the skeletal structure of the polymer chain.

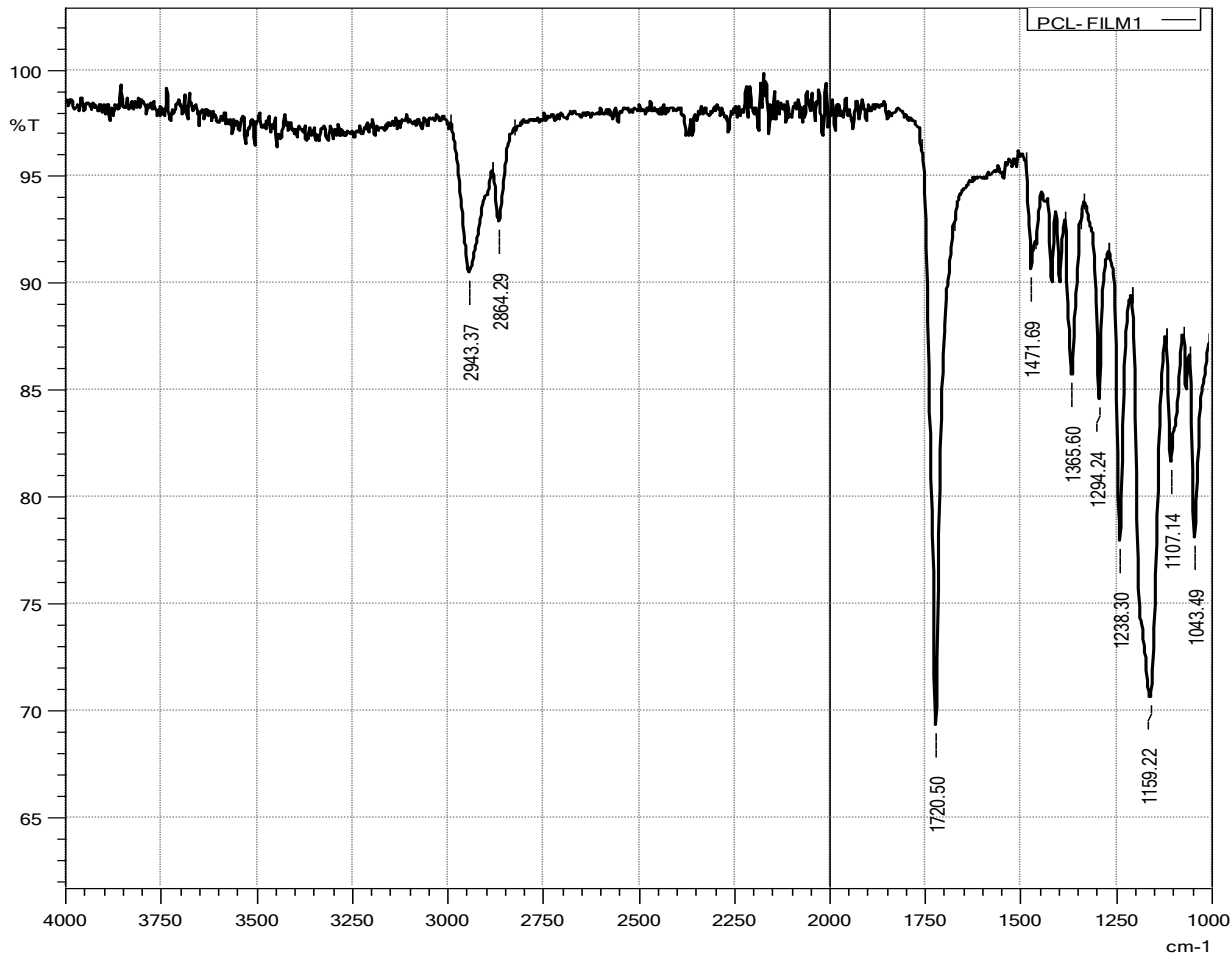


**Figure 4.17:** FTIR spectrum of pure  $\epsilon$ -PCL

#### 4.4: Characterization of Poly( $\epsilon$ -caprolactone) - Rice Husks Films

##### 4.4.1: Thermogravimetric Analysis of PCL - RH

The material exhibited three distinct thermal phases (Fig. 4.18). In the first phase which started from 25 to 126.4 °C, there was 1.171 mg (4.47 %) material weight loss. The observed loss was due to the evaporation of the residue moisture adsorbed on the PCL - RH material. Phase two occurred within the temperature gradient of 126.4 – 426.52 °C and it was characterized by a substantial weight loss of 18.59 mg which is equivalent to 70.93 %. The weight loss is ascribed to the loss of light volatiles at 126 up to approximately 200 °C. Within the same phase, there was

thermal degradation of PCL which started from 220 °C and ended at 446.52 °C (Hoidy *et al.*, 2010). Finally, decomposition of hemicellulose, lignin and cellulose occurred owing to the presence of rice husks in the blend as demonstrated in Fig. 4.4. From 426.52 to 525.51 °C was the final stage of decomposition with a residue of 5.78 mg which was attributed to char and undecomposed material due to incomplete combustion. The TGA results revealed that the PCL-RH material is a thermally stable material hence it is an ideal candidate for the sorption of organic water contaminants from high-temperature effluents.

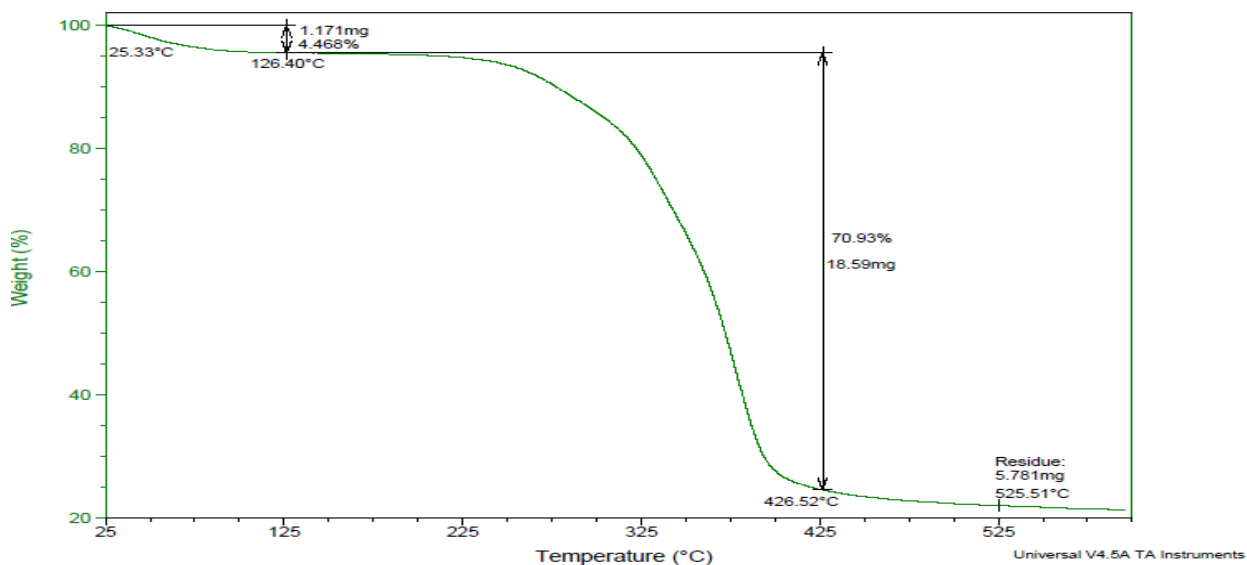


**Figure 4.18:** TGA thermogram of PCL- RH blend films

#### 4.4.2: X-Ray Diffraction Analysis

Fig. 4.19 illustrates the XRD pattern for poly ( $\epsilon$ -caprolactone)- rice husks (PCL-RH) blend films. The material exhibited two peaks at  $2\theta = 21.2^\circ$  and  $23.4^\circ$  which were ascribed to (110) and (200) orientation planes correspondingly owing to the orthorhombic framework of  $\epsilon$ -PCL (Abdelrazek

*et al.*, 2016). The film blend depicts a more crystalline material compared to the neat amorphous rice husks (Fig. 4.3) ascribable to the existence of semi-crystalline PCL in the blend.

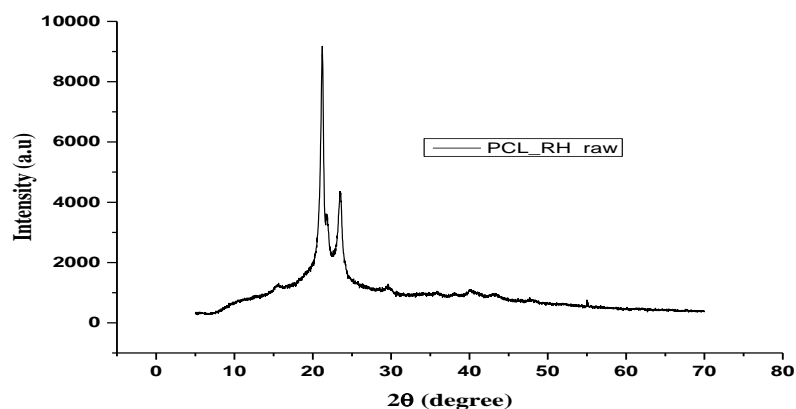


**Figure 4.19:** XRD diffractogram of PCL-RH blend film.

#### 4.4.3: FTIR Spectra Analysis of Raw and MG Loaded PCL-RH Films

After blending the PCL with rice husks through the solvent casting method, several surface organic groups moved to either lower or higher absorption bands. For example, the absorption band at  $1043.49\text{ cm}^{-1}$  moved to  $1045.42\text{ cm}^{-1}$ ,  $1159.22\text{ cm}^{-1}$  moved to  $1161.15\text{ cm}^{-1}$ ,  $1238.30\text{ cm}^{-1}$  changed to  $1240.23\text{ cm}^{-1}$  and  $1365.60\text{ cm}^{-1}$  moved to  $1363.67\text{ cm}^{-1}$  (Figs. 4. 17 & 4.20). This is evident that new bonds between the pure PCL and RH were formed and thus the blending process was effective.

After the adsorption of malachite green (MG), only three absorption peaks were detectable (Fig. 4.21). This indicates that the peaks which vanished were involved in forming adsorbent-adsorbate bonds for the abstraction of the colorant from the aqueous media. Among the three bonds which were detected after adsorption, two of them shifted from the original position implying that they were also responsible for the process. For instance, the peak at  $2943.37\text{ cm}^{-1}$

in the unreacted material shifted to  $2918.30\text{ cm}^{-1}$  while the band detected at  $1161.15\text{ cm}^{-1}$  changed to  $1166.93\text{ cm}^{-1}$ . Although the carbonyl band at  $1720.50\text{ cm}^{-1}$  did not shift from the original position, it reduced in intensity (Fig. 4.21).

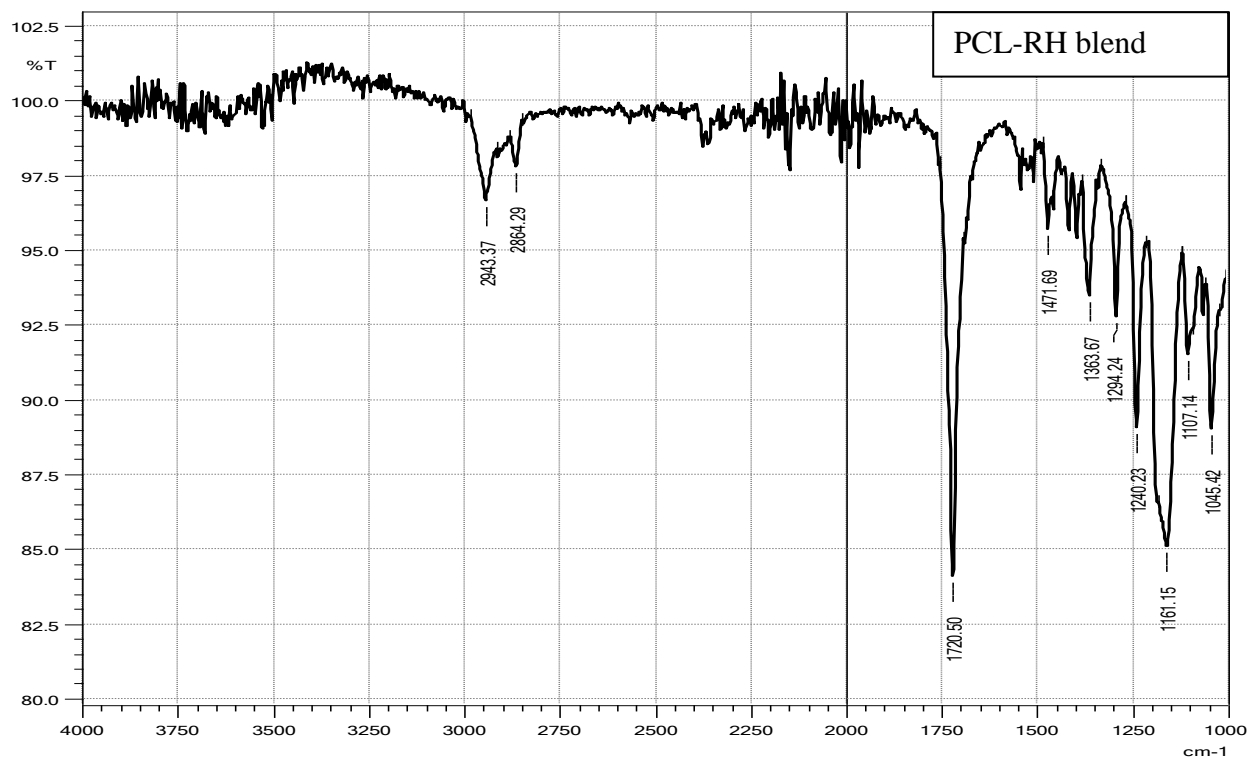


**Figure 4.20:** FTIR spectrum for unreacted/raw PCL-RH blend films.

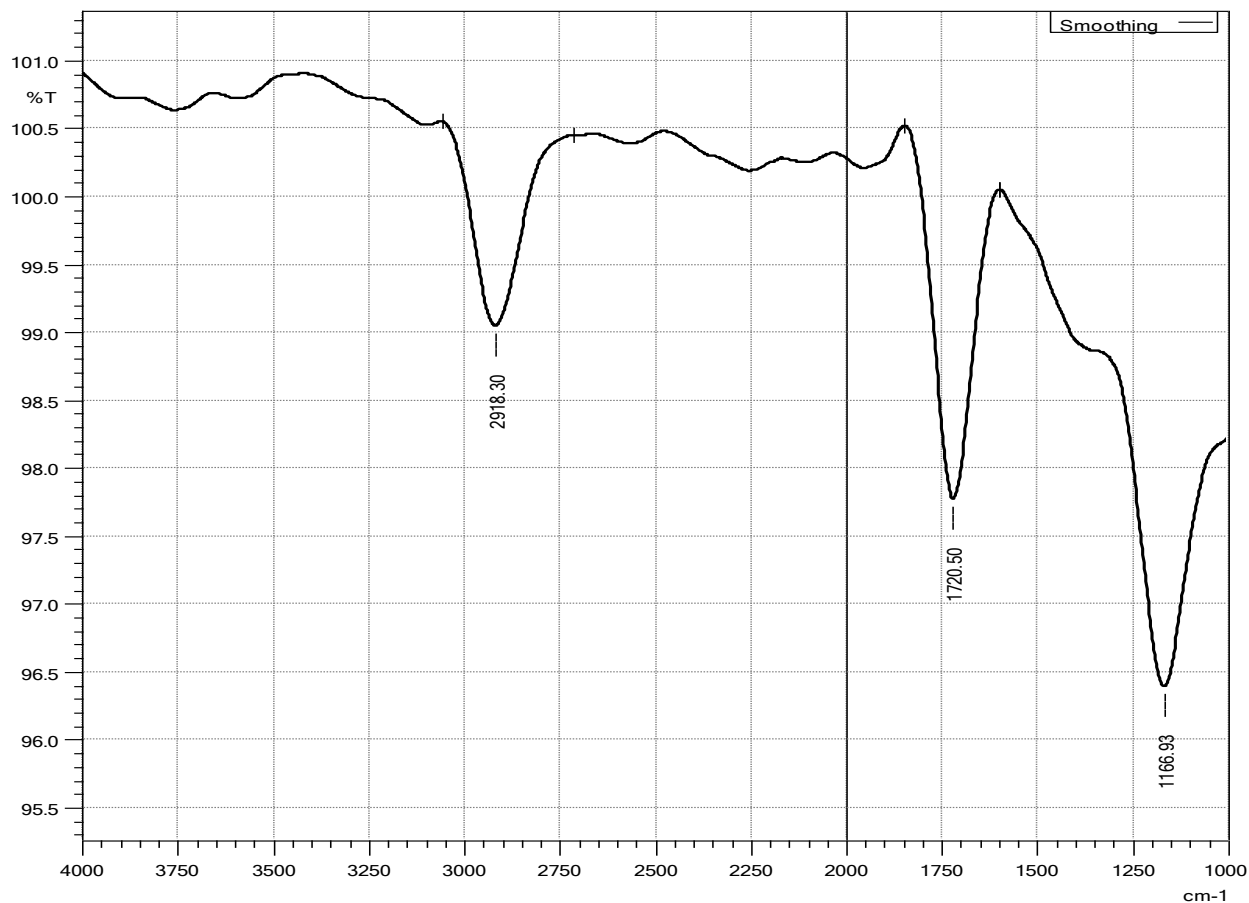


**Figure 4.21:** FTIR spectrum for malachite green loaded PCL-RH blend.

#### **4.5: Batch Experiments for Uptake of Malachite Green on Rice Husks**

The experiments were performed to explore the possible application of rice husks (RH) as an affordable, feasible and sustainable material for uptake of recalcitrant malachite green (MG) from an aqueous media. Parameters that influence the sorption process for instance interaction time, pH, concentration, sorbent dosage and material particle size were examined. Both chemical kinetics and equilibrium models were also studied to provide some insight into the processes involved in the entire sorption reaction.

#### 4.5.1: Determined Maximum Absorption Wavelength of MG

The determined  $\lambda_{\text{max}}$  for malachite green was found to be 620 nm (Fig. 4.22) using a concentration of  $1 \times 10^{-5}$  M to scan through various wavelengths (400 – 700 nm) in the UV-visible spectrophotometer. All other analysis were done at 620 nm and in triplicates.

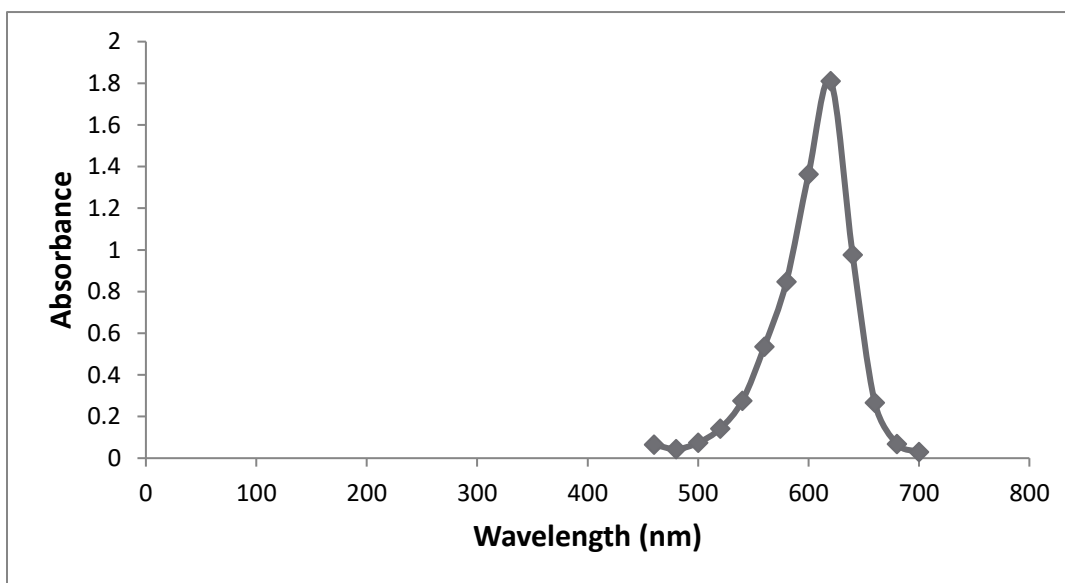


**Figure 4.22:** Maximum absorption curve for malachite green dye

#### 4.5.2: Calibration Curve

Beer -Lambert's law was adopted for the construction of the malachite green calibration curve. A graph of the recorded absorbance ( $\lambda_{620}$  nm) from the spectrophotometer was plotted against the concentration (moles/L) of the prepared standard solutions (Fig. 4.23). The graph was linear with a coefficient of determination of 0.999 and hence it was used to compute the data from the batch adsorption experiments.

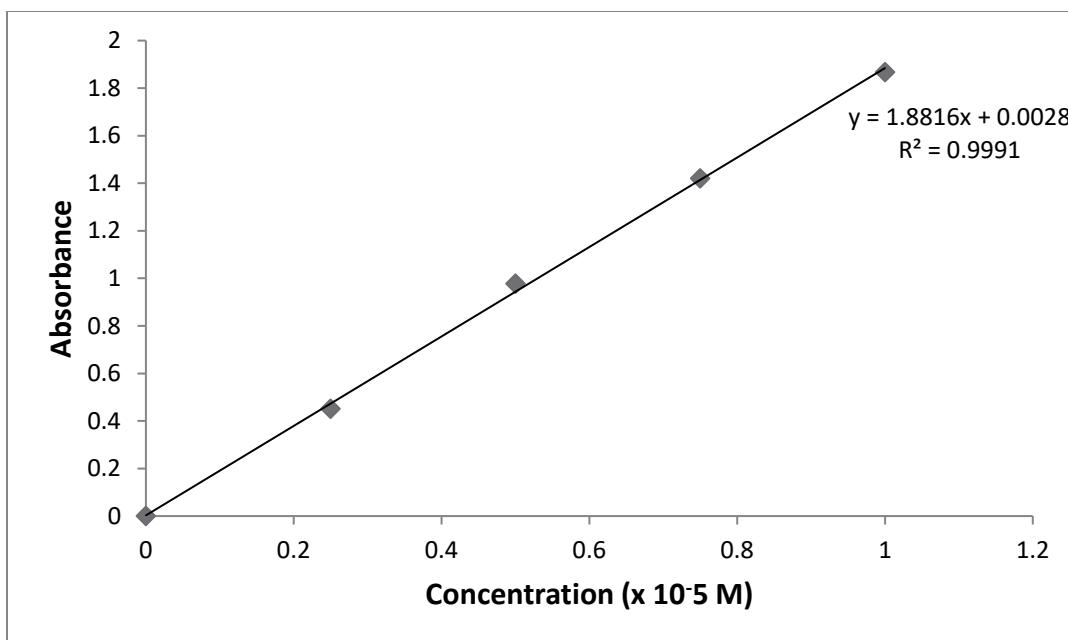


**Figure 4.23:** Malachite green calibration curve

#### 4.5.3: Influence of Interaction Time on Malachite Green Uptake onto Rice Husks

Contact time has a direct influence on sorption kinetics and the overall economic efficacy of the process. The results depicted a rapid uptake (87 %) of the dye within 5 minutes of sorption kinetics using 0.1g of RH and subsequently, an equilibrium for the reaction was achieved at 100 minutes (Fig. 4.24). This trend is imputed to the significant quantity of unoccupied sorption sites accessible for removal of the colorant at the early periods of the reaction. Conversely, as the chemical reaction moved towards equilibrium nearly all the sorption sites were filled with the colorant leading to saturation thus the slow removal process at the plateau stage.

Rapid equilibrium time is suitable for (removal of MG) wastewater treatment since it indicates decreased residence time. Oloo and co-workers (2020) reported similar results for the removal of crystal violet onto *Rhizophora mucronata* biomass. Previous studies by Gündüz & Bayrak (2017) reported a comparable trend for the removal of MG onto pomegranate peel.

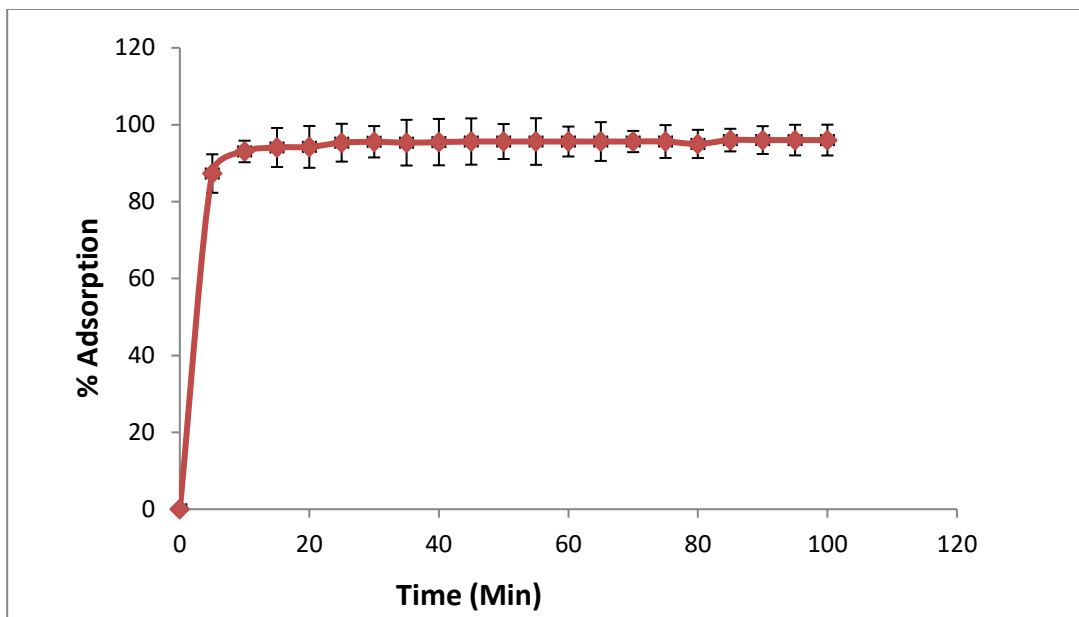


**Figure 4.24:** Influence of interaction time on MG sorption

#### 4.5.4: Influence of Initial Colorant Strength

The impact of the malachite green (MG) strength was explored utilizing colorant concentrations varying from 2.3 to 9.3 mg/L with an optimal RH dose of 0.1g. The (%) uptake of MG by RH reduced from 97.5 to 88.1% after the initial dye strength was raised from 2.3 to 9.3 mg/L (Fig. 4.25). The % decline in sorption is imputed to saturation of all sorption sites of the RH at higher dye concentrations.

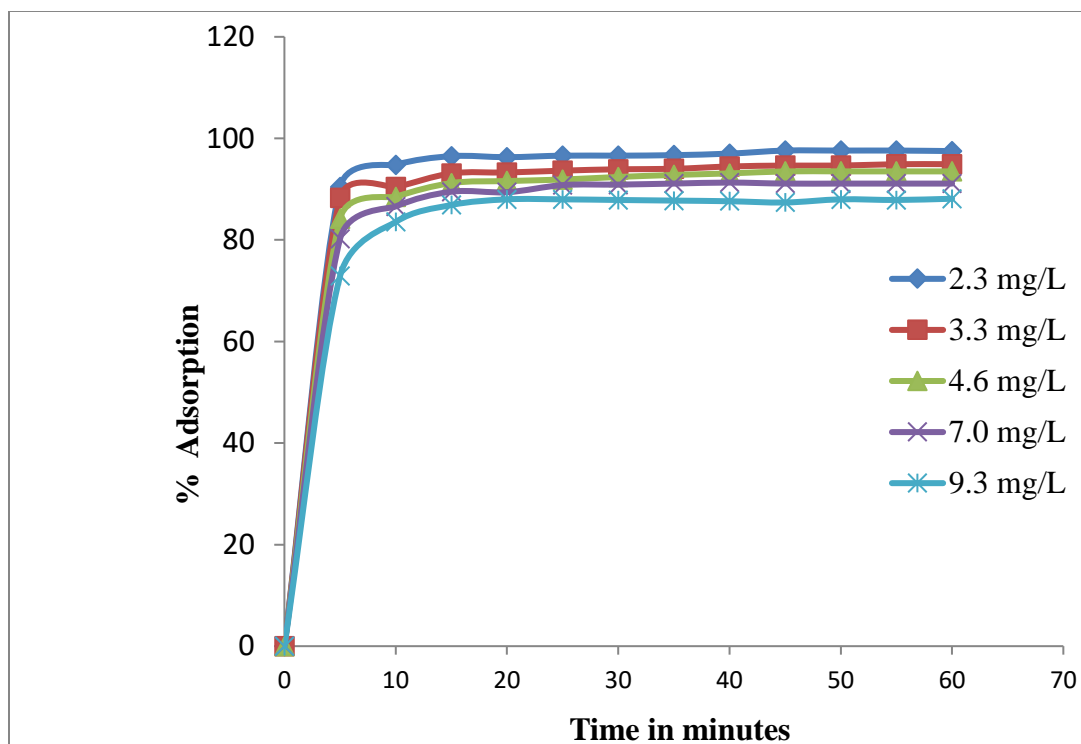


**Figure 4.25:** Variation of % MG adsorbed onto RH as a function of time

#### 4.5.5: Influence of Dosage on Malachite Green Adsorption

Generally, the amount of sorption material influences strongly the adsorbate–adsorbent interactions hence the efficacy of the overall process. In this study, the quantity of rice husks (RH) was varied from 0.1 to 1.5g and 40 cm<sup>3</sup> of 9.3 mg/L MG solution was used for the experiments at 25 °C. At the initial 5 minutes, there was a 74.9 % removal using 0.1g RH which increased steeply to 98.8 % when the amount of dosage was increased to 1.5 g (Fig. 4. 26). The upsurge in MG removal capability is attributed to increased active exchangeable sorption sites which is correlated to surface functional groups on the RH. A comparable trend was reported by Chanzu and co-workers (2019) for the abstraction of Congo red and MG on brewers’ spent grain.

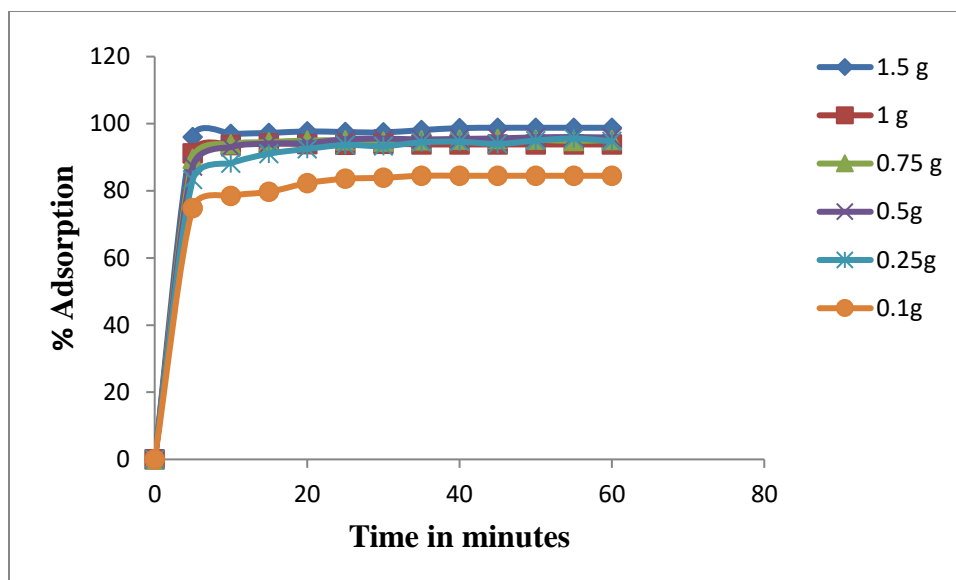


**Figure 4.26:** Plot of % sorption vs time for removal of MG by RH

#### 4.5.6: Effect of Monovalent Ions on Malachite Green Adsorption

Textile wastewater constitutes of substantial quantities of salts that may interfere with the sorption process (Iftekhhar *et al.*, 2018). To gain insight into the sorption kinetics and efficacy, NaCl was used as a model salt with concentrations varying from 0.0125 to 0.1M. There was a considerable reduction in MG removal onto RH with an increase in salt strength (Fig. 4.27). The percentage adsorption capacity decreased from 80.1 to 58.3 % after increasing NaCl quantities from 0 to 4 mL of 1M solution utilized. This phenomenon is attributed to competitive sorption on the surface of the RH due to co-existing ions in the solution. The addition of ions suppresses adsorbate – adsorbent electrostatic interaction owing to the existence of ions ( $\text{Na}^+$ ) having a comparable charge to that of cationic MG. A comparable observation was described for the removal of MG by walnut (Dahri *et al.*, 2014).

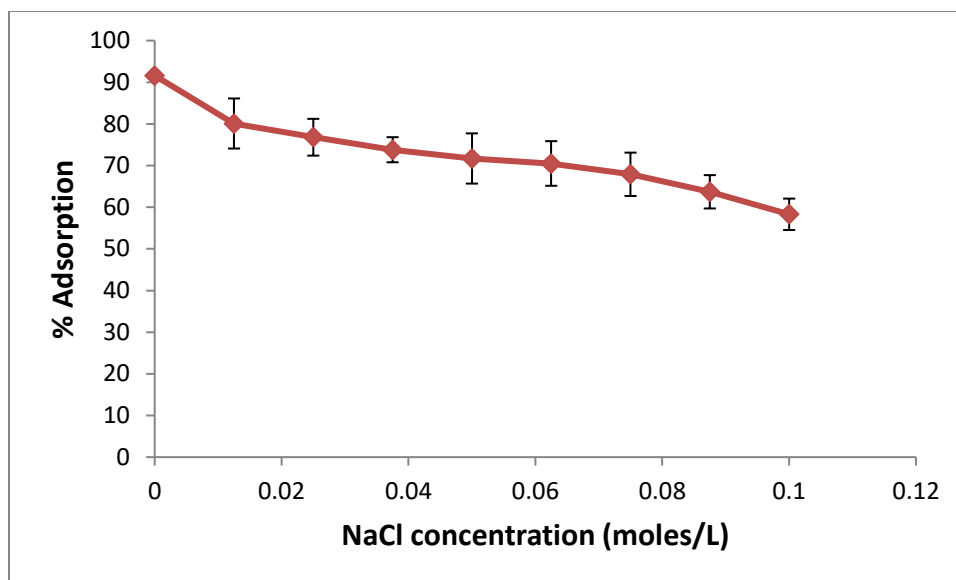


**Figure 4.27:** Variation of % adsorption vs NaCl concentration for removal of MG onto RH

#### 4.5.7: Impact of Rice Husks Particle Size on Malachite Green Adsorption

The impact of sorbent mesh size on removal of MG was investigated by utilizing three distinct sizes (< 300, > 300 < 425, & > 425  $\mu\text{m}$ ). The RH dose was fixed at 0.1 g; the volume of the neutral 9.3 mg/L MG solution utilized for the test was 40 mL while a 200-rpm agitating speed was adopted. The % uptake of MG by RH reduced from 98 up to 95 % after raising the sorbent mesh size from < 300 to > 425  $\mu\text{m}$  (Fig. 4.28). The elevated removal of MG colorant by the smaller RH mesh size (high surface area) is ascribed to the increased accessibility of the sorbent active sites by the MG molecules. Comparable findings were reported by Oloo *et al.*, (2020) for the abstraction of recalcitrant crystal violet colorant from aqueous media by *Rhizophora mucronata* stem-barks.

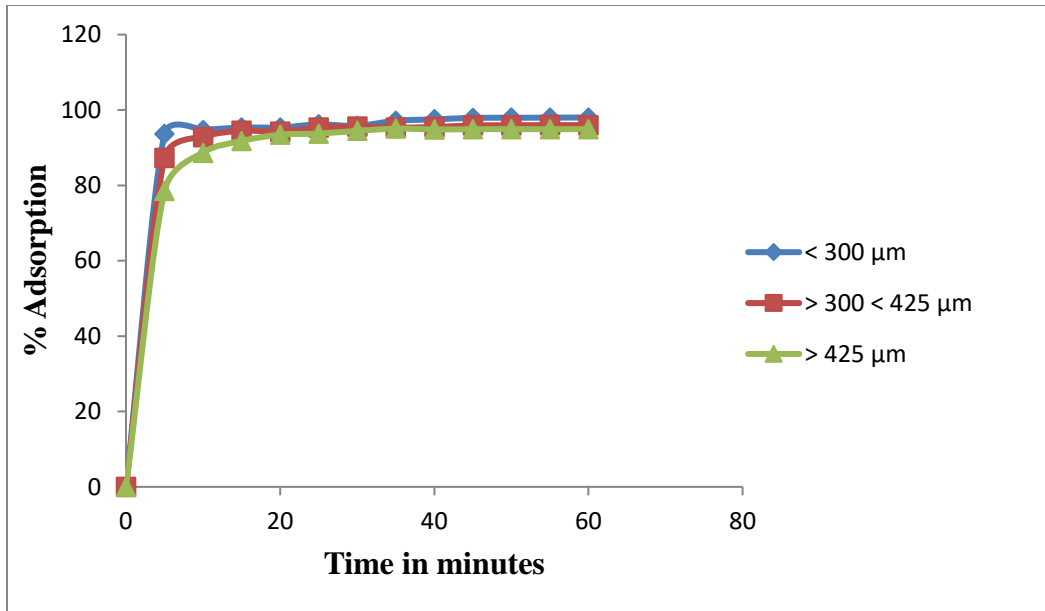


**Figure 4.28:** Impact of RH mesh size on MG uptake

#### 4.5.8: Impact of Solution pH on Malachite Green Uptake by Rice Husks

The MG solution pH impacts the surface charge (Hameed, 2009) of the sorbent material and the extent of ionization of the colorant (Chanzu *et al.*, 2012). In this work, the pH of the tested MG solution ranged from 3 to 9 (Fig. 4.29) as the other sorption factors remained constant. To achieve the required pH, 0.1M HCl and 0.1M NaOH solutions were utilized for specific pH amendments. The % sorption of the colorant increased with an upsurge in pH up to an optimum of pH 7.

For pH values above 7 (neutral), the % removal of the MG reduced and therefore the subsequent tests were performed at pH 7. The reduced uptake of MG by RH at pH 3 to 6 can be ascribed to excess  $H^+$  ions in the solution that compete with the colorant cations for the sorption active sites (Hameed & El- Khaiary, 2008b).

For the pH varying from 8 to 9, the uptake of MG reduced owing to carbinol formation (Appendix 9) due to hydroxylation at the methane carbon at elevated pH where 0% ionization prevails (Das *et al.*, 2009).

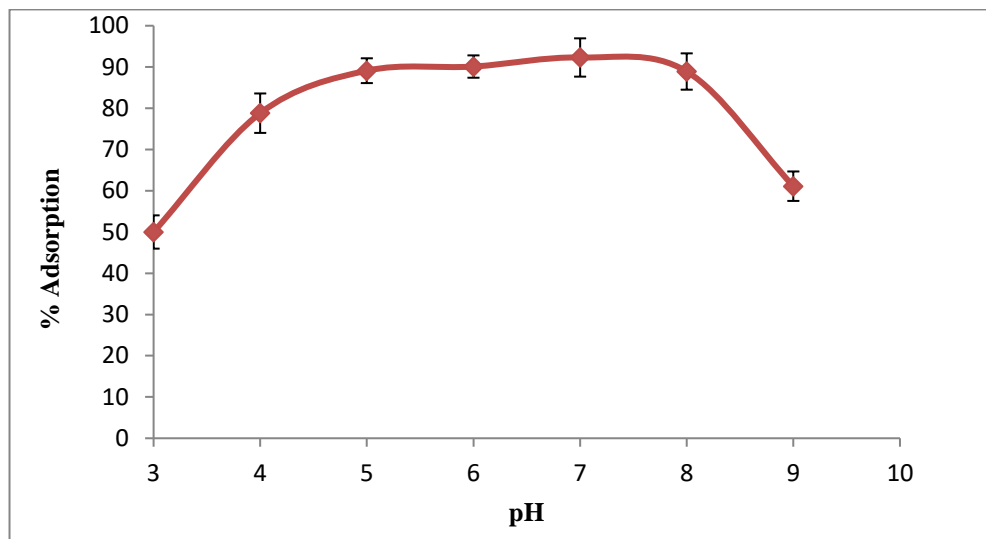


**Figure 4.29:** Impact of solution pH on uptake of MG by RH.

#### 4.5.9: Impact of Agitation Speed on Malachite Green Uptake

The experiment was performed by varying the shaker speed from 50 to 250 rpm. The RH dosage was fixed at 0.1g, mesh size utilized was  $> 300 < 425 \mu\text{m}$ , neutral pH and the quantity of the colorant solution was  $40 \text{ cm}^3$ . The highest uptake (93.4 %) of MG by RH was attained at 200 rpm and then the uptake reduced once the stirring speed was intensified to 250 rpm (Fig. 4.30). Increasing the shaking speed reduced the boundary of the diffusion of MG particles from the bulk solution to the sorbent surface. The results from this work concur with the findings depicted by Crini *et al.*, (2007).

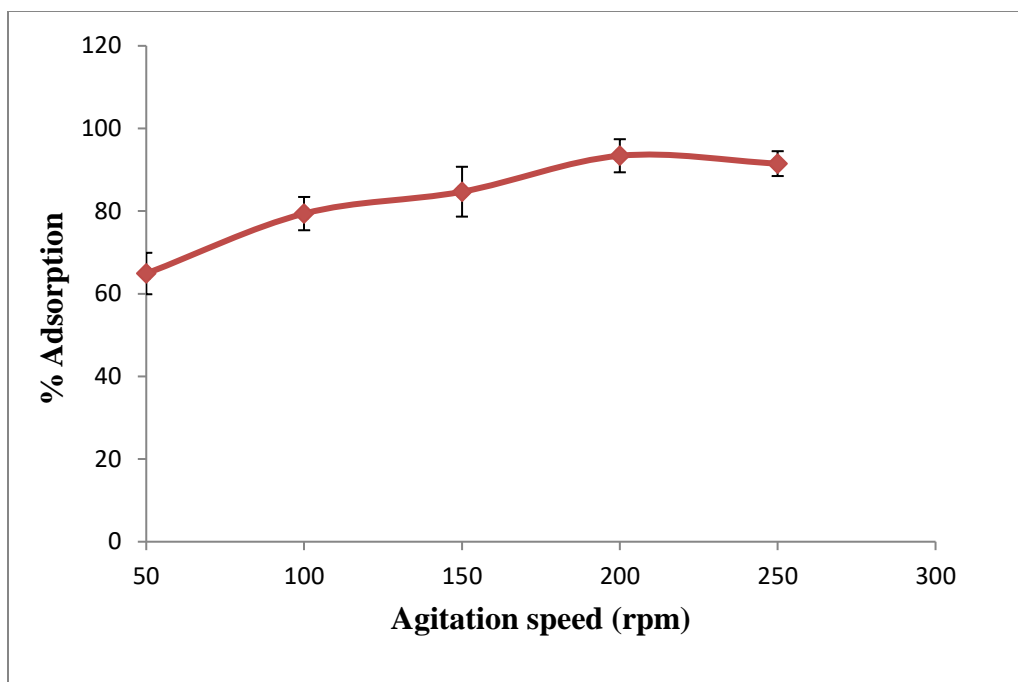


**Figure 4.30:** Impact of shaking rate on sorption of MG on RH

#### **4.5.10: Impact of Temperature on Malachite Green Adsorption**

The temperature of the solution media affects the motion of ions and adsorbate-adsorbent interface performance (Iftekhhar *et al.*, 2018). The current study was performed at temperature ranges of 296.15 to 323.15 K. The % removal of the colorant declined (97.3 to 79.0 %) after raising the solution temperature inferring that the reaction process was exothermic (Fig. 4.31). This phenomenon can be imputed to the decline of sorption strength between the active sites of the RH and MG. Comparable research findings were stated for the abstraction of MG by sugarcane bagasse (Sharma & Nandi, 2013).

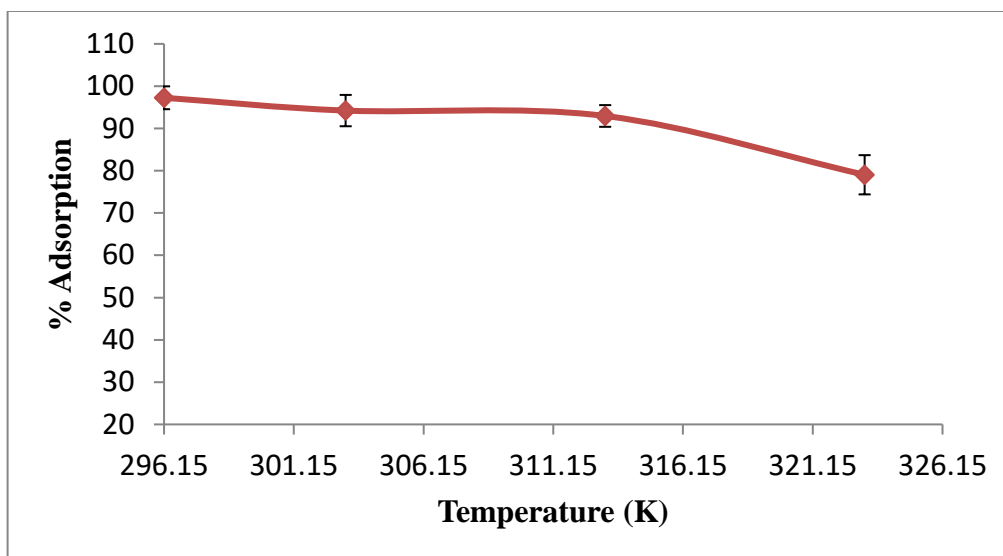


**Figure 4.31:** Influence of temperature for the uptake of MG onto RH adsorbent

#### 4.6: Equilibrium Isotherms for Uptake of MG by RH

The equilibrium data for uptake of MG dye was fitted into three isotherms namely: Langmuir, Freundlich and Temkin.

##### 4.6.1: Langmuir Isotherm for Uptake of Malachite Green

The Langmuir isotherm appropriately described the equilibrium sorption data, with a  $r^2 = 0.97$  (Fig. 4.32) as compared to both Freundlich (Fig. 4.33) and Temkin (Fig. 4.34) isotherms which gave  $r^2$  values of 0.93 and 0.89 respectively. The monolayer sorption capacity from this work was 6.5 mg/g, a value which is greater than the 1.48 mg.g<sup>-1</sup> value reported by Chanzu *et al.*, (2012) for the abstraction of MG by PLA/spent brewery grain films. This implies that the uptake of the MG colorant by RH was through the formation of a monolayer film and thus the interaction between MG particles was negligible (Ofomaja and Ho, 2008). The  $R_L$  value was 0.61 signifying a favorable sorption process (Table 4.2) while the  $K_L$  parameter was 0.28 L mg<sup>-1</sup>.

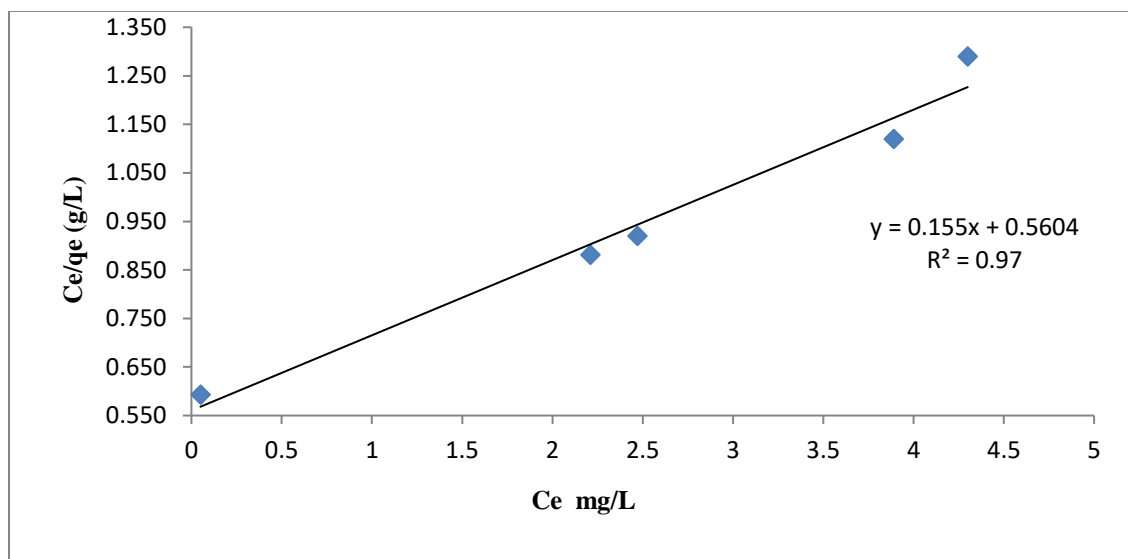


**Figure 4.32:** Langmuir model for the uptake of MG onto rice husks

**Table 4. 2:** Isotherm Values for the Removal of MG by Unmodified Rice Husks

Langmuir model				Freundlich model			Temkin model		
$Q_m$ (mg. g <sup>-1</sup> )	$K_L$ (L.mg <sup>-1</sup> )	$R_L$	$R^2$	$K_F$ (mg. g <sup>-1</sup> )	n	$R^2$	$K_t$	B	$R^2$
6.5	0.28	0.61	0.97	0.43	27	0.93	0.83	0.16	0.89

#### 4.6.2: Freundlich Isotherm for Malachite Green Adsorption

This isotherm presumes a multilayer uptake of adsorbate from an aqueous media by a heterogeneous surface. The Freundlich model was employed to assess the initial colorant concentration data acquired from equilibrium experiments.

Freundlich isotherm graph (Fig. 4.33) gave a  $r^2$  value of 0.93, a value which was lower than that acquired from the Langmuir model plot. From the findings, it was evident that the isotherm was not suitable to illustrate the data since it yielded a reduced maximum uptake capacity (0.43 mg/g) as compared to the Langmuir quantity of 6.5 mg/g (Table 4.2).

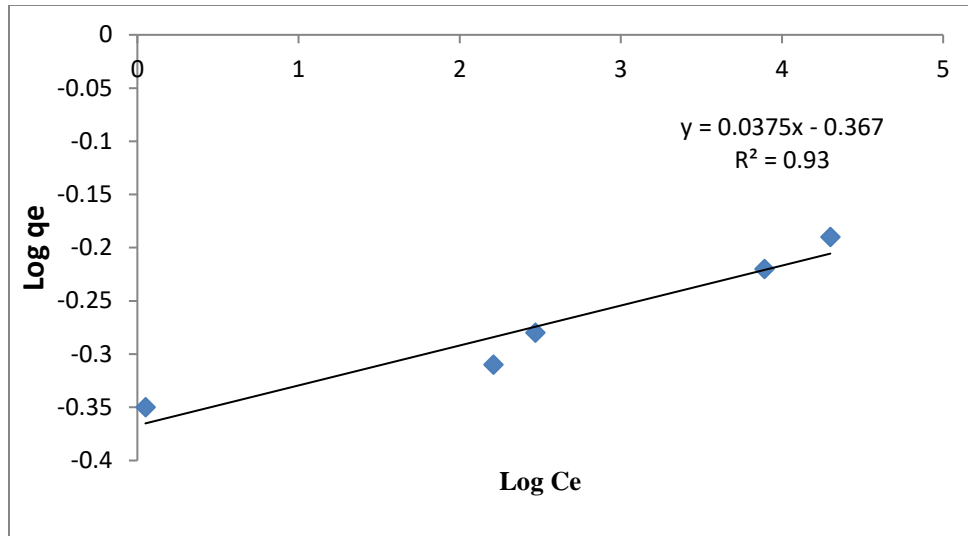


**Figure 4.33:** Freundlich model for the uptake of MG on rice husks

#### 4.6.3: Temkin Isotherm for Malachite Green Adsorption on RH

Figure 4.34 represents the Temkin isotherm. This model gave a  $r^2 = 0.89$  which was the lowest amongst the three isotherms utilized in this work and therefore it was the least appropriate isotherm to illustrate the equilibrium data. Table 4.2 gives the values of the computed constants.

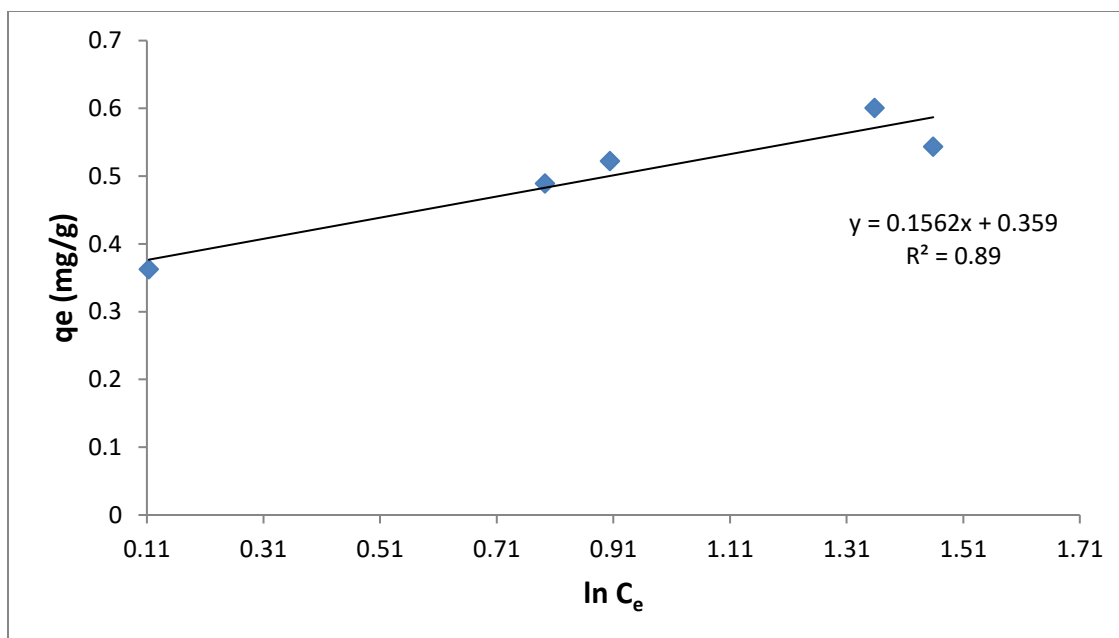


**Figure 4.34:** Temkin isotherm for the uptake of MG onto rice husks

#### **4.7: Kinetic Studies of Malachite Green Adsorption onto RH**

Kinetic modelling was done to evaluate the performance of the RH, the rate-controlling step and the mechanisms involved in the sorption reaction process. The slopes and intercepts (Figs. 4.35 and 4.36) were utilized in computing the rate constants and sorption at equilibrium.

##### **4.7.1: Pseudo- First-Order Rate Kinetics on MG uptake**

The pseudo-first-order (PFO) graph (Fig. 4.35) yielded a  $r^2 = 0.78$ . From the obtained results, it was apparent that the uptake of MG colorant by RH sorbent did not obey the PFO model because no clear conformity between the experimental (Exp  $q_e$ ) and computed ( $q_e$ , cal) sorption capacities was observed (Table 4.3). Moreover, its  $r^2$  value (0.78) was comparatively lower (Fig. 4.35) than the pseudo-second-order (PSO) quantity of 0.987 (Fig. 4.36).

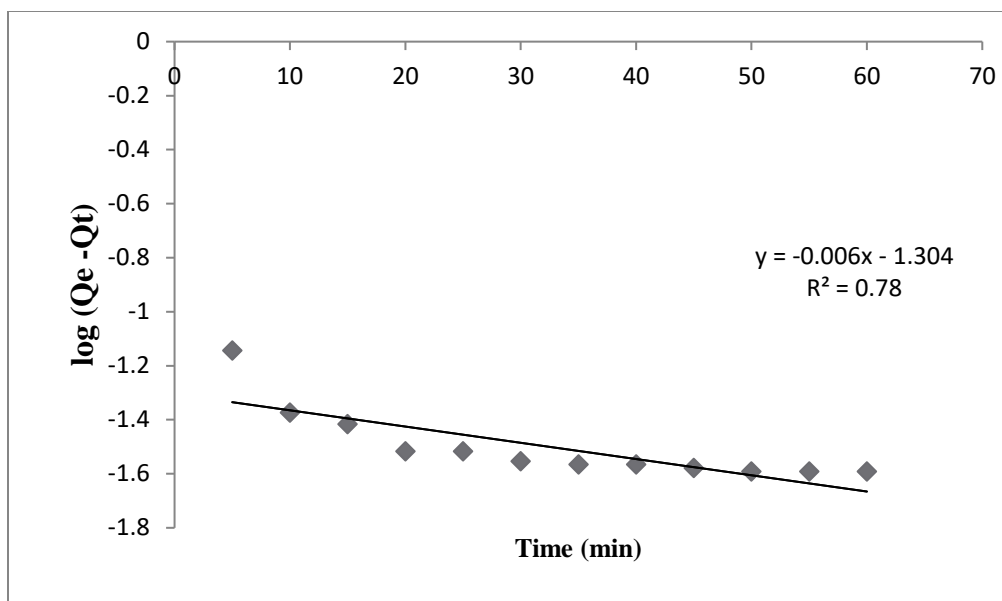


**Figure 4.35:** PFO kinetics graph for the uptake of MG by rice husks

#### 4.7.2: Pseudo- Second - Order Reaction Rate for Uptake of MG on Rice Husks

The equilibrium data was suitably explained by the PSO model with a  $r^2 = 0.987$  (Fig. 4.36) and a  $k_2 = 4.3 \text{ g mg}^{-1} \text{ min}^{-1}$ . The model depicted an excellent correlation between the experimental and computed  $q_e$  (Table 4.3) demonstrating that the sorption experiment obeyed the PSO kinetics than the PFO model. Comparable research findings were described for the abstraction of cationic colorant (methylene blue) from aqueous media by *Eichhornia Crassipes* (Wanyonyi *et al.*, 2013).

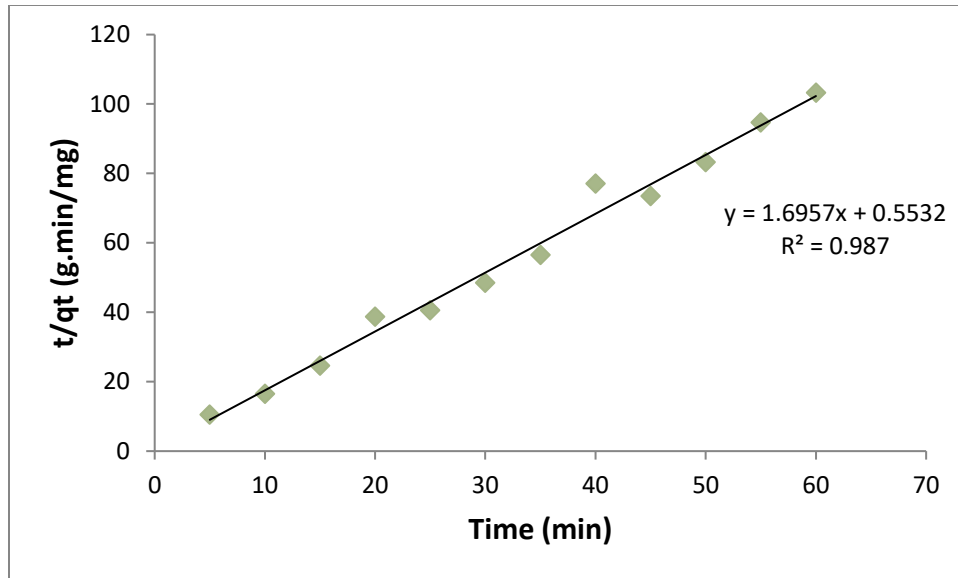


**Figure 4.36:** PSO kinetic reaction for the uptake of MG by RH

#### 4.7.3: Intraparticle Diffusion Model

The Weber (Weber & Chakravorti, 1974) diffusion model was utilized to demonstrate the presence of competing uptake processes in the abstraction of MG by rice husks. In this model, the removal rate of the pollutant is assumed to be directly proportional to  $t^{1/2}$  rather than the interaction time,  $t$  (Sartape *et al.*, 2017). From the graph (Fig. 4.37), the  $r^2$  was 0.966 whereas the  $K_{id}$  was  $0.057 \text{ mg g}^{-1}\text{min}^{0.5}$  with a  $c$  value of 0.303 as determined from the gradient and the intercept of the plot. The line of the graph (Fig. 4.37) did not traverse via the zero-point signifying that intraparticle diffusion was not solely the operating uptake rate mechanism for the abstraction of MG colorant by the RH. Hameed *et al.*, (2008) stated comparable findings for uptake of 2,4,6-trichlorophenol by coconut husk-derived activated carbon.

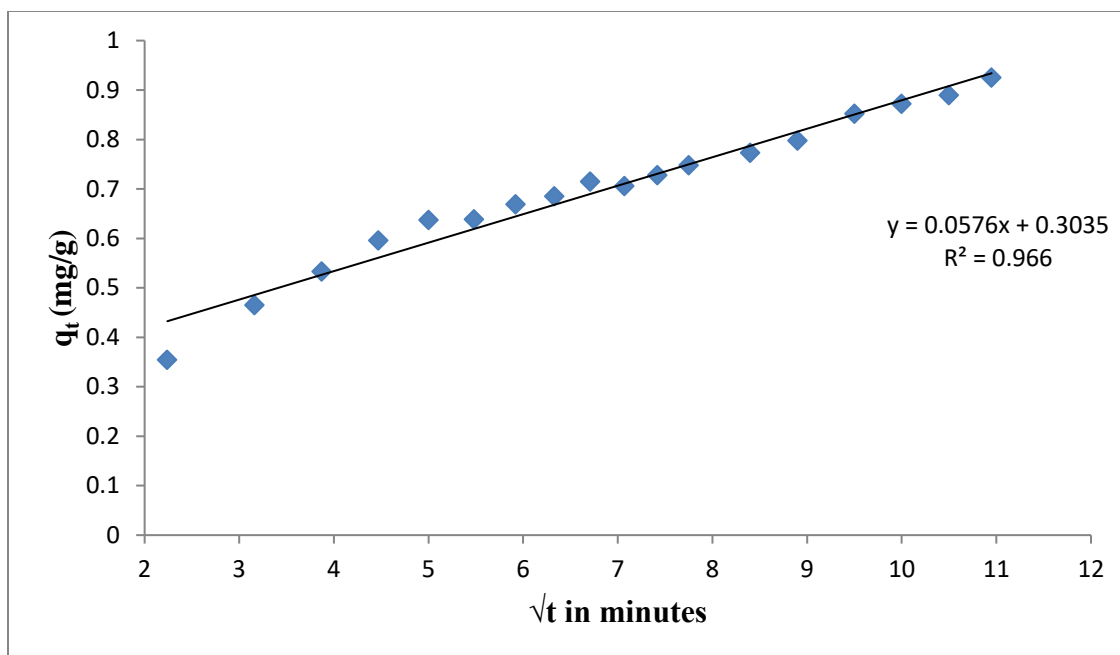


**Figure 4.37:** Intra particle diffusion graph for uptake MG by RH

**Table 4. 3:** Kinetic Rate Values for Sorption of MG by Rice Husks.

Exp $q_e$ , (mgg <sup>-1</sup> )	Pseudo -first order			Pseudo- second - order		
	$q_e$ , cal. (mgg <sup>-1</sup> ) 1)	$K_1$ (min <sup>-1</sup> )	$R^2$	$q_e$ , cal. (mgg <sup>-1</sup> ) 1)	$K_2$ (g mg <sup>-1</sup> min <sup>-1</sup> )	$R^2$
0.622	0.05	0.014	0.78	0.625	4.3	0.986

#### 4.7.4: Thermodynamic Studies

Temperature variations influence the position of the equilibrium for adsorption processes (Shikuku *et al.*, 2018). Figure 4.38 represents the thermodynamic linear plot of the uptake of MG by the RH material. The computed thermodynamic quantities are given in Table 4.4. The negative quantity of  $\Delta G$  at all temperatures denotes a viable and spontaneous process whereas the negative quantity of  $\Delta H$  implies that the removal rate was exothermic. Further, the positive quantity of  $\Delta S$  is an indication of increased randomness of the uptake process (Hameed *et al.*,

2007) and a good affinity of MG towards the rice husks. The activation energy,  $E_a$  was obtained from the slope of the linear plot of  $\ln K_d$  vs  $1/T$  and it was found to be  $56.2 \text{ kJmol}^{-1}$  thus confirming that the uptake of MG by the RH was a chemisorption process.

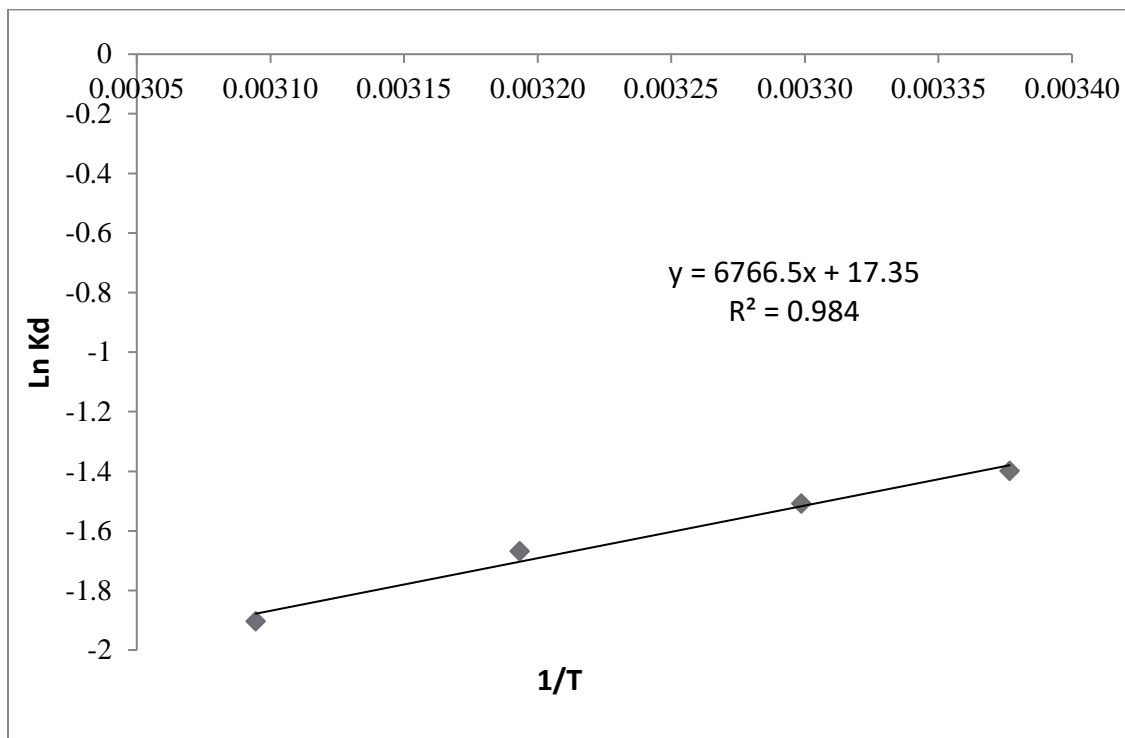


**Figure 4.38:** Thermodynamic graph of removal of MG by RH material

**Table 4.4:** Activation Energy and Thermodynamic Values for MG Uptake by RH

$E_a$ ( $\text{kJmol}^{-1}$ )	Temp (K)	Removal %	$\Delta G$ ( $\text{kJmol}^{-1}$ )	$\Delta H$ ( $\text{kJmol}^{-1}$ )	$\Delta S$ ( $\text{kJmol}^{-1}\text{K}^{-1}$ )
56.2 $\text{kJmol}^{-1}$	296.15	97.3	-99.23	-56.3	0.14
	303.15	94.2	-90.14		
	313.15	93	-78.76		
	323.15	79	-56.16		

## 4.8: Batch Adsorption Experiments for Chitosan- ZnO Material

### 4.8.1: Impact of Dye Concentration

The concentration of the colourant was varied from 2.3 to 9.3 mg/L, while the quantity of chitosan-ZnO composite adsorbent was 0.6 g. The greater the dye strength, the lesser the quantity of adsorbed dye (Fig. 4.39). The maximum removal of 98.5% was attained with a MG concentration of 2.3 mg/L whereas a concentration of 9.3 mg/L gave 66.1 % adsorption. The uptake efficacy reduced with the increasing initial MG concentration because all the sorbent surface was loaded with the colourant particles (Alqadami *et al.*, 2018).

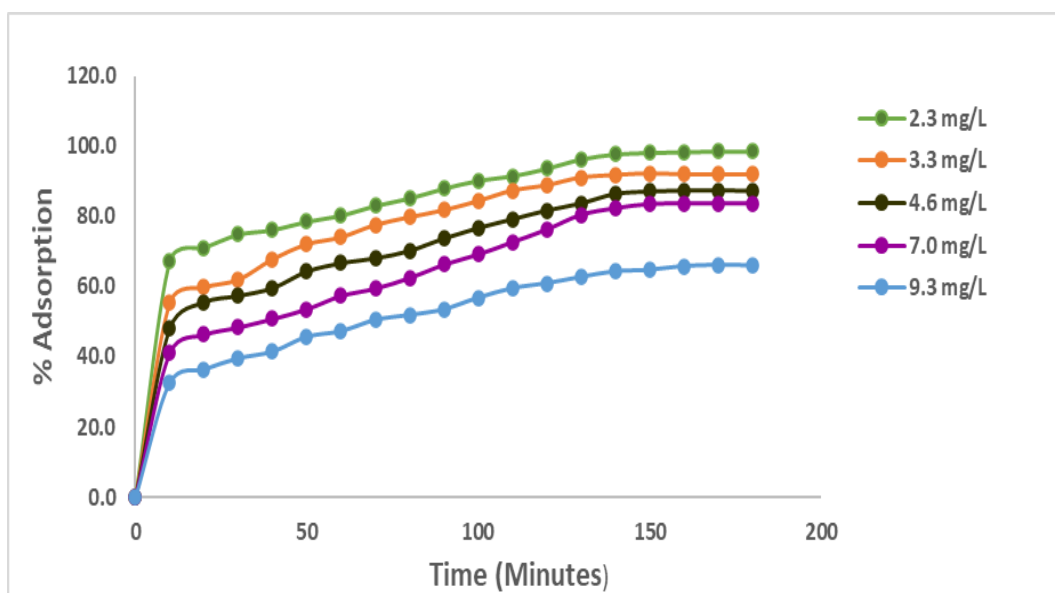


**Figure 4.39:** Impact of initial dye concentration on the % sorption of MG.

### 4.8.2: Impact of Interaction Time

The impact of interaction time was investigated by utilizing 0.6 g of sorbent and 40 mL of 9.3 mg/L solution. The uptake of MG by CS-ZnO sorbent was rapid in the initial steps of the chemical reaction and gradually decreased as it approached equilibrium (Fig. 4.40). The reaction

equilibrium was realized in 180 minutes with a 80.1% removal. The detected trend is imputed to the significant quantity of vacant active sorbent sites accessible for abstracting the colourant at the initial phases and as the experiment began to stabilize, all the active sites were covered up by the MG particles hence the reduced uptake process (Bulut *et al.*, 2008).

On the other hand, the abstraction of MG by pure chitosan gave a 59.7 % adsorption (Fig. 4.40). The lower removal value (59.7 %) of MG by the plain CS is ascribed to fewer sorption sites available for adsorption. The higher colorant removal by the nanocomposite compared to the plain CS was ascribed to the joint effect of the sorption process by the nanocomposite and the photodegradation effect by the ZnO nanoparticles.

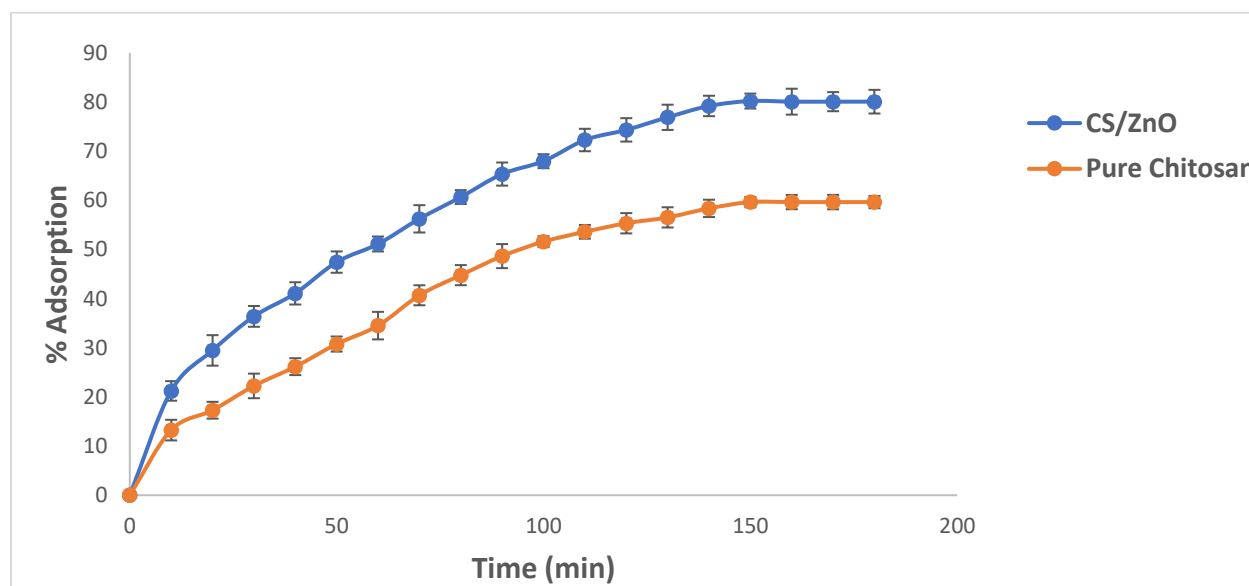


**Figure 4.40:** Influence of interaction time on MG abstraction onto plain chitosan and CS-ZnO materials.

#### 4.8.3: Impact of CS-ZnO Dose

The amount of sorbent utilized ranged from 0.4 to 1.2 g in 40 mL of 9.3 mg/L of the colourant solution at a neutral pH. The fraction of removed MG colourant increased with a cumulative

sorbent amount due to intensified uptake sites (Fig. 4.41). For example, 1.2 g yielded a 93.6% MG uptake in comparison to 0.4 g which produced a 67.4 % uptake. Similar findings were depicted for the abstraction of MG from aqueous solution on activated carbon (AC) produced from low-priced material (Santhi *et al.*, 2010). For successive experiments, 0.6 g of the CS-ZnO material was utilized.

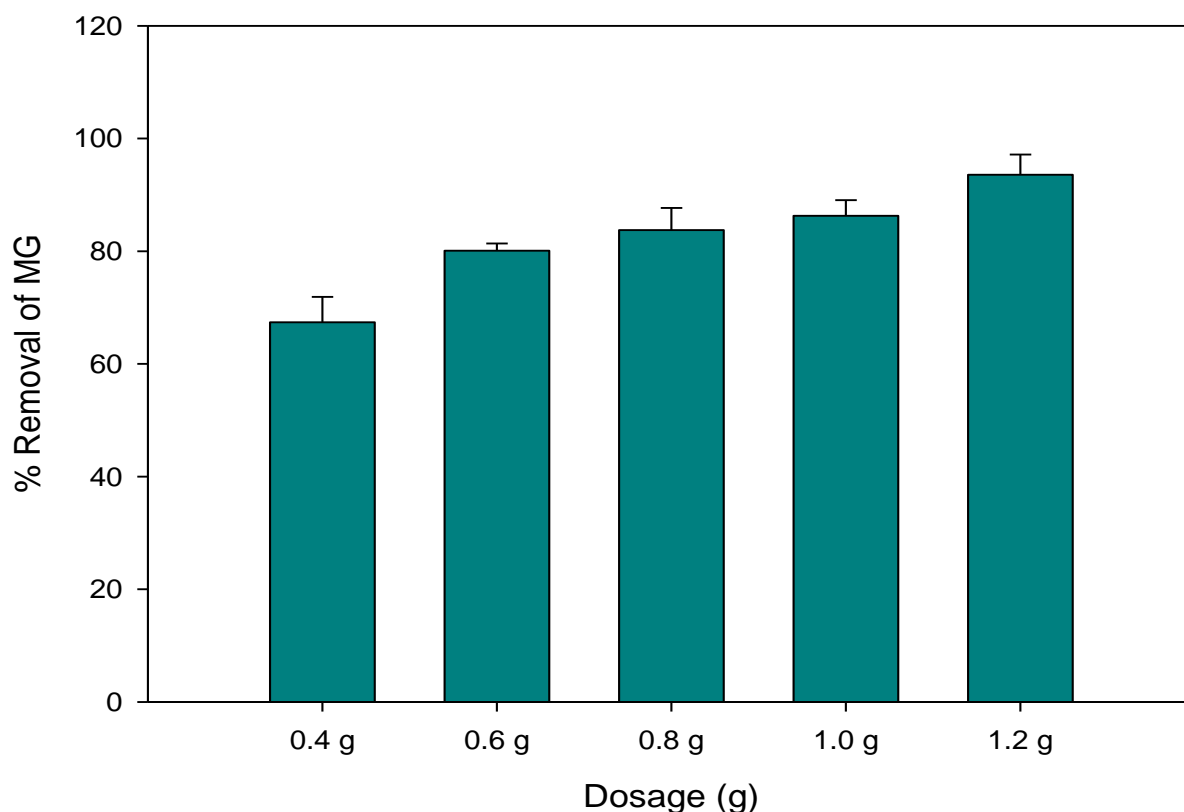


**Figure 4.41:** Influence of dosage on uptake of MG on CS-ZnO composite.

#### 4.8.4: Influence of pH

The uptake of malachite green by the ZnO-based nanocomposite material varies with the solution pH. The pH influences the scope of ionization and speciation of adsorbate material

(Kumar *et al.*, 2017). The fate of MG contaminant in the ecosystem is impacted by its pka (6.9) (Singh *et al.*, 2016) because its steadiness fluctuates with pH and therefore the uptake tests in this work were achieved at pH varied from 3 to 8 where the colorant is stable and exists in its typical green colour (Nghah & Fatinathan, 2008).

When the pH is low, there is protonation of amino (-NH<sub>2</sub>) surface groups (Equation 4.1) of CS hence raising the pH of the solution (Dotto & Pinto, 2011). The decrease in abstraction rate for the colorant which was evidenced at pH 3 (59.8 %) is imputable to unsteady CS molecules at subdued pH.



The highest percentage adsorption (98.6 %) was realized at pH 8 (Fig. 4.42). In a basic medium (pH > 6), a reduction in positive charge of CS amine surface groups may arise due to surplus -OH molecules, which might cause deprotonation and consequently, the surface charge of CS material develops a negative charge (Nghah *et al.*, 2006). This phenomenon leads to an electrostatic pull between the positively charged malachite green and oppositely charged ions of chitosan, due to the excess <sup>-</sup>OH molecules (Nghah & Fatinathan, 2008). Conversely, at pH > 10 (characterized by 0 % ionization) hydroxylation commences resulting to the production of a colorless carbinol (Appendix 9) thus the diminished removal capacity of the MG colorant (Das *et al.*, 2009).

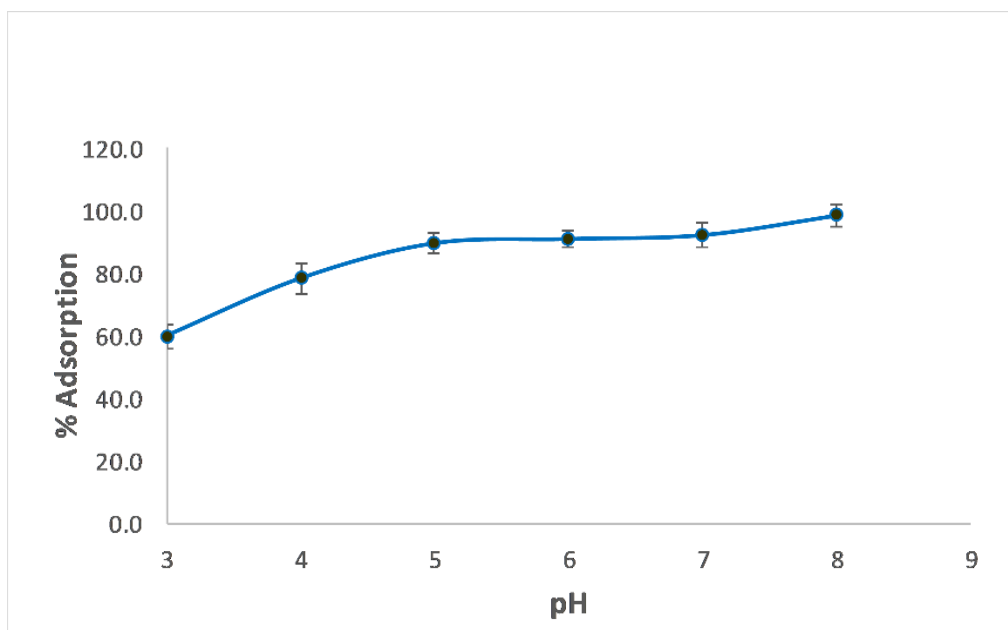


**Figure 4.42:** Influence of pH on the abstraction of malachite green on CS-ZnO composite.

#### **4.9: Equilibrium Isotherms for Removal of MG by the Chitosan-ZnO Sorbent**

To explore the most suitable isotherm for the data, three commonly known models were utilized i.e. Langmuir, Freundlich and Temkin sorption isotherms.

##### **4.9.1: Langmuir Model for the Uptake of MG by CS-ZnO Material**

From the  $r^2$  quantity of 0.998, it is apparent that the Langmuir model (Fig 4.43) suitably illustrated the equilibrium data effectively than the Freundlich and Temkin isotherms which yielded  $r^2$  values of 0.973 and 0.951 correspondingly. The monolayer adsorption capacity ( $q_m$ ) was 11 mg/g, a value which is larger than 3.55 mg/g described by Beak and collaborators for the uptake of MG by poultry chicken feathers (Beak *et al.*, 2009).

The  $R_L$  value for the present study was 0.49 at 25 °C, suggesting a favourable abstraction of the MG onto CS-ZnO because it is below one (unity). The value of  $K_L$  was found to be 0.57 L/mg.

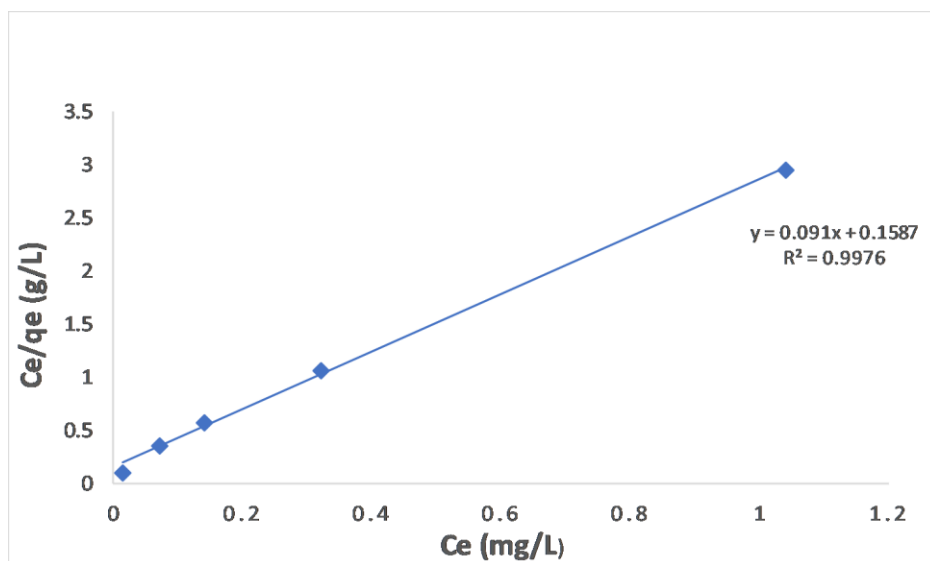


**Figure 4.43:** Langmuir model for the abstraction of MG by chitosan-ZnO composite.

#### 4.9.2: Freundlich Model for Uptake of MG on CS-ZnO Nanocomposite

This is an experimental expression based on the formation of a multilayer film during the uptake process (Liu *et al.*, 2012).

The  $K_f$  quantity was found to be 0.37 mg/g, a figure that is lesser than the Langmuir model one (11 mg/g). Furthermore, the  $n$  value from this study was greater than one thus demonstrating a powerful correlation between MG and the CS-ZnO sorbent material. Although the  $r^2$  for the linearized Freundlich plot was high (0.97), It was still lower than the Langmuir one of 0.998. This implies that the Freundlich model did not describe the equilibrium sorption data appropriately.

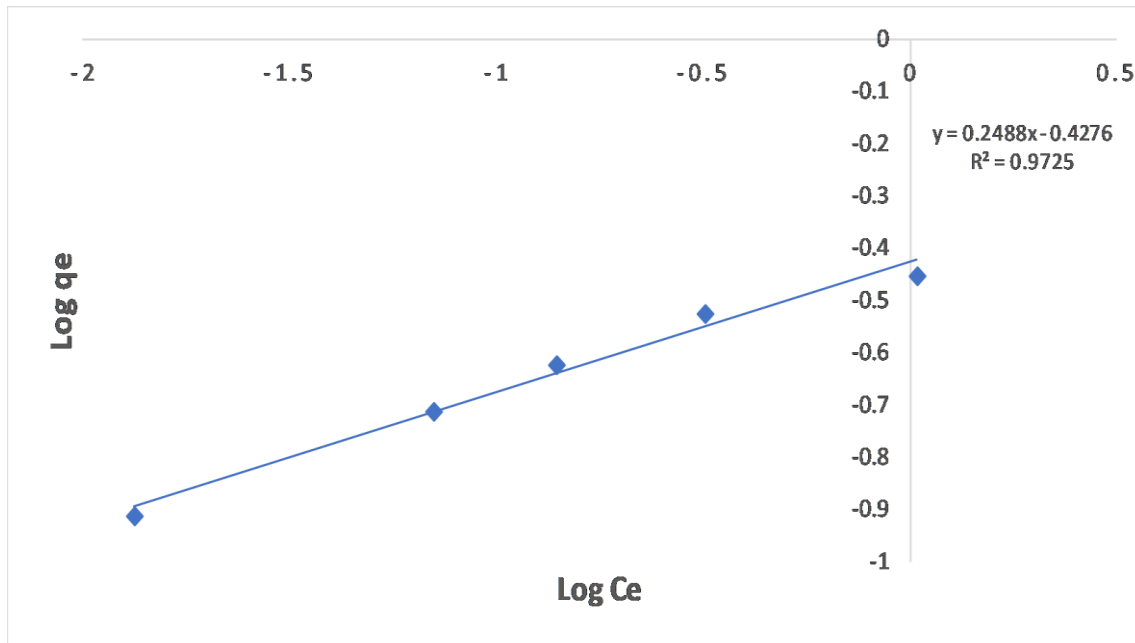


**Figure 4.44:** Freundlich sorption model for the uptake of MG on CS-ZnO composite.

#### 4.9.3: Temkin Uptake Model

This isotherm deduces that the reduction in the heat of uptake obtained is linear instead of logarithmic (Dotto & Pinto, 2011). The model yielded the lowest  $r^2$  ( $r^2 = 0.951$ ) value in relation to both Langmuir and Freundlich isotherms (Table 4.5). These findings unveil that the Temkin model was the least appropriate (Fig. 4.45) to elucidate the uptake equilibrium data of the MG colorant on CS – ZnO sorbent. The  $K_t$  and  $B$  values were found to be 1.91 and 0.54 respectively.

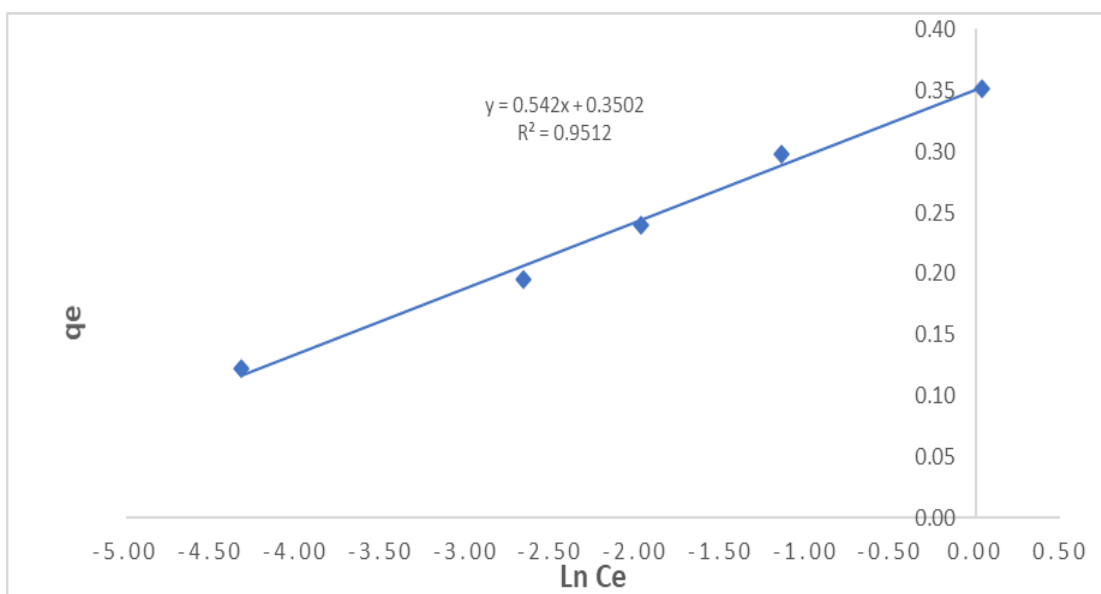


**Figure 4.45: Temkin model for the abstraction of MG dye onto CS-ZnO composite**

**Table 4. 5:** Isotherm values for the abstraction of MG by CS-ZnO composite

Langmuir model				Freundlich model			Temkin model		
$Q_m$ (mg. g <sup>-1</sup> )	$K_L$ (L.mg <sup>-1</sup> )	$R_L$	$R^2$	$K_F$ (mg. g <sup>-1</sup> )	n	$R^2$	$K_t$	B	$R^2$
11	0.57	0.49	0.998	0.37	4.01	0.973	1.91	0.54	0.951

#### 4.10: Kinetic Modelling for Uptake of MG by CS-ZnO Composite

##### 4.10.1: Mechanism for Adsorption of MG onto CS-ZnO Material

To obtain some understanding of both the mechanisms and chemical rate reactions for the uptake of malachite green by the CS-ZnO sorbent, the chemical reaction data was fitted into pseudo-first-order (PFO) (Ho & McKay, 1998) and pseudo-second-order (PSO) (Ho & McKay, 1999) rate models. The  $K_1$  and  $K_2$  rate constants for the models were computed from the gradients of the corresponding linearized graphs and are provided in table 4.6. The suitability of the kinetic model was determined by obtained  $r^2$  values. Even though the maximum uptake capacities ( $q_e$ ) for both experimental (0.51 mg/g) and computed (0.59 mg/g) figures for the PFO model

corresponded perfectly (Table 4.6), they were conversely lesser than the  $q_e$  of PSO (6.71 mg/g) model. It was apparent that the uptake reaction agreed appropriately to the PSO chemical rate with a  $r^2$  of 0.98 (Fig: 4.47) which was higher than the PFO one (Fig. 4.46). The study outcome unveiled that chemisorption was the reaction-controlling step with a possible electron exchange between the MG particles and CS-ZnO uptake material (Nodeh *et al.*, 2016). Comparable research findings were described by Hameed, (2009) for the uptake of methylene blue dye onto grass waste.

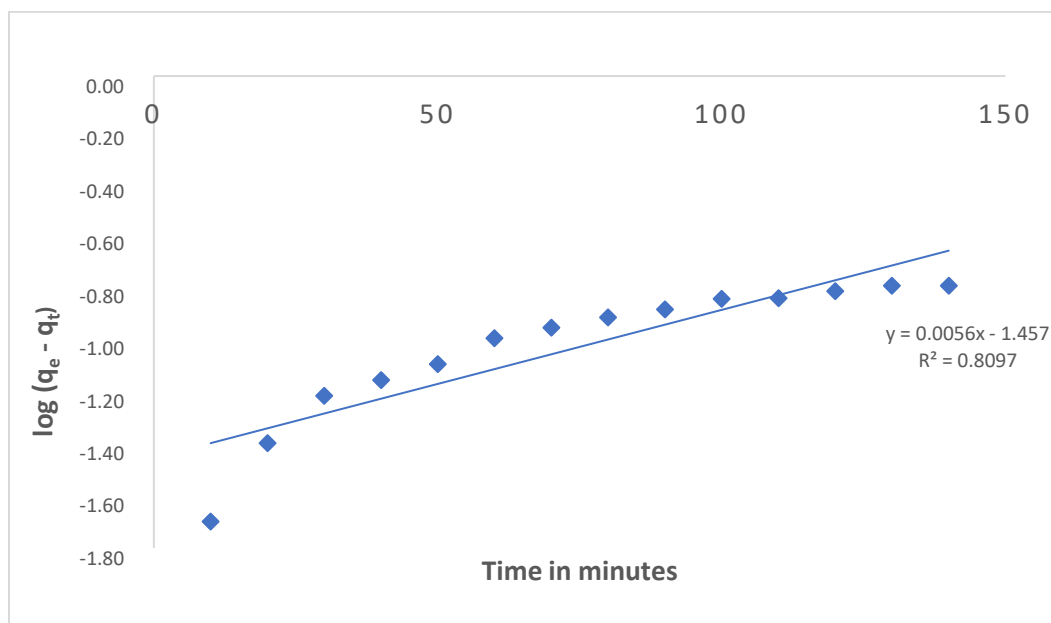


**Figure 4.46:** PFO kinetics graph for the abstraction of MG by CS-ZnO nanocomposite

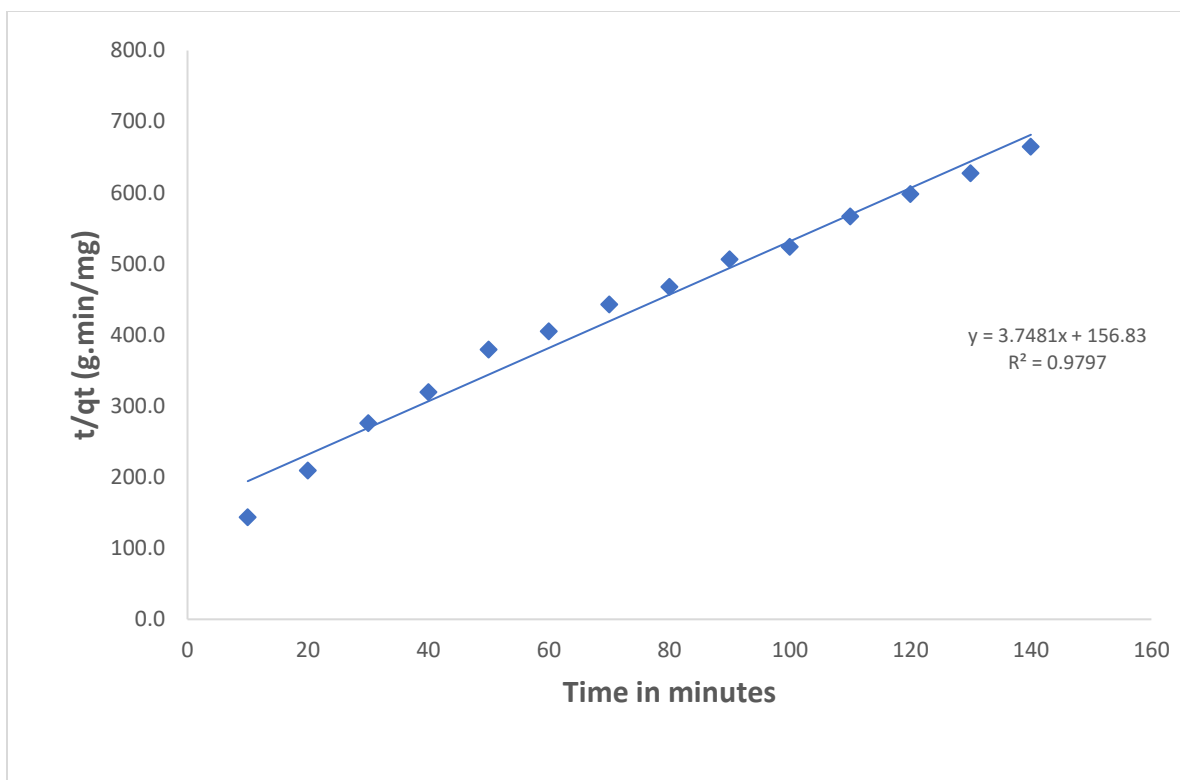


**Figure 4.47:** Second-order rate graph for removal of MG on CS- ZnO

#### 4.10.2: Intra- Particle Diffusion Rate Model for Uptake of MG on CS-ZnO Material

From the graph (Fig. 4.48), it is clear that the plotline did not cross through the origin ( $C = 0$ ) of the graph thus signifying that the intraparticle diffusion model was not controlling the uptake process exclusively (Saha *et al.*, 2010). It can be concluded that the model was operating simultaneously with other mechanisms e.g. film diffusion (Stavrinou *et al.*, 2018) for the abstraction of MG on CS-ZnO biosorbent material.

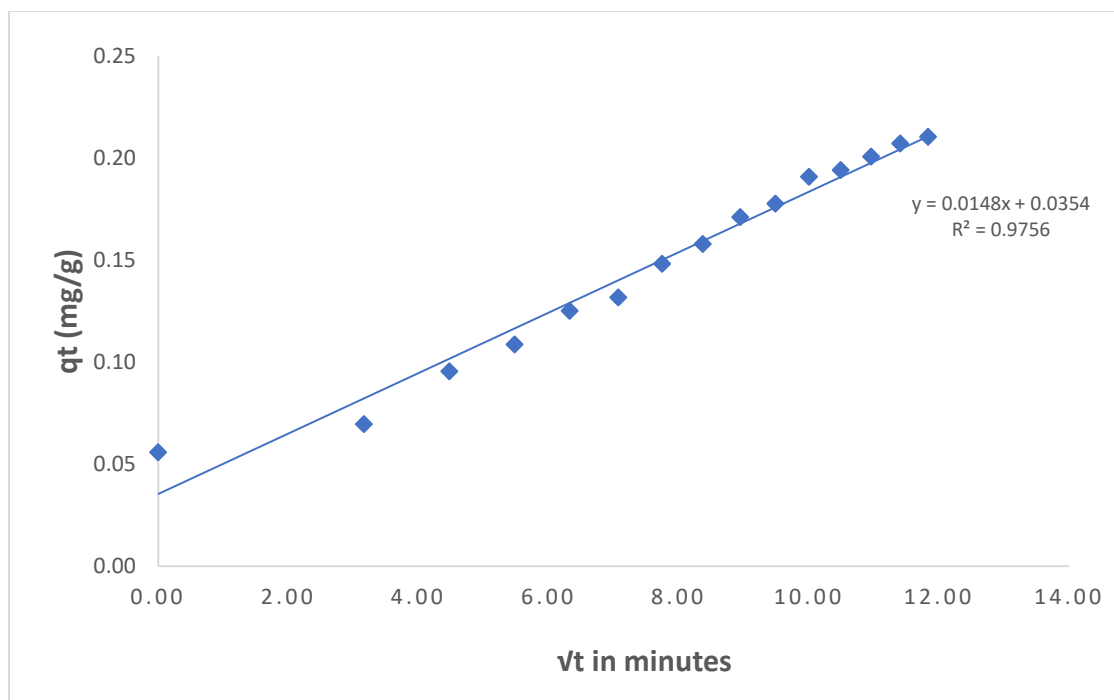


**Figure 4.48:** Intraparticle diffusion plot for biosorption of MG on CS – ZnO material

**Table 4. 6:** Chemical Kinetics Values for the Abstraction of MG by CS-ZnO nanomaterial

Pseudo- first-order				Pseudo-second-order		
$\text{Log}(q_e - q_t) = \text{log } q_e - K_1 t / 2.303$				$t/q_t = 1/K_2 q_e^2 + 1/q_e t$		
Exp $q_e$ (mg/g)	$q_e$ cal (mg/g)	$K_1$ (min <sup>-1</sup> )	$R^2$	$q_e$ (mg/g)	$K_2$ (g/mg.min)	$R^2$
0.51	0.59	0.013	0.81	6.71	0.040	0.98

#### 4.11: Batch Uptake for MG on Poly( $\epsilon$ -Caprolactone)-Rice Husks (PCL-RH) Blend Films

##### 4. 11.1: Impact of Dose on the Uptake of MG on PCL-RH

The bio sorbent quantity ranged from 0.1 to 0.5 g versus a fixed dye amount of 40 mL, pH 7 and fixed dye concentration of 9.3 mg/L. It is evident that as the amount of PCL-RH (*1:1 ratio*) was increased, the % uptake of the colorant also increased owing to the increase of vacant uptake

sites on the sorbent plane. The highest uptake of 99 % of the MG was achieved within an equilibration time of 150 minutes (Fig.4.49).

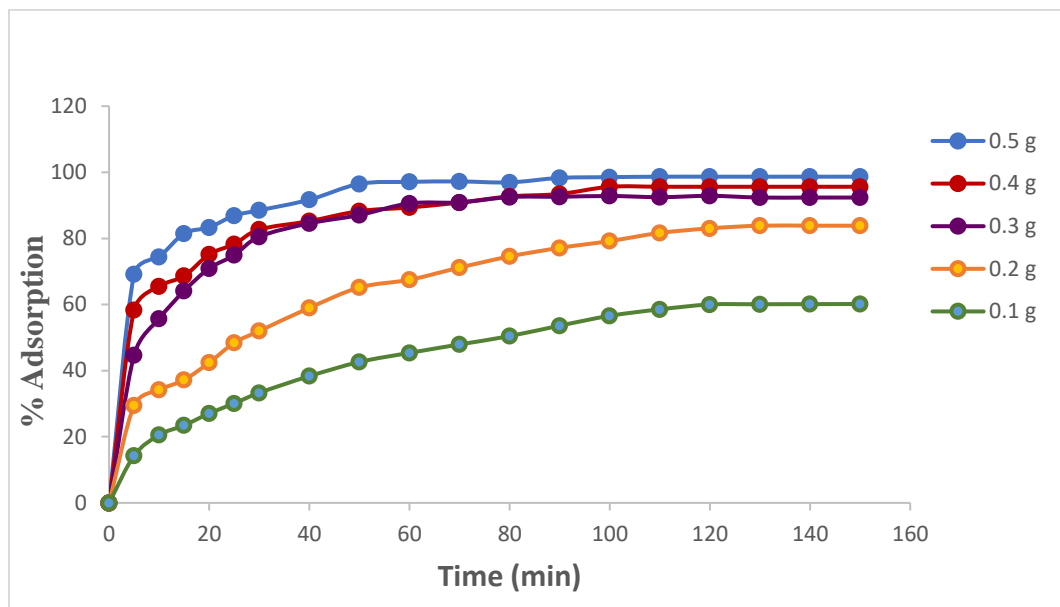


**Figure 4.49:** Impact of dose on % abstraction of MG on PCL-RH film blend

#### 4.11.2: Impact of Interaction Time on the Abstraction of MG by Plain PCL and PCL-RH Materials

The time required for a reaction to reach equilibrium is essential when designing batch experiments for wastewater treatment. Contact time measurements were done using 0.3 g of PCL-RH films. The adsorption rate of MG by PCL-RH (*1:1 ratio*) rose rapidly with an upsurge in time up to 80 minutes with a maximum % adsorption of 93 % indicating strong adsorbent-adsorbate interactive forces (Mohammad & Rahbar-kelishami, 2015). Further increase in sorption time did not improve the removal efficacy of the dye but it only led to the attainment of the reaction equilibrium at 150 minutes. (Fig. 4.50). The fast removal rate in the initial stages is imputed to the accessibility of vacant uptake sites on the PCL-RH plane by the dye molecules.

At the final stages, most of the adsorption sites were already saturated with the dye hence the reduced uptake rate of the colorant (Njoku *et al.*, 2015). On the other hand, 0.3 g of the plain PCL gave a 62.1 % removal for the MG dye (Fig. 4.50). The low removal rate by the pure PCL material is imputed to the limited number of available sorption sites on its surface. Chanzu *et al.*, (2012) also demonstrated a similar phenomenon (low removal) for the uptake of MG by plain polylactide (PLA) film material.

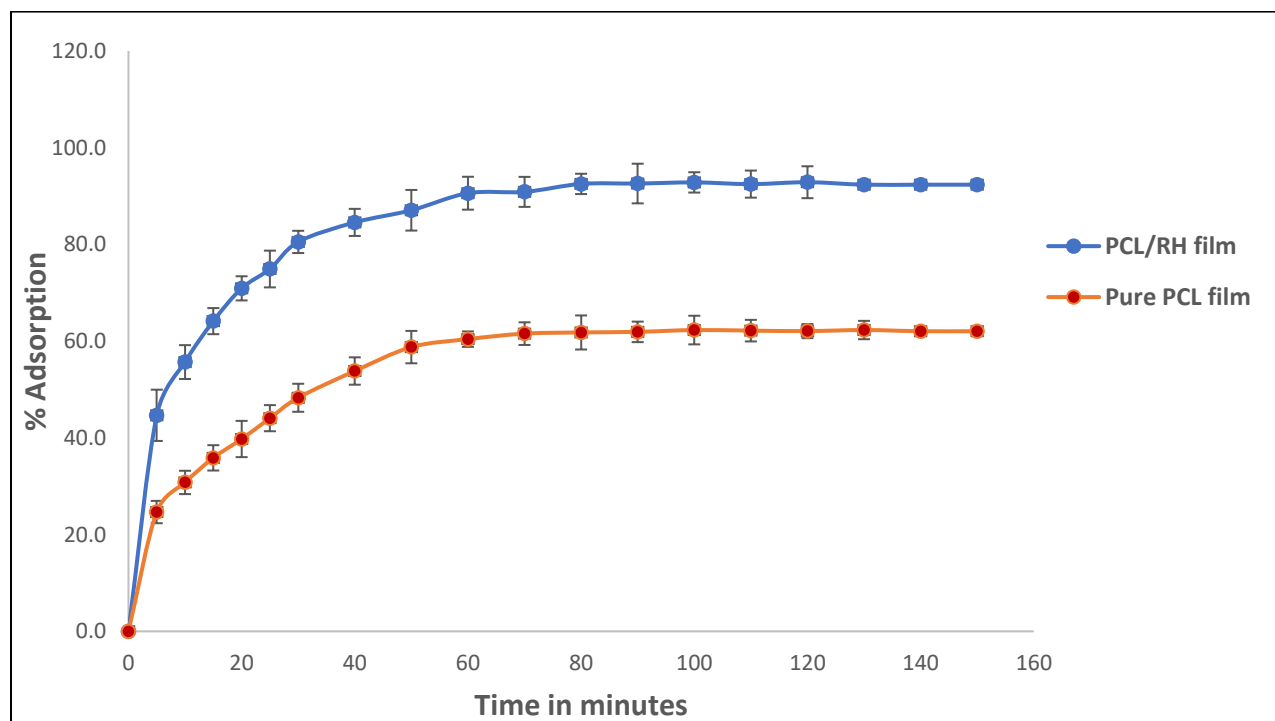


**Figure 4.50:** Influence of interaction time on % removal of MG on plain PCL & PCL-RH films

#### 4.11.3: Impact of Initial Colourant Strength on MG Removal by PCL-RH Films

The initial colourant strength of wastewater is significant because a certain mass of PCL-RH sorbent material can only remove a fixed quantity of colorant (Bharathi & Ramesh, 2013). The impact of the initial colourant strength strongly depends on the relationship between the strength of the colourant and the accessible active sorption sites on the material surface (Mahmoud *et al.*,

2012). For this work, the initial colourant concentration varied from 2.3 to 9.3 mg/L. The highest % removal (98.2 %) was realized using 2.3 mg/L within 150 minutes (Fig. 4.51). Furthermore, figure 4.51 illustrates that the rate of MG removal by PCL-RH reduced with an upsurge in initial dye strength. This is because at low concentrations of the MG colourant there is considerable number of vacant sorption sites on the PCL-RH surface. Once the initial MG strength upsurges, the active removal sites needed for MG uptake lessens.

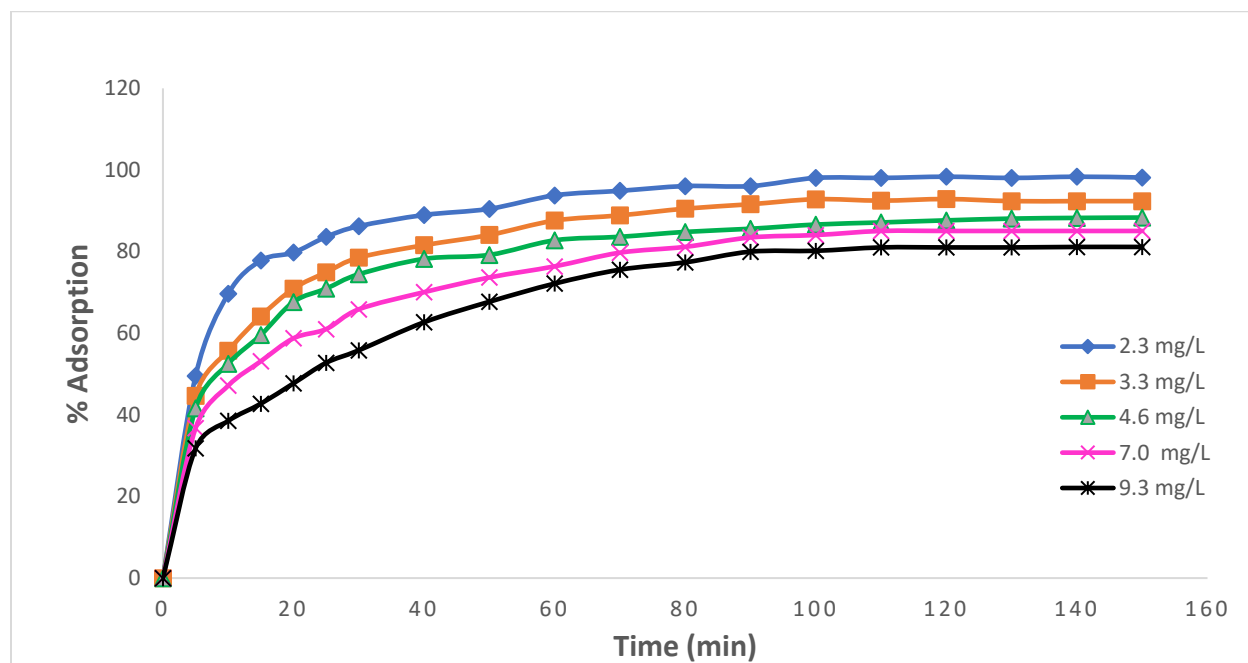


**Figure 4.51:** Influence of initial dye strength with time on abstraction of MG by PCL-RH films

#### 4.12: Sorption Kinetics for the Abstraction of MG by PCL-RH

To understand the sorption dynamics, the data was evaluated by use of the pseudo-first-order (Ho & McKay, 1998) and pseudo-second-order (Ho & McKay, 1999) rate mechanisms. The applicability of the models was assessed using coefficient of determination ( $r^2$ ) value (Shikuku *et al.*, 2018) and comparison of both the experimental ( $q_{exp}$ ) and theoretical ( $q_e$ , cal) adsorption capacity values calculated from the plotted models (Ghaedi *et al.*, 2015). The pseudo-first-order

(PFO) biosorption rate inadequately described the kinetic data for the removal of MG by PCL-RH with a  $r^2$  value of 0.96 (Fig. 4.52). The pseudo-second-order (PSO) rate was the highly applicable mechanism for the biosorption data with a  $r^2$  value of 0.99 (Fig. 4.53) which is close to unity. Further, the model gave a higher adsorption capacity ( $q_e = 9.09$  mg/g) compared to the PFO model which yielded 5.13 mg/g demonstrating that chemisorption was responsible for the uptake process. The rate coefficients for PFO and PSO reaction models ( $K_1$  &  $K_2$ ) were calculated from their linearized graphs and their corresponding values are provided in table 4.7.

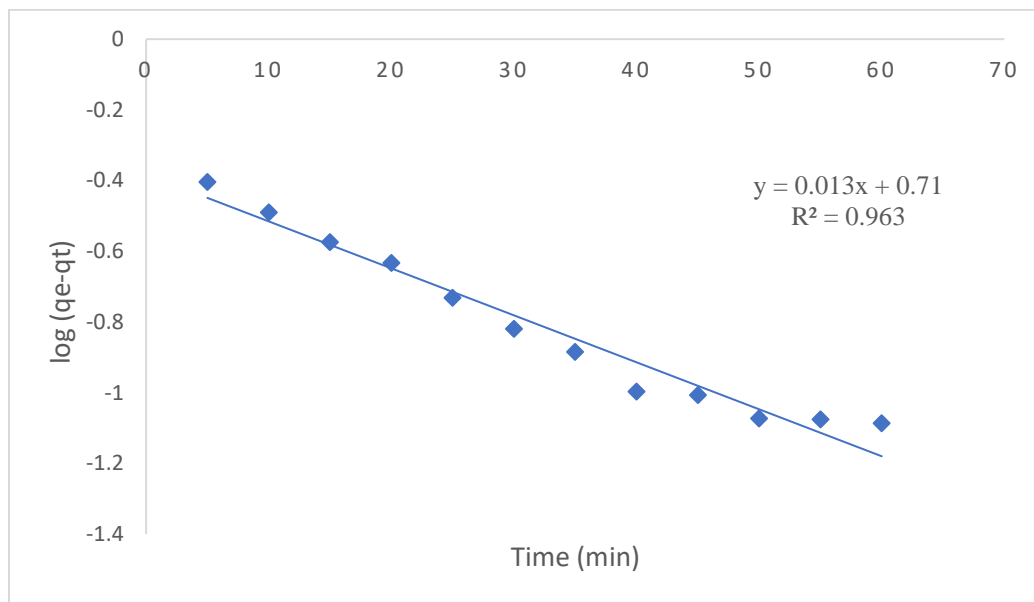


**Figure 4.52:** Pseudo first-order graph for the abstraction of MG on PCL-RH films

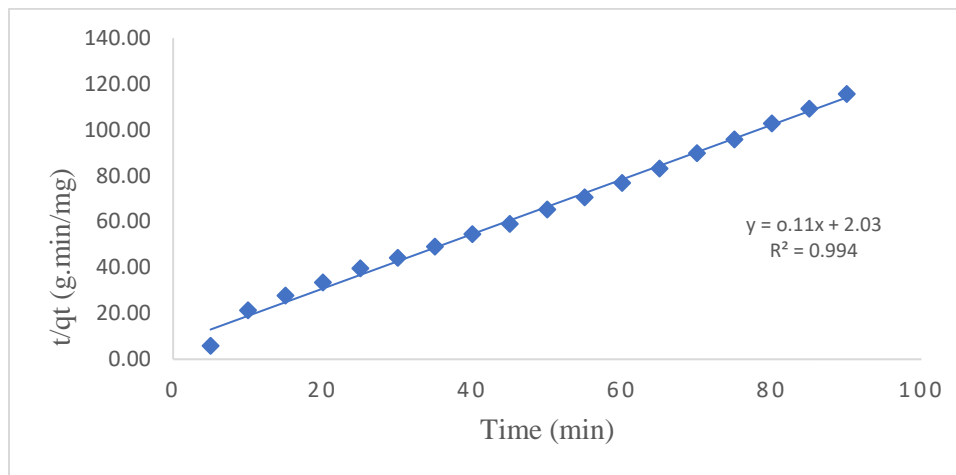


**Figure 4.53:** PSO reaction for the abstraction of MG by PCL-RH nanomaterial

**Table 4.7:** Chemical Kinetic Components for Biosorption of MG onto PCL-RH

Pseudo- first-order				Pseudo-second-order		
Log (q <sub>e</sub> - q <sub>t</sub> ) = log q <sub>e</sub> - K <sub>1</sub> t/2.303				t/q <sub>t</sub> = 1/K <sub>2</sub> q <sub>e</sub> <sup>2</sup> + 1/q <sub>e</sub> t		
Exp q <sub>e</sub> (mg/g)	q <sub>e</sub> cal (mg/g)	K <sub>1</sub> (min <sup>-1</sup> )	R <sup>2</sup>	q <sub>e</sub> (mg/g)	K <sub>2</sub> (g/mg.min)	R <sup>2</sup>
4.98	5.13	0.030	0.96	9.09	0.006	0.99

#### 4.13: The Intra-Particle Diffusion Model for Uptake of MG by PCL-RH

This is a model that is commonly applied for the prediction of the rate-controlling step of a biosorption process (Weber & Chakravorti 1974). The model assumes that if the graph of q<sub>t</sub> vs √t is linear, implying that the line of the graph crosses through the origin/ zero (C = 0), then pore diffusion controls the reaction and therefore intra-particle diffusion is the exclusive reaction-determining step (Hameed *et al.*, 2007). Results from this work (Fig.4.54) have revealed that pore diffusion was not singly controlling the biosorption of the recalcitrant dye on the PCL-RH material since the plot did not traverse via the origin of the graph. Comparable kinetic behavior

has been stated for the removal of basic methylene blue on activated carbon (AC) obtained from phosphoric acid-modified eucalyptus ( Han *et al.*, 2020).

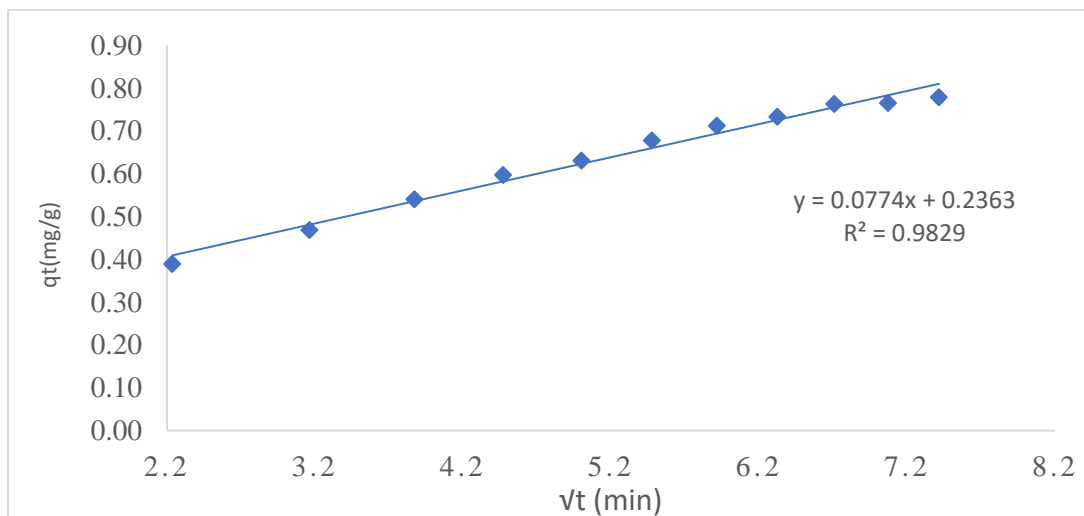


**Figure 4.54:** Intraparticle particle diffusion graph for the uptake of MG by PCL-RH films

#### 4.14 Comparison of RH, CS-ZnO and PCL-RH with other Sorbents for Uptake of MG from Aqueous Media

The elevated removal capacity of the three adsorbents utilized in this work on the targeted MG colorant compared to the other sorbents by various researchers (Table 4.8), demonstrates their appropriateness in wastewater management.

**Table 4. 8:** Comparison of Various Literature Sorbents with the three Adsorbents Used in this Study for MG Uptake

Bio sorbent	Uptake capability (mg/g)	Reference
Brewer’s spent grain	2.55	(Chanzu <i>et al.</i> , 2019)
Neem sawdust	4.354	(Khattri & Singh, 2009)
Poultry feathers	3.55	(Beak <i>et al.</i> , 2009)
PLA/spent brewery grain	1.48	(Chanzu <i>et al.</i> , 2012)
Rice husks	6.5	This work
Chitosan-ZnO	11	This work
PCL-RH	9.09	This work

## **4.2: Equilibrium Isotherms for Uptake of MG by $\epsilon$ -Polycaprolactone-Rice Husks Films**

Equilibrium studies provide the sorption capacity of the sorbent material and additionally can be utilized to predict the most appropriate model applicable when fabricating a sorption system.

### **4.2.1: Langmuir model for the abstraction of MG on PCL-RH biofilms**

This model presumes a monolayer sorption on a homogeneous surface containing a fixed amount of active uptake sites with no migration of the sorbate molecules on the surface. The Langmuir maximum uptake capacity ( $Q_m$ ) was 6.58 mg/g whereas the  $K_L$  factor was 0.74 L/mg (Table 4.9). The computed  $R_L$  constant of 0.48 was less than unity implying that it fulfilled the condition ( $0 < R_L < 1$ ) and therefore abstraction of MG on PCL-RH blend films was favorable. Compared to both Freundlich and Temkin isotherms, Langmuir was the most suitable in describing the data since it yielded the highest  $r^2$  of 0.99 (Fig. 4.55).

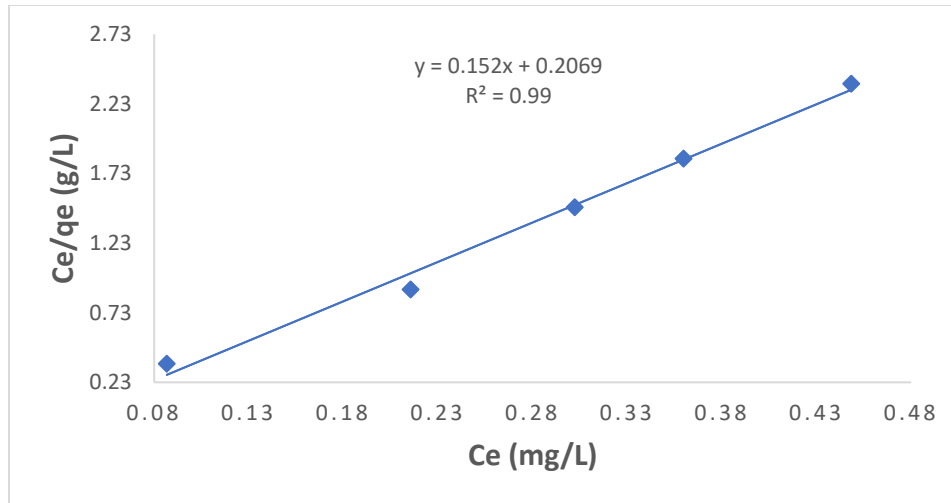


**Figure 4.55:** Langmuir model for the abstraction of MG on PCL-RH films

#### 4.2.2: Freundlich isotherm for the abstraction of MG by PCL-RH blend films

This model presumes a multilayer removal of the adsorbate on a heterogeneous surface. Its linearized equation is provided in table 4.9. The Freundlich sorption capacity was 4.9 mg/g whereas the  $n$  value was 0.93 (Fig. 4.56). Although this model demonstrated a high  $r^2$  of 0.94 (Fig. 4.56), it was less applicable in explaining the equilibrium data compared to Langmuir's  $r^2 = 0.99$ .

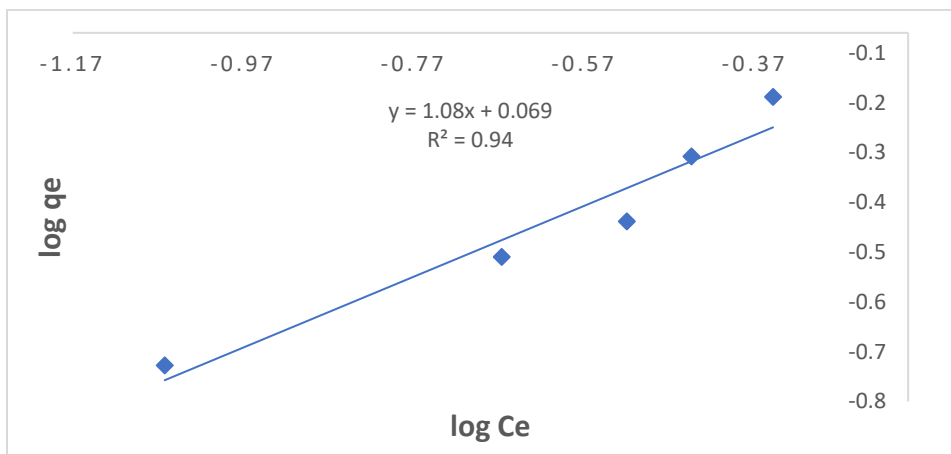


**Figure 4.56:** Freundlich model for uptake of MG by PCL-RH material

### 4.2.3: Temkin Isotherm for Abstraction of MG on PCL-RH Blend Films

This model presumes that the drop in the heat of adsorption is linear instead of logarithmic (Bharathi & Ramesh, 2013). The linear mode of this equation is provided in table 4.9. The model yielded a B value of 0.68 and a  $K_t$  constant of 1.4 (Table 4.9). It is evident that from Temkin's  $r^2$  value of 0.89 (Fig. 4.47), it was the least applicable model to illustrate the sorption data. Based on the  $r^2$  values, the best fitting isotherms were categorized as Langmuir > Freundlich > Temkin.

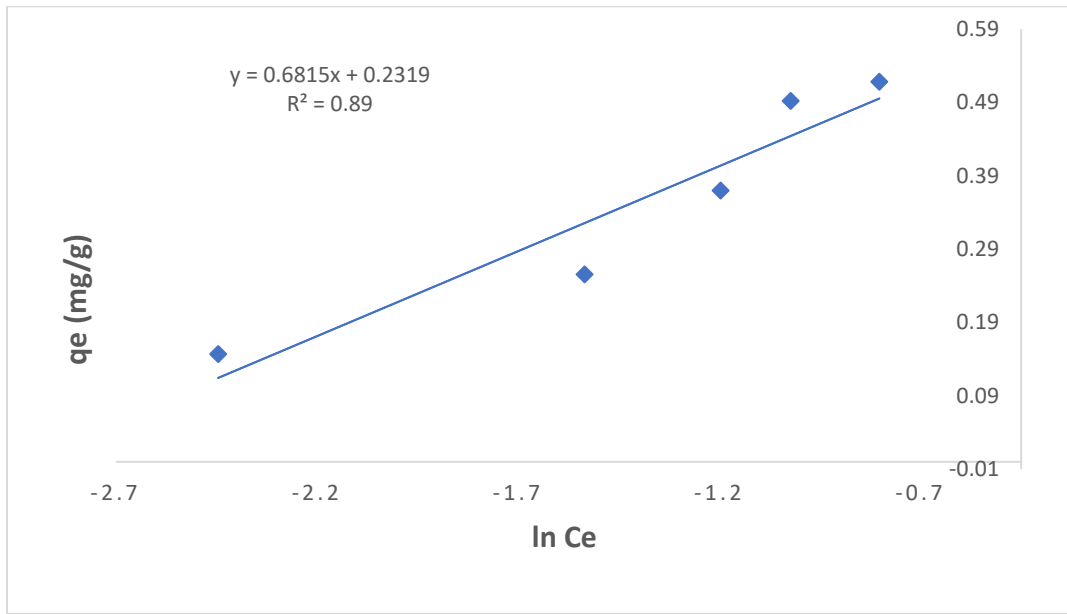


**Figure 4.57:** Temkin model for removal of MG by PCL-RH biofilms

**Table 4. 9:** Isotherm Constants for the Abstraction of MG by PCL-RH Biofilms

<b>Langmuir isotherm</b> $C_e/q_e = 1/K_L q_m + C_e/q_m$				<b>Freundlich isotherm</b> $\log q_e = \log K_f + 1/n \log C_e$			<b>Temkin model</b> $q_e = B \ln K_t + B \ln C_e$		
$Q_m$ (mg. g <sup>-1</sup> )	$K_L$ (L.mg <sup>-1</sup> )	$R_L$	$R^2$	$K_F$ (mg. g <sup>-1</sup> )	n	$R^2$	$K_t$	B	$R^2$
6.58	0.74	0.48	0.99	4.9	0.93	0.94	1.4	0.68	0.89

### **4.3: Adsorbent Cost Evaluation**

The cost of sorbents has a considerable influence on the capital required to operate a textile dye purification process. Moreover, the cost evaluation is a fundamental factor for assessing the industrial application of sorbent materials (Saha *et al.*, 2010). The price of the sorbent depends on various components such as its availability, reuse and the processing required (Chowdhury *et al.*, 2011).

Rice husks is an agricultural waste obtained from a rice processing factory. This industry is very popular in Kenya since rice is one of the staple foods consumed by most people. The unmodified RH which was used in this study was donated by the Mwea Tembere factory for free. However, there were transportation and preparation costs involved which were about 5 US Dollars.

Currently, the most preferred sorbent for the uptake of dyes is commercial activated carbon (AC). The cheapest type of AC costs 168 US Dollars whereas chitosan (100 - 300 kDa, 95 % deacetylation) costs 50 US Dollars and PCL per Kg costs 526 US Dollars (Sigma Aldrich, UK). Although the price of PCL per kg is 526 US Dollars, its cost reduces significantly when blended with the unmodified RH. Comparing the prices of the adsorbents utilized in this study with commercial AC and their adsorption capacities with other low-cost sorbents reported in the literature, it is evident that the materials are cheaper and therefore they can be commercialized to be used as alternative sustainable adsorbents for textile wastewater purification.

## CHAPTER FIVE

### CONCLUSIONS AND RECOMMENDATIONS

#### 5.1: CONCLUSIONS

The study has demonstrated that rice husks (RH), chitosan- ZnO (CS-ZnO) and poly( $\epsilon$ -caprolactone)- rice husks (PCL-RH) film blend sorbent materials are viable and cost-effective in removing hazardous MG colorant from textile wastewater effluents. The BET surface area and thermogravimetric analysis revealed that, the materials were mesoporous and thermally stable and therefore they can effectively remove cationic colourants from high-temperature textile effluents. Further, the FTIR analysis showed that the materials possessed surface functional groups (-OH, -NH & -C=O) which were responsible for the uptake of the dye through electrostatic interactions.

Poly( $\epsilon$ -caprolactone) (PCL) was successfully synthesized in bulk through the ring-opening polymerization route for water purification application. The synthesized PCL was blended with RH through simple solvent casting method. The sorbent material (PCL blended RH) demonstrated a better performance (93 % removal) than the neat PCL (62.1 %) thus making it a better candidate for dye removal from textile wastewater.

The mesoporous (33 nm) chitosan-zinc oxide (CS-ZnO) was successfully synthesized through the precipitation technique. The presence of a substantial amount of Zn in this thermally stable material proved efficacious in the integration of ZnO into the chitosan matrix.

This work has demonstrated that batch abstraction of MG from aqueous media is affected by components such as initial dye strength, solution pH, stirring speed, interaction time and

temperature. The uptake efficacy rose with the increase in time, adsorbent dose and reduction in particle sizes and initial dye concentration.

These sorbents proved their cost-effectiveness in MG removal by adsorbing better at neutral pH, low salt concentration and room temperature. In each case, over 90% removal was achieved within 150 minutes or less. This suggests that these materials can be utilized for textile wastewater purification owing to their short residence time.

The equilibrium data for all the sorbent materials was perfectly described by the Langmuir model indicating a monolayer sorption on a homogeneous surface. The maximum sorption capacities were as follows: unmodified rice husks yielded 6.5 mg/g, chitosan-ZnO gave 11.0 mg/g whereas PCL-RH gave 9.09 mg/g. Overall, CS-ZnO nanocomposite proved to be a superior adsorbent than both RH and PCL-RH film blends due to the possible combined effect of the sorption process and photodegradation effect by the ZnO nanoparticles. The  $R_L$  value of MG removal indicated a favourable process. The negative values of  $\Delta G$  and  $\Delta H$  revealed that the uptake of MG colorant by the unmodified RH was a spontaneous and exothermic process.

To understand the mechanisms responsible for the MG bio sorption, kinetics models were adopted. The pseudo-second-order rate mechanism depicted the kinetics data appropriately for all the experiments with  $r^2$  values  $> 90$  %. This infers that chemisorption dominated the abstraction of MG from the aqueous media. The intraparticle diffusion was involved in the uptake process however, it was not exclusively controlling the uptake process. The conclusion therefore, is that the surface sorption and intraparticle diffusion were concurrently operational during the MG removal.

In summary, this study has demonstrated the potential of low-cost RH, CS-ZnO and PCL-RH films as effective and eco-friendly materials for remediation of wastewaters containing dyes. In conclusion, the developed sorbent materials from this work can be applied to overcome water pollution problems at a reasonably low cost.

## **5.2: RECOMMENDATIONS**

1. Investigation of anionic dyes using rice husks, chitosan- ZnO and PCL-RH materials should be explored since the present work focused on the uptake of malachite green as a model cationic dye.
2. Further work to be done using continuous flow experiments since this study focused on batch adsorption experiments.
3. Real dye-loaded wastewater from textile industries should be tested using the adsorbents adopted in this study for comparison purposes since this work tested simulated water spiked with the MG dye.
4. To get some insight into the mechanism involved in the malachite green (MG) dye, adsorption-desorption studies should be performed.
5. Synthesis of  $\epsilon$ -PCL using supercritical carbon dioxide (SCO<sub>2</sub>) should be explored for comparison purposes.

## REFERENCES

- Abdelrazek, E. M., Hezma, A. M., El-khodary, A., & Elzayat, A. M. (2016). Spectroscopic studies and thermal properties of PCL / PMMA biopolymer blend. *Egyptian Journal of Basic and Applied Sciences*, **3**: 10–15. <https://doi.org/10.1016/j.ejbas.2015.06.001>
- Ahmad, R., & Kumar, R. (2010). Adsorption studies of hazardous malachite green onto treated ginger waste. *Journal of Environmental Management*, **91**: 1032–1038.
- Ahmadzadeh, Y., Babaei, A., & Goudarzi, A. (2018). Assessment of localization and degradation of ZnO nano-particles in the PLA/PCL biocompatible blend through a comprehensive rheological characterization. *Polymer Degradation and Stability*, **158**: 136–147.
- Akar, E., Altinisik, A., & Seki, Y. (2013). Using activated carbon produced from spent tea leaves for the removal of malachite green from aqueous solution. *Ecological Engineering*, **52**: 19–27. <https://doi.org/10.1016/j.ecoleng.2012.12.032>
- Albertsson, A., & Varma, I. K. (2003). Recent Developments in Ring Opening Polymerization of Lactones for Biomedical Applications. *Biomacromolecules*, **4**: 1466–1486.
- Allen, S. J., Mckay, G., & Porter, J. F. (2004). Adsorption isotherm models for basic dye adsorption by peat in single and binary component systems. *Journal of Colloid and Interface Science*, **280**: 322–333. <https://doi.org/10.1016/j.jcis.2004.08.078>
- Alqadami, A. A., Naushad, M., Alothman, Z. A., & Ahamad, T. (2018). Adsorptive performance of MOF nanocomposite for methylene blue and malachite green dyes : Kinetics, isotherm

- and mechanism. *Journal of Environmental Management*, **223**: 29–36.
- Ana, M. D., & Angel, L. D. (2015). Wound Healing Bionanocomposites Based on Castor Oil Polymeric Films Reinforced with Chitosan-Modified ZnO Nanoparticles. *Biomaterials*, **16**: 2631–2644. <https://doi.org/10.1021/acs.biomac.5b00447>
- Attallah, O. A., Al-Ghobashy, M. A., Nebsen, M., & Salem, M. Y. (2016). Removal of cationic and anionic dyes from aqueous solution with magnetite/pectin and magnetite/silica/pectin hybrid nanocomposites: Kinetic, isotherm and mechanism analysis. *RSC Advances*, **6**: 11461–11480. <https://doi.org/10.1039/c5ra23452b>
- Aydın, Y.A & Aksoy, N. D. (2009). Adsorption of chromium on chitosan: Optimization, kinetics and thermodynamics. *Chemical Engineering Journal*, **151**: 188–194.
- Baheti, P., Gimello, O., Bouilhac, C., Lacroix-desmazes, P., & Howdle, S. M. (2018). Polymer Chemistry. *Polymer Chemistry*, **9**: 5594–5607. <https://doi.org/10.1039/c8py01266k>
- Beak, M. H., Ijagbemi, C. O., & Kim, D. S. (2009). Treatment of malachite green-containing wastewater using poultry feathers as adsorbent. *Journal of Environmental Science and Health - Part A*, **44**: 536–542. <https://doi.org/10.1080/10934520902720132>
- Bekçi, Z., Özveri, C., Seki, Y., & Yurdakoç, K. (2008). Sorption of malachite green on chitosan bead. *Journal of Hazardous Materials*, **154**: 254–261.
- Bharathi & Ramesh. (2013). Removal of dyes using agricultural waste as low-cost adsorbents: a review. *Journal of Applied Water Science*, **3**: 773–790. <https://doi.org/10.1007/s13201-013-0117-y>

- Bhatnagar, A. & Minocha, A. K. (2006). Conventional and non-conventional adsorbents for removal of pollutants from water – A review. *Indian Journal of Chemical Technology*, **13**: 203–217.
- Bhatnagar, A., & Jain, A. K. (2005). A comparative adsorption study with different industrial wastes as adsorbents for the removal of cationic dyes from water. *Journal of Colloid and Interface Science*, **281**: 49–55. <https://doi.org/10.1016/j.jcis.2004.08.076>
- Bulut, E. O'zacar, M. & Sengil, I. A. (2008). Adsorption of malachite green onto bentonite : Equilibrium and kinetic studies and process design. *Microporous and Mesoporous Materials*, **115**: 234–246. <https://doi.org/10.1016/j.micromeso.2008.01.039>
- Chanzu, H. A., Onyari, J. M., & Shiundu, P. M. (2012). Biosorption of Malachite Green from Aqueous Solutions onto Polylactide / Spent Brewery Grains Films : Kinetic and Equilibrium Studies. *Journal of Polymers and the Environment*, **20**: 665–672.
- Chanzu H. Shiundu P. & Onyari J. (2019). Brewers ' spent grain in adsorption of aqueous Congo Red and malachite Green dyes : Batch and continuous flow systems. *Journal of Hazardous Materials*, **380**: 120897. <https://doi.org/10.1016/j.jhazmat.2019.120897>
- Chen, S., Zhang, J., Zhang, C., Yue, Q., Li, Y., & Li, C. (2010). Equilibrium and kinetic studies of methyl orange and methyl violet adsorption on activated carbon derived from *Phragmites australis*. *Desalination*, **252**: 149–156. <https://doi.org/10.1016/j.desal.2009.10.010>
- Chowdhury, S., Mishra, R., Saha, P., & Kushwaha, P. (2011). Adsorption thermodynamics , kinetics and isosteric heat of adsorption of malachite green onto chemically modified rice

- husk. *Desalination*, **265**: 159–168. <https://doi.org/10.1016/j.desal.2010.07.047>
- Chu, H., Cao, D., Jin, W., & Dong, B. (2008). Characteristics of bio-diatomite dynamic membrane process for municipal wastewater treatment. *Journal of Membrane Science*, **325**: 271–276. <https://doi.org/10.1016/j.memsci.2008.07.040>
- Chuah, T. G., Jumariah, A., Azni, I., Katayon, S., & Thomas Choong, S. Y. (2005). Rice husk as a potentially low-cost biosorbent for heavy metal and dye removal: An overview. *Desalination*, **175**: 305–316. <https://doi.org/10.1016/j.desal.2004.10.014>
- Crini, G., Peindy, H.N., Gimbert, F., & Capucine, R. (2007). Removal of C. I. Basic Green 4 ( Malachite Green ) from aqueous solutions by adsorption using cyclodextrin-based adsorbent : Kinetic and equilibrium studies. *Separation and Purification Technology*, **53**: 97–110. <https://doi.org/10.1016/j.seppur.2006.06.018>
- Culp, S. J., & Beland, F. A. (1996). Malachite Green : A Toxicological Review. *Journal of the American College of Toxicology*, **15**: 219–238.
- Dahri, M. K., Kooh, M. R. R., & Lim, L. B. L. (2014). Water remediation using low cost adsorbent walnut shell for removal of malachite green: Equilibrium, kinetics, thermodynamic and regeneration studies. *Journal of Environmental Chemical Engineering*, **2**: 1434–1444. <https://doi.org/10.1016/j.jece.2014.07.008>
- Darensbourg, D. J., & Karroonnirun, O. (2010). Ring-opening polymerization of l-lactide and  $\epsilon$ -caprolactone utilizing biocompatible zinc catalysts. random copolymerization of l-lactide and  $\epsilon$ -caprolactone. *Macromolecules*, **43**: 8880–8886. <https://doi.org/10.1021/ma101784y>

- Das, A., Pal, A., Saha, S. & Maji, S. K. (2009). Behaviour of fixed-bed column for the adsorption of malachite green on surfactant-modified alumina. *Journal of Environmental Science and Health Part A*, **44**: 265–272. <https://doi.org/10.1080/10934520802597929>
- Dehaghi, S. ., Rahmanifar, B., Moradi, A. M., & Azar, P. A. (2014). Removal of permethrin pesticide from water by chitosan-zinc oxide nanoparticles composite as an adsorbent. *Journal of Saudi Chemical Society*, **18**: 348–355. <https://doi.org/10.1016/j.jscs.2014.01.004>
- Dezhampanah, H., Mousazadeh, A., & Mousazadeh, I. (2014). Sugarcane Bagasse and Modified Rice Husk for the Removal of Malachite Green From Aqueous. *European Chemical Bulletin*, **3**: 400–406.
- Dhanavel, S., Nivethaa, E.A.K., Narayanan, V. & Stephen, A. (2014). Photocatalytic activity of Chitosan / ZnO nanocomposites for degrading Photocatalytic activity of Chitosan / ZnO nanocomposites for degrading methylene blue. *International Journal of ChemTech Research*, **6**: 1880–1882.
- Dotto, G.L. & Pinto, L. A. A. (2011). Adsorption of food dyes onto chitosan : Optimization process and kinetic. *Carbohydrate Polymers*, **84**: 231–238.
- Dubey, S. P., & Gopal, K. (2007). Adsorption of chromium ( VI ) on low cost adsorbents derived from agricultural waste material : A comparative study. *Journal of Hazardous Materials*, **145**: 465–470. <https://doi.org/10.1016/j.jhazmat.2006.11.041>
- Farajzadeh, M.A., & Fallahi, M. R. (2005). Study of Phenolic Compounds Removal from Aqueous Solution by Polymeric Sorbent. *Journal of the Chinese Chemical Society*, **52**:

295–301.

Feng, Q., Lin, Q., Gong, F., Sugita, S., & Shoya, M. (2004). Adsorption of lead and mercury by rice husk ash. *Journal of Colloid and Interface Science*, **278**: 1–8.

Ferrero, F. (2007). Dye removal by low cost adsorbents : Hazelnut shells in comparison with wood sawdust. *Journal of Hazardous Materials*, **142**: 144–152.

Freundlich, H. M. (1906). Over the Adsorption in Solution. *Journal of Physical Chemistry A*, **57**: 385–470.

Fu, J., Chen, Z., Wang, M., Liu, S., Zhang, J. & Zhang, J. (2015). Adsorption of methylene blue by a high-efficiency adsorbent (polydopamine microspheres): Kinetics, isotherm, thermodynamics and mechanism analysis. *Chemical Engineering Journal*, **259**: 53–61.  
<https://doi.org/10.1016/j.cej.2014.07.101>

Fulmer, G.R., Miller, A.J.M., Sherden, N.H., Gottlieb, H.E., Nudelman, A., Stoltz, B.M., Bercaw, J.E. & Goldberg, K. I. (2010). NMR Chemical Shifts of Trace Impurities : Common Laboratory Solvents, Organics, and Gases in Deuterated Solvents Relevant to the Organometallic Chemist. *Organometallics*, **29**: 2176–2179.

Gadzinowski, M., Sosnowski, S., & Słomkowski, S. (1996). Kinetics of the Dispersion Ring-Opening Polymerization of  $\epsilon$ -Caprolactone Initiated with Diethylaluminum Ethoxide. *Macromolecules*, **29**: 6404–6407.

Genieva, S. D., Turmanova, S. C., Dimitrova, A. S., & Vlaev, L. T. (2008). Characterization of rice husks and the products of its thermal degradation in air or nitrogen atmosphere. *Journal*

*of Thermal Analysis and Calorimetry*, **93**: 387–396.

Ghaedi, M., Hajjati, S., Mahmudi Z., , Tyagi, I., Agarwal, S., Maity, A. & Gupta, V. K. (2015).

Modeling of competitive ultrasonic-assisted removal of the dyes – Methylene blue and Safranin-O using Fe<sub>3</sub>O<sub>4</sub> nanoparticles. *Chemical Engineering Journal*, **268**: 28–37.

<https://doi.org/10.1016/j.cej.2014.12.090>

Goswami, L., Kumar, R. V., Pakshirajan, K., & Pugazhenti, G. (2018). A novel integrated

biodegradation—Microfiltration system for sustainable wastewater treatment and energy recovery. *Journal of Hazardous Materials*, **365**: 707–715.

Govindan, S., Nivethaa, E. A. K., Saravanan, R., Narayanan, V., & Stephen, A. (2012).

Synthesis and characterization of Chitosan–Silver nanocomposite. *Applied Nanoscience*, **2**: 299–303. <https://doi.org/10.1007/s13204-012-0109-5>

Gündüz, F., & Bayrak, B. (2017). Biosorption of malachite green from an aqueous solution using

pomegranate peel: Equilibrium modelling, kinetic and thermodynamic studies. *Journal of Molecular Liquids*, **243**: 790–798. <https://doi.org/10.1016/j.molliq.2017.08.095>

Haldorai, Y., & Shim, J. J. (2013). Chitosan-Zinc Oxide hybrid composite for enhanced dye

degradation and antibacterial activity. *Composite Interfaces*, **20**: 365–377.

Hameed, B.H., Tan, I.A.W. & Ahmad, A. L. (2008). Adsorption isotherm, kinetic modeling and

mechanism of 2,4,6-trichlorophenol on coconut husk-based activated carbon. *Chemical Engineering Journal*, **144**: 235–244. <https://doi.org/10.1016/j.cej.2008.01.028>

Hameed, B.H. & El- Khaiary, M. I. (2008a). Kinetics and equilibrium studies of malachite green

- adsorption on rice straw-derived char. *Journal of Hazardous Materials*, **153**: 701–708.  
<https://doi.org/10.1016/j.jhazmat.2007.09.019>
- Hameed, B.H. & El- Khaiary, M. I. (2008b). Malachite green adsorption by rattan sawdust : Isotherm, kinetic and mechanism modeling. *Journal of Hazardous Materials*, **159**: 574–579. <https://doi.org/10.1016/j.jhazmat.2008.02.054>
- Hameed, B. H. (2009). Grass waste : A novel sorbent for the removal of basic dye from aqueous solution. *Journal of Hazardous Materials Journal*, **166**: 233–238.
- Hameed, B. H., & Ahmad, A. A. (2009). Batch adsorption of methylene blue from aqueous solution by garlic peel, an agricultural waste biomass. *Journal of Hazardous Materials*, **164**: 870–875. <https://doi.org/10.1016/j.jhazmat.2008.08.084>
- Hameed, B. H., Ahmad, A. A., & Aziz, N. (2007). Isotherms, kinetics and thermodynamics of acid dye adsorption on activated palm ash. *Chemical Engineering Journal*, **133**: 195–203.  
<https://doi.org/10.1016/j.cej.2007.01.032>
- Hameed, B. H., Krishni, R. R., & Sata, S. A. (2009). A novel agricultural waste adsorbent for the removal of cationic dye from aqueous solutions. *Journal of Hazardous Materials*, **162**: 305–311. <https://doi.org/10.1016/j.jhazmat.2008.05.036>
- Han, X., Yuan, J. & Ma, X. (2014). Adsorption of malachite green from aqueous solutions onto lotus leaf: Equilibrium, kinetic, and thermodynamic studies. *Desalination and Water Treatment*, **52**: 5563–5574. <https://doi.org/10.1080/19443994.2013.813102>
- Han, Q., Wang, J., Goodman, B. A., Xie, J., & Liu, Z. (2020). High adsorption of methylene blue

- by activated carbon prepared from phosphoric acid treated eucalyptus residue. *Powder Technology*, **366**: 239–248. <https://doi.org/10.1016/j.powtec.2020.02.013>
- Ho, Y.S. & McKay, G. (1998). Sorption of dye from aqueous solution by peat. *Chemical Engineering Journal*, **70**: 115–124.
- Ho, Y.S. & McKay, G. (1999). Pseudo-second order model for sorption processes. *Process Biochemistry*, **34**, 451–465.
- Hoidy, W.H., Al-Mulla, E.A.J., & Al -Janabi, K. W. (2010). Mechanical and Thermal Properties of PLLA / PCL Modified Clay Nanocomposites. *Journal of Polymers and the Environment*, **18**: 608–616. <https://doi.org/10.1007/s10924-010-0240-x>
- Hu, L., Sun, Y., & Wu, Y. (2013). Advances in chitosan-based drug delivery vehicles. *Nanoscale*, **5**: 3103–3111. <https://doi.org/10.1039/c3nr00338h>
- Iftekhhar,S., Ramasamy, D. L., Srivastava, V., Asif, M. B., S. M. (2018). Understanding the factors affecting the adsorption of Lanthanum using different adsorbents : A critical review. *Chemosphere*, **204**: 413–430. <https://doi.org/10.1016/j.chemosphere.2018.04.053>
- Jaman, H., Chakraborty, D., & Saha, P. (2009). A study of the thermodynamics and kinetics of copper adsorption using chemically modified rice husk. *Clean - Soil, Air, Water*, **37**: 704–711. <https://doi.org/10.1002/clen.200900138>
- Jiang, N., Shang, R., Heijman, S.G.J. & Rietveld, L. C. (2018). High-silica zeolites for adsorption of organic micro-pollutants in water treatment: A review. *Water Research*, **144**: 145–161. <https://doi.org/10.1016/j.watres.2018.07.017>

- Johar, N., Ahmad, I., & Dufresne, A. (2012). Extraction, preparation and characterization of cellulose fibres and nanocrystals from rice husk. *Industrial Crops and Products*, **37**: 93–99. <https://doi.org/10.1016/j.indcrop.2011.12.016>
- John, S., Joseph, A., Jose, A. J., & Narayana, B. (2015). Enhancement of corrosion protection of mild steel by chitosan/ZnO nanoparticle composite membranes. *Progress in Organic Coatings*, **84**: 28–34. <https://doi.org/10.1016/j.porgcoat.2015.02.005>
- Kaneko, K. (1994). Determination of pore size and pore size distribution. Adsorbents and catalysts. *Journal of Membrane Science*, **96**: 59–89.
- Kang, S. X., Sun, X., & Ju, X. (2002). Measurement and calculation of escape peak intensities in synchrotron radiation X-ray fluorescence analysis. *Nucl. Instr. and Meth. in Phys. Res. B*, **192**: 365–369.
- Khan, R., Bhawana, P., & Fulekar, M. H. (2013). Microbial decolorization and degradation of synthetic dyes : a review. *Rev Environ Sci Biotechnol*, **12**: 75–97.
- Khattri, S. D., & Singh, M. K. (2009). Removal of malachite green from dye wastewater using neem sawdust by adsorption. *Journal of Hazardous Materials Journal*, **167**: 1089–1094. <https://doi.org/10.1016/j.jhazmat.2009.01.101>
- Kumar, B. & Kumar, U. (2015). Adsorption of malachite green in aqueous solution onto sodium carbonate treated rice husk. *Korean J. Chem. Eng.*, **32**: 1655–1666.
- Kumar, K. V., & Sivanesan, S. (2005). Prediction of optimum sorption isotherm : Comparison of linear and non-linear method. *Journal of Hazardous Materials*, **126**: 198–

201.

- Kumar, T., Naba, R., & Mondal, K. (2017). Biosorption of Congo Red from aqueous solution onto burned root of *Eichhornia crassipes* biomass. *Applied Water Science*, **7**: 1841–1854. <https://doi.org/10.1007/s13201-015-0358-z>
- Kumari, S., & Kumar, P. (2014). Extraction and Characterization of Chitin and Chitosan from ( *Labeo rohita* ) Fish Scales. *Procedia Materials Science*, **6**: 482–489.
- Kurniawan, T. A., Chan G. Y.S., & Lo W. Babel, S. (2006). Comparisons of low-cost adsorbents for treating wastewaters laden with heavy metals. *Science of the Total Environment*, **366**: 409–426. <https://doi.org/10.1016/j.scitotenv.2005.10.001>
- Kushwaha, A. K., Gupta, N., & Chattopadhyaya, M. C. (2014). Removal of cationic methylene blue and malachite green dyes from aqueous solution by waste materials of *Daucus carota*. *Journal of Saudi Chemical Society*, **18**: 200–207.
- Kweon, H.Y., Yoo, M.K., Park, I.K., Kim, T.H., Lee, H.C., Lee, H., Oh, J., Akaike, T. & Cho, C. (2003). A novel degradable polycaprolactone networks for tissue engineering. *Biomaterials*, **24**: 801–808.
- Kyzas, G. Z., & Deliyanni, E. A. (2015). Modified activated carbons from potato peels as green environmental-friendly adsorbents for the treatment of pharmaceutical effluents. *Chemical Engineering Research and Design*, **97**: 135–144.
- Labet, M., & Thielemans, W. (2009). Synthesis of polycaprolactone : A review. *Chemical Society Reviews*, **38**: 3484–3504. <https://doi.org/10.1039/b820162p>

- Langmuir, I. (1916). The Constitution and Fundamental properties of solids and liquids. Part 1. Solids. *Journal of the American Chemical Society*, **38**: 2221–2295.
- Li, Q., Yue, Q. Y., Sun, H. J., Su, Y., & Gao, B. Y. (2010). A comparative study on the properties, mechanisms and process designs for the adsorption of non-ionic or anionic dyes onto cationic-polymer/bentonite. *Journal of Environmental Management*, **91**: 1601–1611.
- Liu, T., Li, Y., Du, Q., Sun, J., Jiao, Y., Yang, G., Wang, Z., Xia, Y., Zhang, W., Wang, K., Zhu, H., & Wu, D. (2012). Adsorption of methylene blue from aqueous solution by graphene. *Colloids and Surfaces B: Biointerfaces*, **90**: 197–203.
- Mahmoodi, N. M. (2013). Zinc ferrite nanoparticle as a magnetic catalyst: Synthesis and dye degradation. *Materials Research Bulletin*, **48**: 4255–4260.
- Mahmoodi, N. M. (2014). Binary catalyst system dye degradation using photocatalysis. *Fibers and Polymers*, **15**: 273–280. <https://doi.org/10.1007/s12221-014-0273-1>
- Mahmoud, D.K., Salleh, M.A.M., Karim, W.A.W.A., Idris, A. & Abidin, Z. Z. (2012). Batch adsorption of basic dye using acid treated kenaf fibre char: Equilibrium, kinetic and thermodynamic studies. *Chemical Engineering Journal*, **181**: 449–457.
- Makeswari, M., & Santhi, T. (2013). Removal of Malachite Green Dye from Aqueous Solutions onto Microwave Assisted Zinc Chloride Chemical Activated Epicarp of *Ricinus communis*. *Journal of Water Resource and Protection*, **5**: 222–238.
- Mansaray, K. G., & Ghaly, A. E. (1998). Thermal degradation of rice husks in nitrogen atmosphere. *Bioresource Technology*, **65**: 13–20.

- Mbui, D. N., Shiundu, P. M., Ndonye, R. M., & Kamau, G. N. (2002). Adsorption and detection of some phenolic compounds by rice husk ash of Kenyan origin. *The Royal Society of Chemistry*, **4**: 978–984. <https://doi.org/10.1039/b207257m>
- Memon, G. Z., Bhangar, M. I., Akhtar, M., Talpur, F. N., & Memon, J. R. (2008). Adsorption of methyl parathion pesticide from water using watermelon peels as a low cost adsorbent. *Chemical Engineering Journal*, **138**: 616–621. <https://doi.org/10.1016/j.cej.2007.09.027>
- Mishra, V. K., & Tripathi, B. D. (2009). Accumulation of chromium and zinc from aqueous solutions using water hyacinth (*Eichhornia crassipes*). *Journal of Hazardous Materials*, **164**:1059–1063. <https://doi.org/10.1016/j.jhazmat.2008.09.020>
- Mittal, A., Mittal, J., Malviya, A., & Gupta, V. K. (2010). Removal and recovery of Chrysoidine Y from aqueous solutions by waste materials Structure of Chrysoidine Y. *Journal of Colloid and Interface Science*, **344**: 497–507. <https://doi.org/10.1016/j.jcis.2010.01.007>
- Mohammad, P. & Rahbar-kelishami, A. (2015). Adsorption of methylene blue onto *Platanus orientalis* leaf powder: Kinetic, equilibrium and thermodynamic studies. *Journal of Industrial and Engineering Chemistry*, **21**: 1014–1019.
- Mohammed, M. A., Shitu, A., & Ibrahim, A. (2014). Removal of Methylene Blue Using Low Cost Adsorbent : A Review. *Research Journal of Chemical Sciences*, **4**: 91–102.
- Moradi, S., Rahmanifar, B., & Mashinchian, A. (2014). Removal of permethrin pesticide from water by chitosan – zinc oxide nanoparticles composite as an adsorbent. *Journal of Saudi Chemical Society*, **18**: 348–355. <https://doi.org/10.1016/j.jscs.2014.01.004>

- Moussout, H., Ahlafi, H., Aazza, M., & Maghat, H. (2018). Critical of linear and nonlinear equations of pseudo-first order and pseudo-second order kinetic models. *Karbala International Journal of Modern Science*, **4**: 244–254.
- Mujeeb, R. P., Mujeeb, V. M., Muraleedharan, K., & Thomas, S. K. (2018). Chitosan/nano ZnO composite films: Enhanced mechanical, antimicrobial and dielectric properties. *Arabian Journal of Chemistry*, **11**: 120–127. <https://doi.org/10.1016/j.arabjc.2016.09.008>
- Nethaji, S., Sivasamy, A., Thennarasu, G., & Saravanan, S. (2010). Adsorption of Malachite Green dye onto activated carbon derived from *Borassus aethiopum* flower biomass. *Journal of Hazardous Materials*, **181**: 271–280. <https://doi.org/10.1016/j.jhazmat.2010.05.008>
- Ngah, W.S.W., Kamari, A., Fatinathan, S. & Ng, P. W. (2006). Adsorption of chromium from aqueous solution using chitosan beads. *Adsorption*, **12**: 249–257.
- Ngah, W. S. W., & Fatinathan, S. (2008). Adsorption of Cu ( II ) ions in aqueous solution using chitosan beads , chitosan – GLA beads and chitosan – alginate beads. *Chemical Engineering Journal*, **143**: 62–72. <https://doi.org/10.1016/j.cej.2007.12.006>
- Nguyen, N.T., Thurecht, K.J., Howdle, S.M. & Irvine, D. J. (2014). Facile one-spot synthesis of highly branched polycaprolactone. *Journal of Polymer Chemistry*, **5**: 2997–3008.
- Njoku, V. O., Asif, M., & Hameed, B. H. (2015). 2,4-Dichlorophenoxyacetic acid adsorption onto coconut shell-activated carbon: isotherm and kinetic modeling. *Desalination and Water Treatment*, **55**: 132–141. <https://doi.org/10.1080/19443994.2014.911708>
- Nodeh, H. R., Aini, W., Ibrahim, W., & Sanagi, M. M. (2016). Development of magnetic

- graphene oxide adsorbent for the removal and preconcentration of As ( III ) and As ( V ) species from environmental water samples. *Environmental Science and Pollution Research*, **23**: 9759–9773. <https://doi.org/10.1007/s11356-016-6137-z>
- Ofomaja, A. E., & Ho, Y. (2008). Effect of temperatures and pH on methyl violet biosorption by *Mansonia wood* sawdust. *Bioresource Technology*, **99**: 5411–5417.
- Oloo, C. M., Onyari, J. M., Wanyonyi, W. C., Wabomba, J. N., & Muinde, V. M. (2020). Adsorptive removal of hazardous crystal violet dye from aqueous solution using *Rhizophora mucronata* stem-barks: Equilibrium and kinetics studies. *Environmental Chemistry and Ecotoxicology*, **2**: 64–72.
- Özbay, I., Özdemir, U., Özbay, B., & Veli, S. (2013). Kinetic, thermodynamic, and equilibrium studies for adsorption of azo reactive dye onto a novel waste adsorbent: Charcoal ash. *Desalination and Water Treatment*, **51**: 6091–6100.
- Phillipson, K., Hay, J., & Jenkins, M. (2014). Thermal analysis FTIR spectroscopy of poly ( $\epsilon$ -caprolactone ). *Thermochimica Acta*, **595**: 74–82. <https://doi.org/10.1016/j.tca.2014.08.027>
- Poojari, A.C., Maind, S.D., & Bhalerao, S. A. (2015). Effective removal of Cr ( VI ) from aqueous solutions using rind of Orange (*Citrus sinensis*), (L.) Osbeck. *International Journal of Current Microbiology and Applied Sciences*, **4**: 653–671.
- Priya, E. S., & Selvan, P. S. (2017). Water hyacinth ( *Eichhornia crassipes* ) – An efficient and economic adsorbent for textile effluent treatment – A review. *Arabian Journal of Chemistry*, **10**: S3548–S3558. <https://doi.org/10.1016/j.arabjc.2014.03.002>

- Rai, H. S., Bhattacharyya, M. S., Singh, J., Bansal, T. K., Vats, P., & Banerjee, U. C. (2005). Removal of dyes from the effluent of textile and dyestuff manufacturing industry: A review of emerging techniques with reference to biological treatment. *Critical Reviews in Environmental Science and Technology*, **35**: 219–238.
- Regel-Rosocka, M. (2010). A review on methods of regeneration of spent pickling solutions from steel processing. *Journal of Hazardous Materials*, **177**: 57–69.
- Rengaraj, S., Yeon, K., & Moon, S. (2001). Removal of chromium from water and wastewater by ion exchange resins. *Journal of Hazardous Materials*, **87**: 273–287.
- Saeed, S. E. S., El-Molla, M. M., Hassan, M. L., Bakir, E., Abdel-Mottaleb, M. M. S., & Abdel-Mottaleb, M. S. A. (2014). Novel chitosan-ZnO based nanocomposites as luminescent tags for cellulosic materials. *Carbohydrate Polymers*, **99**: 817–824.
- Saha, P., Chowdhury, S., Gupta, S., & Kumar, I. (2010). Insight into adsorption equilibrium, kinetics and thermodynamics of Malachite Green onto clayey soil of Indian origin. *Chemical Engineering Journal*, **165**: 874–882. <https://doi.org/10.1016/j.cej.2010.10.048>
- Santhi, T., Manonmani, S., & Smitha, T. (2010). Removal of malachite green from aqueous solution by activated carbon prepared from the epicarp of *Ricinus communis* by adsorption. *Journal of Hazardous Materials*, **179**: 178–186.
- Sanuja, S., Agalya, A., & Umopathy, M. J. (2015). Synthesis and characterization of zinc oxide-neem oil-chitosan bionanocomposite for food packaging application. *International Journal of Biological Macromolecules*, **74**: 76–84. <https://doi.org/10.1016/j.ijbiomac.2014.11.036>

- Sarasam, A., & Madihally, S. V. (2005). Characterization of chitosan-polycaprolactone blends for tissue engineering applications. *Biomaterials*, **26**: 5500–5508.
- Saravanan, R., Gupta, V. K., Narayanan, V., & Stephen, A. (2014). Visible light degradation of textile effluent using novel catalyst. *Journal of the Taiwan Institute of Chemical Engineers*, **45**: 1910–1917.
- Särkkä, H., Bhatnagar, A., & Sillanpää, M. (2015). Recent developments of electro-oxidation in water treatment –A Review. *Journal of Electroanalytical Chemistry*, **754**: 46–56. <https://doi.org/10.1016/j.jelechem.2015.06.016>
- Sartape, A. S., Mandhare, A. M., Jadhav, V. V., Raut, P. D., Anuse, M. A., & Kolekar, S. S. (2017). Removal of malachite green dye from aqueous solution with adsorption technique using *Limonia acidissima* (wood apple) shell as low cost adsorbent. *Arabian Journal of Chemistry*, **10**: S3229–S3238. <https://doi.org/10.1016/j.arabjc.2013.12.019>
- Sattayanon, C., Kungwan, N., & Punyodom, W. (2013). Theoretical investigation on the mechanism and kinetics of the ring-opening polymerization of  $\epsilon$ -caprolactone initiated by tin (II) alkoxides. *Journal of Molecular Modelling*, **19**: 5377–5385.
- Sharma, N. & Nandi, B. K. (2013). Utilization of Sugarcane Baggase , an Agricultural Waste to Remove Malachite Green Dye from Aqueous Solutions. *Journal of Materials and Environmental Science*, **4**: 1052–1065.
- Shikuku, V. O., Zanella, R., Kowenje, C. O., Donato, F. F., Bandeira, N. M. G., & Prestes, O. D. (2018). Single and binary adsorption of sulfonamide antibiotics onto iron-modified clay :

- linear and nonlinear isotherms , kinetics, thermodynamics , and mechanistic studies. *Applied Water Science*, **8**: 1–12. <https://doi.org/10.1007/s13201-018-0825-4>
- Shirmardi, M., Mahvi, A. H., Hashemzadeh, B., Naeimabadi, A., Hassani, G., & Niri, M. V. (2013). The adsorption of malachite green (MG) as a cationic dye onto functionalized multi walled carbon nanotubes. *Korean Journal of Chemical Engineering*, **30**: 1603–1608. <https://doi.org/10.1007/s11814-013-0080-1>
- Shukla, S.K., Mishra, A.K., Arotiba, O.A. & Mamba, B. B. (2013). Chitosan-based nanomaterials: A state-of-the-art review. *International Journal of Biological Macromolecules*, **59**: 46–58. <https://doi.org/10.1016/j.ijbiomac.2013.04.043>
- Singh, H., Chauhan, G., Jain, A. K., & Sharma, S. K. (2016). Adsorptive potential of agricultural wastes for removal of dyes from aqueous solutions. *Journal of Environmental Chemical Engineering*, **5**: 122–135. <https://doi.org/10.1016/j.jece.2016.11.030>
- Sosnowski, S., Gadzinowski, M., & Slomkowski, S. (1996). Poly (L -lactide) Microspheres by Ring-Opening Polymerization. *Macromolecules*, **29**: 4556–4564.
- Srivastava, V.C., Mall, I.D., & Mishra, I. M. (2009). Chemical Engineering and Processing : Process Intensification Competitive adsorption of cadmium ( II ) and nickel ( II ) metal ions from aqueous solution onto rice husk ash. *Chemical Engineering and Processing*, **48**: 370–379. <https://doi.org/10.1016/j.cep.2008.05.001>
- Srivastava, V., Gusain, D., & Sharma, Y. C. (2013). Synthesis, characterization and application of zinc oxide nanoparticles. *Ceramics International*, **39**: 9803–9808.

- Stanford, M. J., & Dove, A. P. (2010). Stereocontrolled ring-opening polymerization of lactide. *Chemical Society Reviews*, **39**: 486–494. <https://doi.org/10.1039/b815104k>
- Stavrinou, A., Aggelopoulos, C. A., & Tsakiroglou, C. D. (2018). Exploring the adsorption mechanisms of cationic and anionic dyes onto agricultural waste peels of banana, cucumber and potato: Adsorption kinetics and equilibrium isotherms as a tool. *Journal of Environmental Chemical Engineering*, **6**: 6958–6970.
- Storey, R. F., & Sherman, J. W. (2002). Kinetics and Mechanism of the Stannous Octoate-Catalyzed Bulk Polymerization of  $\epsilon$ -Caprolactone. *Macromolecules*, **35**: 1504–1512.
- Strokal, M., Yang, H., Zhang, Y., Kroeze, C., Li, L., & Luan, S. (2014). Increasing eutrophication in the coastal seas of China from 1970 to 2050. *Marine Pollution Bulletin*, **85**: 123–140. <https://doi.org/10.1016/j.marpolbul.2014.06.011>
- Suemitsu, R., Uenishi, R., Akashi, I., & Nakano, M. (1986). The Use of Dyestuff-treated Rice Hulls for Removal of Heavy Metals from Waste Water. *Journal of Applied Polymer Science*, **31**: 75–83.
- Swapna, C.J., Prashanth, K. V. H., Rastogi, N. K., Indiramma, A. R., Reddy, S. Y. & Raghavarao, K. S. M. . S. (2011). Optimum Blend of Chitosan and Poly- ( $\epsilon$ -caprolactone) for Fabrication of Films for Food Packaging Applications. *Food Bioprocess Technology*, **4**: 1179–1185. <https://doi.org/10.1007/s11947-009-0203-1>
- Talip, Z., Eral, M., & Hicsonmez, U. (2009). Adsorption of thorium from aqueous solutions by perlite. *Journal of Environmental Radioactivity*, **100**: 139–143.

- Teng, W. L., Khor, E., Tan, T. K., Lim, Y., & Tan, C. (2001). Concurrent production of chitin from shrimp shells and fungi. *Carbohydrate Polymers*, **332**: 305–316.
- Varma, I. K., Albertsson, A. C., Rajkhowa, R., & Srivastava, R. K. (2005). Enzyme catalyzed synthesis of polyesters. *Progress in Polymer Science (Oxford)*, **30**: 949–981.
- Wang, J., Chen, Y., Ge, X., & Yu, H. (2007). Optimization of coagulation-flocculation process for paper-recycling wastewater treatment using response surface methodology. *Colloids and Surfaces A: Physicochemical and Engineering Aspects*, **302**: 204–210.
- Wang, X., Jiang, C., Hou, B., Wang, Y., Hao, C. & Wu, J. (2018). Carbon composite lignin-based adsorbents for the adsorption of dyes. *Chemosphere*, **206**: 587–596.
- Wang, H., Zhai, L., Li, Y., & Shi, T. (2008). Preparation of irregular mesoporous hydroxyapatite. *Materials Research Bulletin*, **43**: 1607–1614.
- Wang, J., Li, A., Xu, L., & Zhou, Y. (2009). Adsorption of tannic and gallic acids on a new polymeric adsorbent and the effect of Cu ( II ) on their removal. *Journal of Hazardous Materials*, **169**: 794–800. <https://doi.org/10.1016/j.jhazmat.2009.04.013>
- Wanyonyi, W.C., Onyari, J. M. & Shiundu, P. M. (2014). Adsorption of Congo Red Dye from Aqueous Solutions Using Roots of *Eichhornia crassipes* : Kinetic and Equilibrium Studies. *Energy Procedia*, **50**: 862–869.
- Wanyonyi, W. C., Onyari, J. M., & Shiundu, P. M. (2013). Adsorption of Methylene Blue Dye from Aqueous Solutions Using *Eichhornia crassipes*. *Bull Environ Contam Toxicol*, **91**: 362 – 366. <https://doi.org/10.1007/s00128-013-1053-0>

- Weber, T. W. & Chakravorti, R. K. (1974). Pore and Solid Diffusion Models for Fixed-Bed Adsorbers. *American Institute of Chemical Engineers*, **20**: 229–238.
- Wekoye, J. N., Wanyonyi, W. C., Wangila, P. T., & Tonui, M. K. (2020). Kinetic and equilibrium studies of Congo red dye adsorption on cabbage waste powder. *Environmental Chemistry and Ecotoxicology*, **2**: 24–31. <https://doi.org/10.1016/j.eneco.2020.01.004>
- Weng, C. H., Lin, Y. T., & Tzeng, T. W. (2009). Removal of methylene blue from aqueous solution by adsorption onto pineapple leaf powder. *Journal of Hazardous Materials*, **170**: 417–424. <https://doi.org/10.1016/j.jhazmat.2009.04.080>
- Xu, J., Song, J., Pispas, S., & Zhang, G. (2014). Polymer Chemistry. *Polymer Chemistry*, **5**: 4726–4733. <https://doi.org/10.1039/c4py00342j>
- Yadamari, T., Yakkala, K., Battala, G., & Gurijala, R. N. (2011). Biosorption of Malathion from Aqueous Solutions Using Herbal Leaves Powder. *American Journal of Analytical Chemistry*, **02**: 37–45. <https://doi.org/10.4236/ajac.2011.228122>
- Yin, C., & Goh, B. (2011). Thermal Degradation of Rice Husks in Air and Nitrogen : Thermogravimetric and Kinetic Analyses. *Energy Sources, Part A*, **34**: 246-252.
- Youssef, A. M., Abou-Yousef, H., El-Sayed, S. M., & Kamel, S. (2015). Mechanical and antibacterial properties of novel high performance chitosan/nanocomposite films. *International Journal of Biological Macromolecules*, **76**: 25–32.
- Yusuff, A. S. (2018). Optimization of adsorption of Cr ( VI ) from aqueous solution by *Leucaena leucocephala* seed shell activated carbon using design of experiment. *Applied Water*

*Science*, **8**: 1–11. <https://doi.org/10.1007/s13201-018-0850-3>

Yuvakkumar, R., Elango, V., Rajendran, V., & Kannan, N. (2014). High-purity nano silica powder from rice husk using a simple chemical method. *Journal of Experimental Nanoscience*, **9**: 272–281. <https://doi.org/10.1080/17458080.2012.656709>

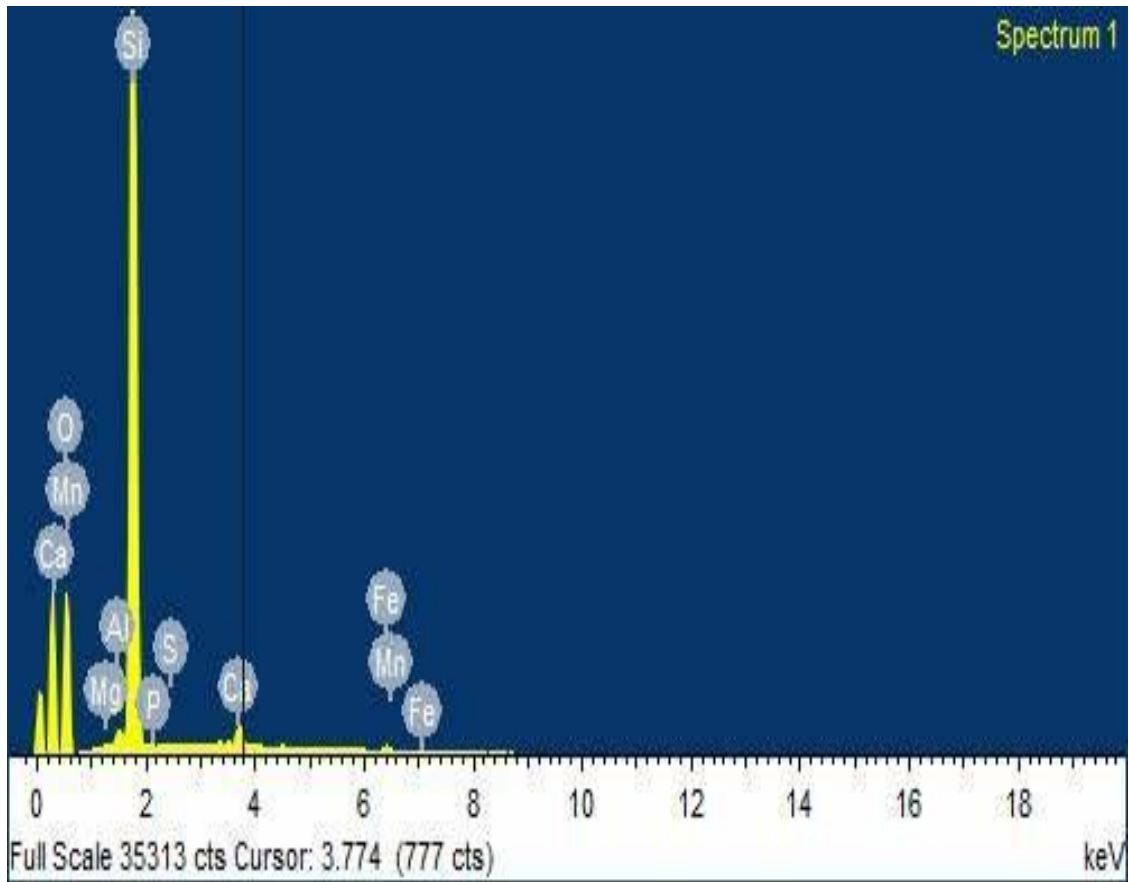
Zhao, Q., Tao, J., Yam, R. C. M., Mok, A. C. K., Li, R. K. Y., & Song, C. (2008). Biodegradation behavior of polycaprolactone/rice husk ecomposites in simulated soil medium. *Polymer Degradation and Stability*, **93**: 1571–1576.

Zheng, J., Su, C., Zhou, J., Xu, L., Qian, Y., & Chen, H. (2017). Disinfection on antibiotic resistance genes in secondary effluents of municipal wastewater treatment plants. *Chemical Engineering Journal*, **317**: 309–316. <https://doi.org/10.1016/j.cej.2017.02.076>

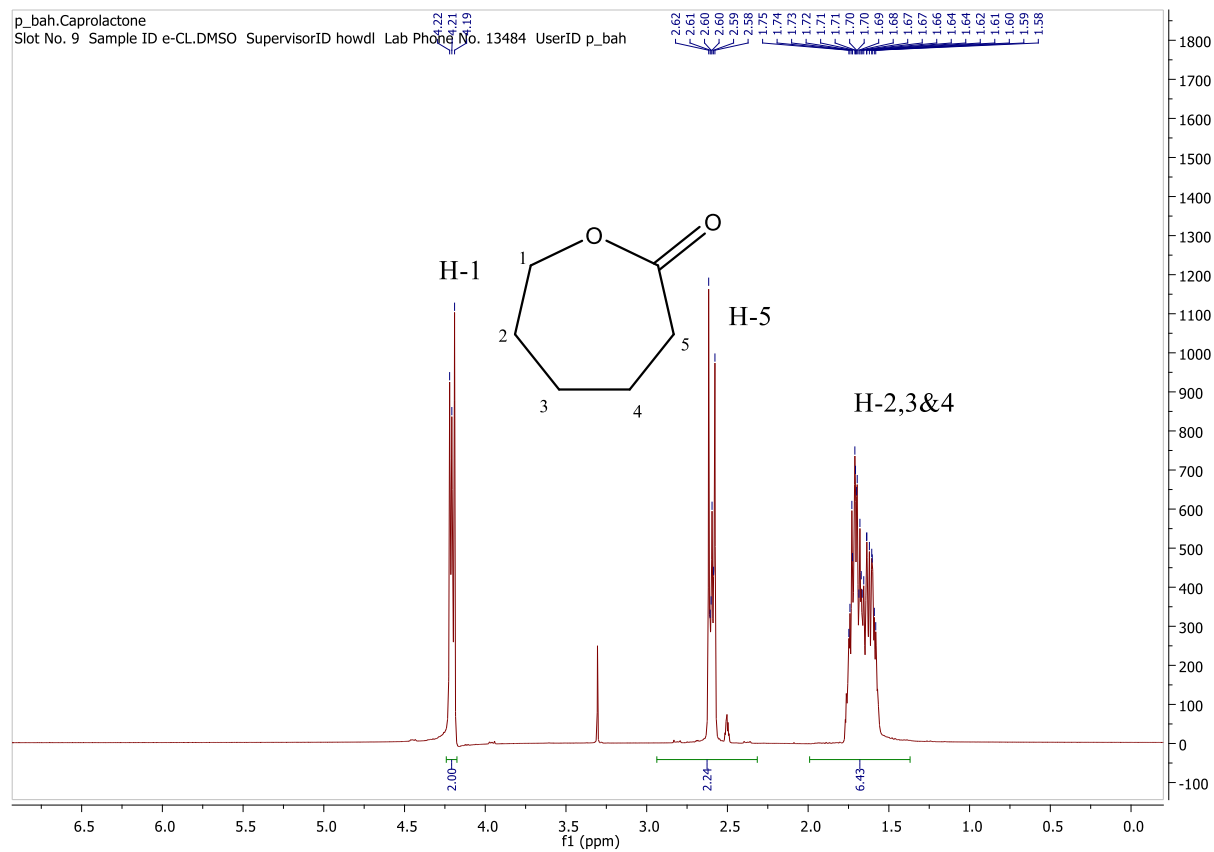
Zou, Z., Tang, Y., Jiang, C., & Zhang, J. (2015). Efficient adsorption of Cr ( VI ) on sunflower seed hull-derived porous carbon. *Journal of Environmental Chemical Engineering*, **3**: 898–905. <https://doi.org/10.1016/j.jece.2015.02.025>

# APPENDICES

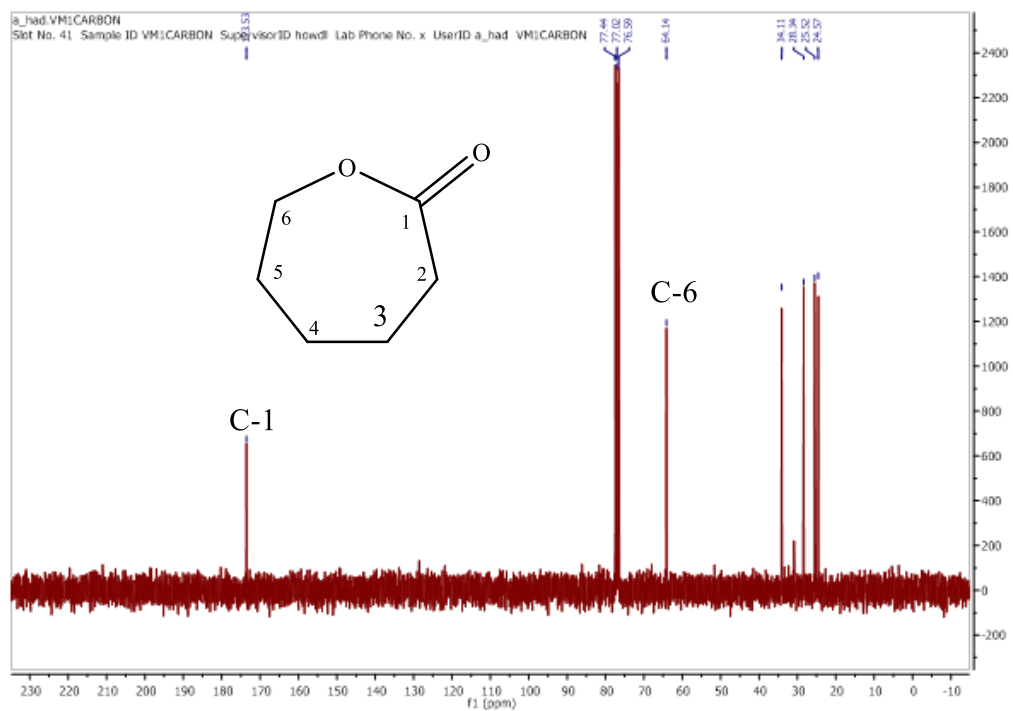
Appendix 1: EDS elemental spectrum for rice husks



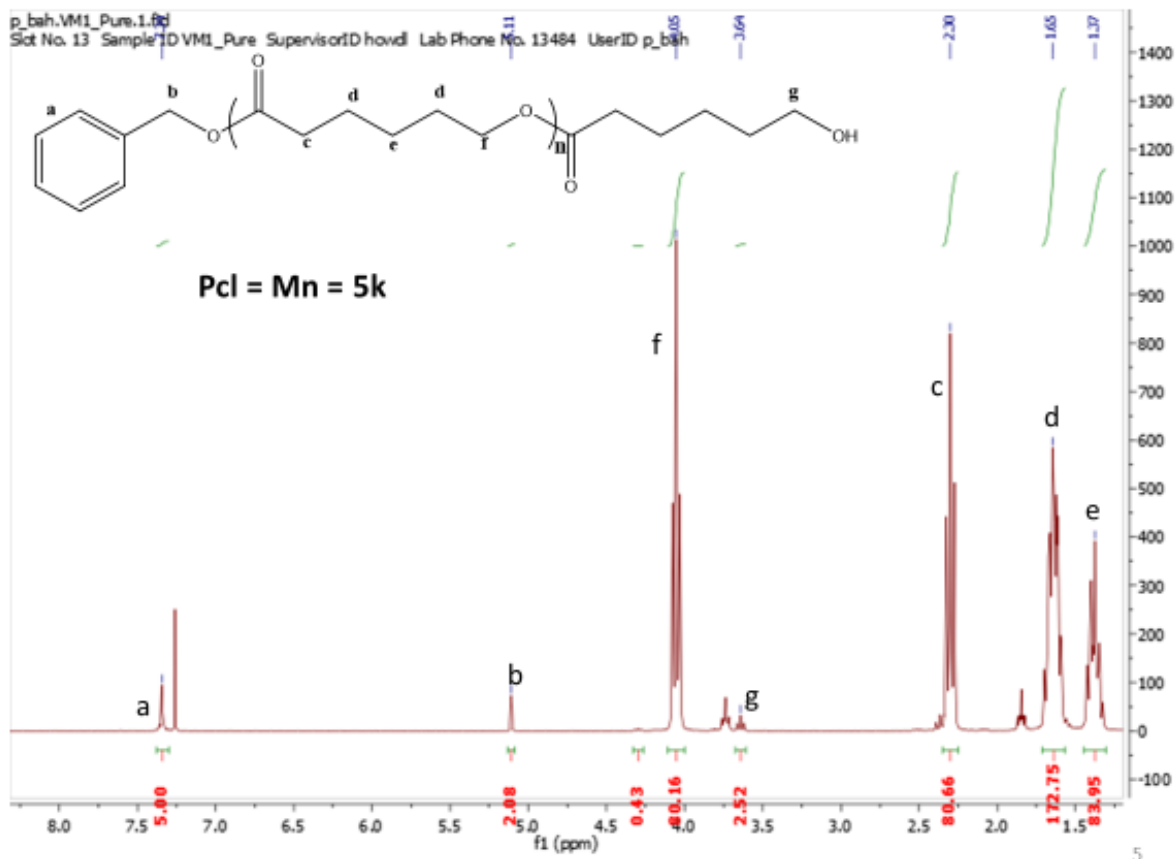
## Appendix 2: $^1\text{H}$ NMR spectrum for $\epsilon$ -Caprolactone



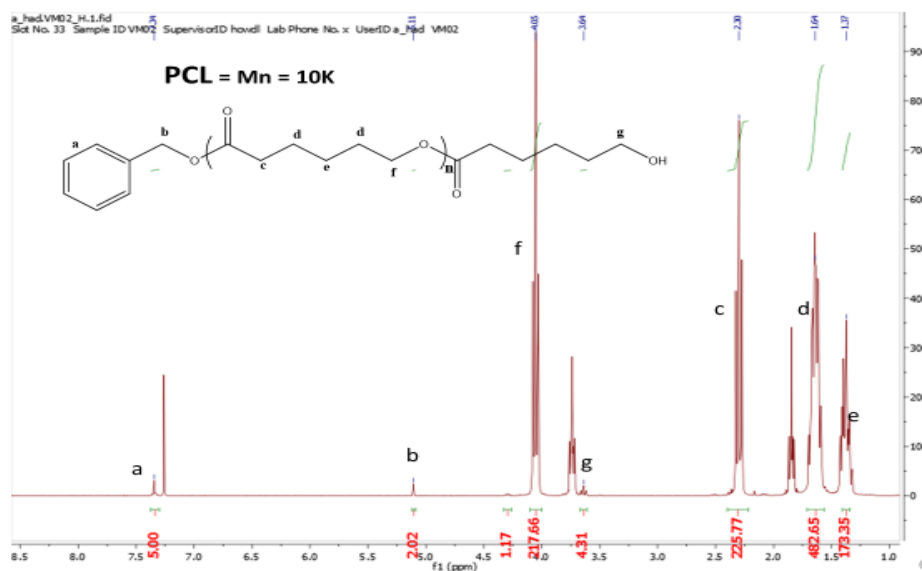
### Appendix 3: $^{13}\text{C}$ NMR spectrum for $\epsilon$ -Caprolactone



Appendix 4:  $^1\text{H}$  NMR spectrum for  $\epsilon$ -PCL (5000g/mol)



**Appendix 5:**  $^1\text{H}$  NMR spectrum for  $\epsilon$ -PCL (10,000g/mol)



**Appendix 6:** Ring opening polymerization of  $\epsilon$ -Caprolactone (CL) with stannous octoate ( $\text{sn}(\text{Oct})_2$ ) as the catalyst and benzyl alcohol as the initiator

Time (Hrs)	Temp ( $^{\circ}\text{C}$ )	[M]: [I] ratio	Initiator	% conv	$M_n$ , Targ g/mol	$M_n$ ( $^1\text{H}$ NMR)	$M_n$ (GPC)	$\text{DP}_n$ (NMR)	PDI
17	120	44.1	BZ(OH)	99.5	5,000	3,653	1,700	32	1.09
21.25	120	88.1	BZ(OH)	99.4	10,000	5,979	8,100	53	1.34
18.42	120	131.1	BZ(OH)	99.9	15,000	5,709	7,100	50	1.28

NB: [M]: [I] = Monomer: Initiator ratio

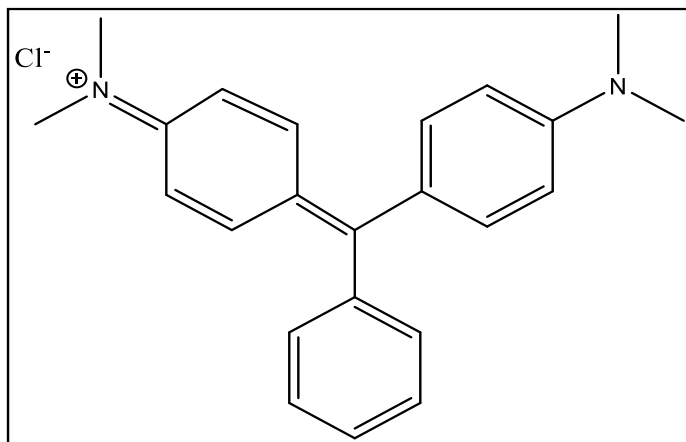
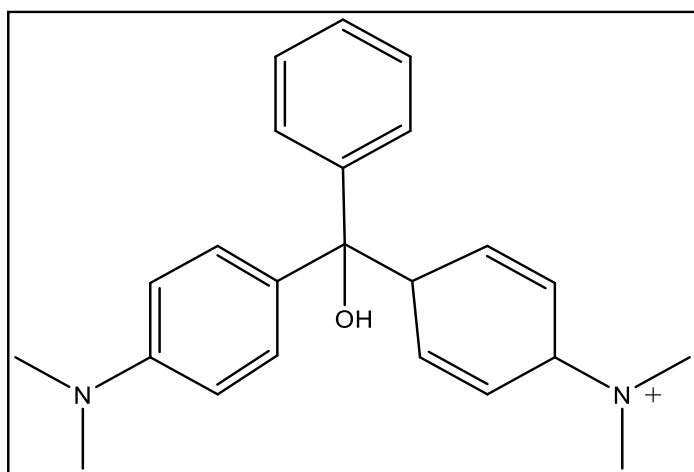
**Appendix 7:** EDXRF analysis settings for CS-ZnO material

Secondary target	Tube voltage (kV)	Tube current (mA)	Analysis time (s)
Mo	50	Auto	50
Cu	50	Auto	50
RX9	25	Auto	50
Al	50	Auto	50

**Appendix 8:** Mean elemental concentration levels of CS-ZnO material

Element	Concentration (mg/kg)
Phosphorus (P)	166 ± 26.6
Iron (Fe)	753 ± 45.3
Zinc (Zn)	965000 ± 53.2

**Appendix 9:** Chemical structure of carbinol form of malachite green



**Appendix 10:** Chemical structure of malachite green chloride